CHARGE MIGRATION AND ONE-ELECTRON OXIDATION AT ADENINE AND THYMIDINE CONTAINING DNA STRANDS AND ROLE OF GUANINE N1 IMINO PROTON IN LONG RANGE CHARGE MIGRATION THROUGH DNA

A Dissertation
Presented to
The Academic Faculty

by

Avik Kumar Ghosh

In Partial Fulfillment
of the Requirements for the Degree
Doctor of Philosophy in Chemistry

Georgia Institute of Technology
August 2007

CHARGE MIGRATION AND ONE-ELECTRON OXIDATION AT ADENINE AND THYMIDINE CONTAINING DNA STRANDS AND ROLE OF GUANINE N1 IMINO PROTON IN LONG RANGE CHARGE MIGRATION THROUGH DNA

Approved by:

Dr. Gary B. Schuster, Advisor
School of Chemistry and Biochemistry
Georgia Institute of Technology

Dr. Christopher Fahrni
School of Chemistry and Biochemistry
Georgia Institute of Technology

Dr. Uwe Bunz
School of Chemistry and Biochemistry
Georgia Institute of Technology

Dr. Roger Wartell
School of Biology
Georgia Institute of Technology

Dr. Donald Doyle
School of Chemistry and Biochemistry
Georgia Institute of Technology

Date approved: 2nd May , 2007

This dissertation is dedicated to my parents Dr. Asit Baran Ghosh and Basusri Ghosh and my beloved wife Tanusree

ACKNOWLEDGEMENTS

I want to take this opportunity to thank many people for helping me in research and for making my stay at Georgia Institute of Technology a memorable one. Firstly, I wish to thank my advisor Dr. Gary Schuster for providing me the chance to work in his group. His guidance and invaluable advices always led my way towards perfect results. Secondly, I want to thank my committee members for their support and important suggestions.

I wish to thank my lab-mates for helping me in learning new things, solving problems and making my life an easy one in Dr. Schuster's lab. I want to specially thank Dr. Sriram Kanvah, Dr. Abraham Joy and Dr. Joshy Joseph for teaching me the general laboratory techniques and helping me in performing the experiments. I also want to express my gratitude to Prolay Das, Gozde Guler, Dr. Huachuan Cao, Dr. Lezah Roberts, Dr.Thabisile Ndlebe, Dr. Nathan Schlientz, Dr.Frank Onyemauwa, Chiko Umeweni, Dr. Bhaskar Dutta, Dr. Rick Redic, Dr. Chu-sheng Liu, Dr. Wen Chen and Dr. Selvi for supporting me and providing me with a memorable experience at Dr. Schuster's lab. . I would also like to thank my friends at Atlanta who helped me in every critical step and never let me feel that I am staying thousands of miles away from my home. I want to thank Dr. Cameron Sullards and Mr. David Bostwick for teaching me various Mass Spectrometric methods and for allowing me to work at the Mass Spectrometry Facilities at Georgia Institute of Technology. I also wish to thank Dr. Bridgette Barry and David Jenson for helping me with EPR experiments and Dr. Jean Cadet and Dr. Thierry Douki at Grenobole, France for running the HPLC-MS analysis which helped my research a lot.

I wish to thank my parents for supporting me through everything. And, lastly I want to thank my wife Tanusree for always being there for me and without her nothing would have been possible.

TABLE OF CONTENTS

LIST OF TABLES

LIST OF FIGURES

LIST OF SYMBOLS AND ABBREVIATIONS

5-HMdUd	5-hydroxymethyl-2’-deoxyuridine
5-FordUd	5-formyl-2’-deoxyuridine
8-oxoA	7,8-dihydro-8-oxoadenine
8-oxoG	7,8-dihydro-8-oxoguanine
α	alpha
Å	Angstrom(s)
A	Adenine
AQ	Anthraquinone
AQ·-	Anthraquinone radical anion
BrF^5dC	5-bromo-2’-deoxycytidine
C	Cytidine
ºC	degree(s) Celcius
CD	Circular Dichroism
cm	centimeter(s)
cpm	count(s) per minute
δA/δT	change in absorbance with respect to the change in temperature
D_2O	deuterium oxide
dC	2’-deoxycytidine
DFT	density functional theory
DMT	4,4'-methoxytrityl
DNA	Deoxyribonucleic Acid
ε	extinction coefficeint

ESI	Electrospray Ionization
E_{ox}	Oxidation Potential
F^5C	5-fluorocytidine
F^5dC	5-fluoro-2'-deoxycytidine
γ	gamma
G	Guanine
G·+	guanine radical cation
h	hour
HPLC	High-Performance Liquid Chromatography
in vacuo	in a vacuum
k_h	rate of hopping
k_t	rate of trapping
k_{ratio}	ratio of rate of hopping to rate of trapping
μ	micro (10^{-6})
M	molar
min	minute(s)
mM	millimolar
nm	nanometer(s)
phen	1,10-phenanthroline
phi	9,10-phenanthrenequinone diimine
PNK	polynucleotide kinase
Rh	Rhodium
ROS	Reactive oxygen species

Ru	Ruthenium
T	Thymine
TdT	terminal dinucleotide transferase
Tm	melting temperature
TMSOTf	Trimethylsilyl Triflate
TPDS	Triisopropyl disiloxane
UV	Ultraviolet
U	2’-deoxyuridine
Vis	Visible

SUMMARY

DNA is the carrier of biological information and damage to DNA has been believed to be responsible for many diseases including aging and cancer. One electron oxidation is one of the processes that lead to DNA damage. This process in duplex DNA results in formation of radical cation that migrates through the nucleobases and eventually gets trapped at guanines G_n (n=1-3) forming guanine radical cation. This can easily react with H_2O and O_2 leading oxidative DNA damage. There are more than one mechanisms reported explaining the charge migration process, the most popular one being the polaron-like hopping mechanism. Some of the minute details of the mechanism are still being developed.

We have tried to figure out the exact role played by the guanine N1 imino proton during the charge migration process. It is known that the guanine N1 imino proton can be transferred to the N3 of cytidine that is hydrogen bonded to it. Some reports have implication that this proton transfer and radical cation migration are coupled to each other. We synthesized 5-fluorocytidine (F^5C) and by titration figured out that it has less pK_a than the normal 2'-deoxycytidine (dC). Then we incorporated 5-fluoro-2'-deoxycytidine (F^5dC) in place of normal dC in DNA duplexes. The lower pK_a of F^5dC should perturb the proton transfer process from the guanine to it and if this process is coupled with charge migration, that process is also going to be affected. Monitoring the charge migration by gel electrophoresis and comparing with the charge migration of the strands having normal dC, we do not see any change in the charge migration ability. However, there is a considerable decrease in the guanine damage, when there is F^5dC

opposite to it. These results indicate that the charge migration is not coupled with proton transfer process, but the change in basicity affects the reactivity of the guanine radical cation.

The charge migration and reactions in guanine containing duplexes are well studied, but very little is known about the charge migration through oligomers that do not have any guanine. We have reported a systematic study on the charge migration through adenine (A) and thymidine (T) containing DNA strands. The damage has predominantly seen in thymidine, although from oxidation potentials reaction at adenine was expected. The thymidine reaction has been analyzed thoroughly. It has similar distance dependence property as the well known guanine damage. Study of thymidine damage in presence of radical scavengers revealed that there are radical intermediates involved in this reaction. The role played by C5-methyl group of thymidine has been studied by replacing some of the thymidines with 2'-deoxyuridines (U). These experiments point toward reactions involving tandem lesion. Although, we were not able to find any conclusive result about the radical intermediates from EPR spectra, the products of the thymidine oxidation reaction has been identified by HPLC-MS analysis. On the basis of these information and molecular modeling study we have proposed a possible pathway leading to one-electron oxidation at the thymidines.

CHAPTER 1

INTRODUCTION

1.1 Structural Overview of DNA

In every organism, the ultimate source of biological information is nucleic acid. The shapes and activities of individual cells are, to large extent, determined by genetic instructions contained in deoxyribonucleic acid or DNA (for some viruses, in ribonucleic acid or RNA)[1]. From the early discovery that DNA is the carrier of genetic information[2] to the structure elucidation by Watson and Crick in 1953[3], DNA has motivated scientists to study its immense physical and chemical properties. The function of DNA is immensely reliant on its structure and its interaction and reactions with other biological molecules and small molecules.

DNA is a polymeric biomolecule and its monomeric units are known as nucleotides. These units are comprise of base, deoxyribose and phosphate backbone and are connected to each other through the phosphate backbone. Nucleotides form DNA strands and two complimentary strands are held together to form DNA double helix structure. The genetic information is encoded in the sequence of nucleotides[1]. The double helix structure protects the nucleotides from damage[4] and thus the integrity of the genetic information is maintained[5]. This information is converted to several functional and structural components *in vivo* through processes such as translation and transcription[6]. Thus, the detailed knowledge of DNA structure is essential to understand and repair pathways that interfere with its normal activity.

1.1.1 Nucleosides & Nucleotides

The basic constituents of DNA are bases, deoxyribose sugar and phosphate groups. Bases and sugars form the nucleosides and they are attached to the phosphate group to form the nucleotides.

Bases:

The primary informational elements of DNA are the heterocyclic aromatic bases. There are two types of bases in DNA: purine and pyrimidine. Adenine (A) and Guanine (G) are the purine bases present in DNA and Thymine (T) and Cytosine (C) are the pyrimidines (Figure 1.1). Uracil (U) is another pyrimidine base and it is present in RNA in place of Thymine. Interestingly, these bases are not synthesized from purine or pyrimidine *in vivo*[1].

Purine is a bicyclic compound where a six member and five member nitrogen containing aromatic rings are fused to each other. In adenine, an amine ($-NH_2$) group is attached to the C6 position. The other purine derivative base guanine has a carbonyl group at C6 position and an amine group at C2 position. On the other hand, pyrimidine is a six member heterocyclic aromatic compound. Pyrimidine derivative base cytosine has an amine group at C4 position and a carbonyl group at C2. Thymine contains carbonyl groups at C2 and C4 positions and a methyl ($-CH_3$) group at C5 position. Uracil has a similar structure as thymine, only it does not have the methyl group at C5.

Sugars:

The sugar moiety present in the DNA is 2'-deoxyribose. Ribose is an aldopentose and present in DNA in its cyclic *furanose* form. 2'-deoxyribose does not have the hydroxyl

group at 2' position (Figure 1.2). RNA has ribose instead of 2'-deoxyribose as the sugar moiety. The conformation of sugar's five member ring is very important in determining the overall conformation of double stranded DNA. One of the atoms in the five member ring tends to "pucker" out of the plane of the ring, potentially affecting the overall shape of the double stranded DNA. For DNA the sugar pucker is mainly 2'-*endo*, which means the C2 position is above the plane of the ring. In RNA the sugar pucker is 3'-*endo*, which means the C3 position is above the plane of the ring (Figure 1.3).

Glycosidic bond:

In a nucleoside the base is attached to the C1 position of sugar (Figure1.4). For purines, N9 position of the base is attached to the sugar and for pyrimidines the connection is through N1 of base. The C-N bond between the sugar and base is known as glycosidic bond (Figure 1.4). The sugar in the nucleosides in DNA adopt β-D-conformation, i.e., the substituent at the C1' (see Figure 1.4 for the numbering) position and C4' positions are both facing up and the substituent at C3' position is facing down.

Phosphate backbone & phosphodiester bond:

Phosphate groups are attached to the C5' and C3' hydroxyl groups of the sugar. The nucleosides with the phosphate group are termed as nucleotides (Figure 1.4). The O-P bonds between the sugar and phosphates are known as phosphodiester bonds. The nucleotides are connected to each other through these phosphate groups. The end where the phosphate is connected to C5' hydroxyl is termed as 5' end and the other end is termed as 3' end (Figure 1.5).

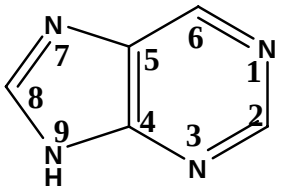

Purine

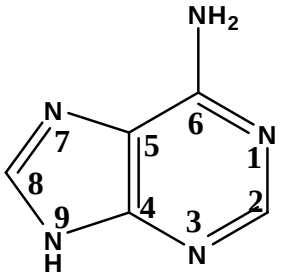

Adenine

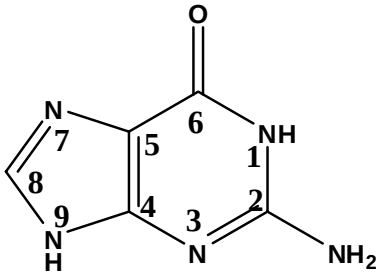

Guanine

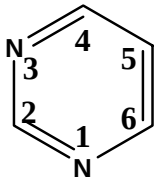

Pyrimidine

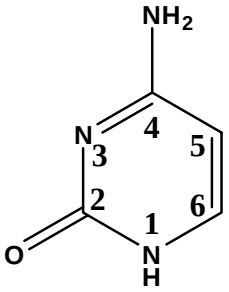

Cytosine

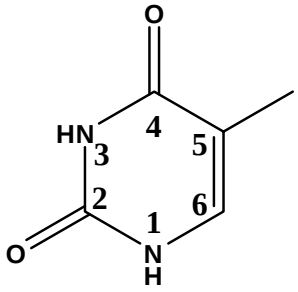

Thymine

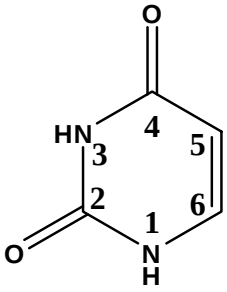

Uracil

Figure 1.1: Structure of Purine, Pyrimidine and DNA bases

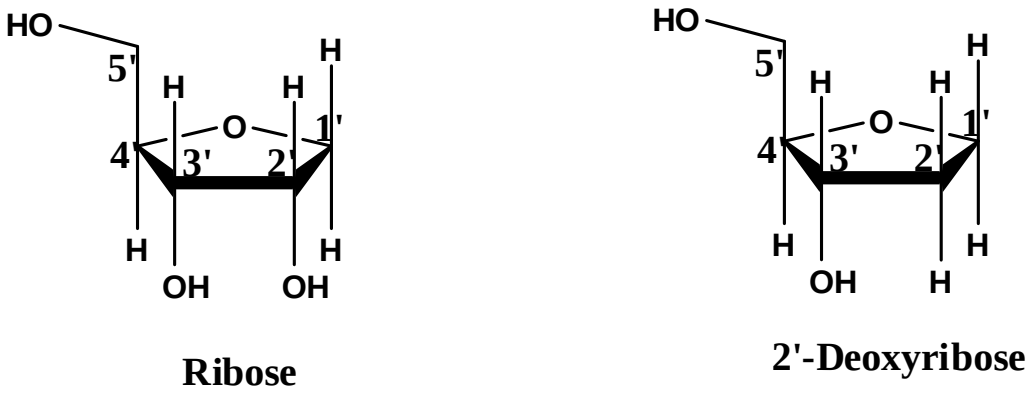

Figure 1.2: Cyclic furanose form of ribose and 2'-deoxyribose

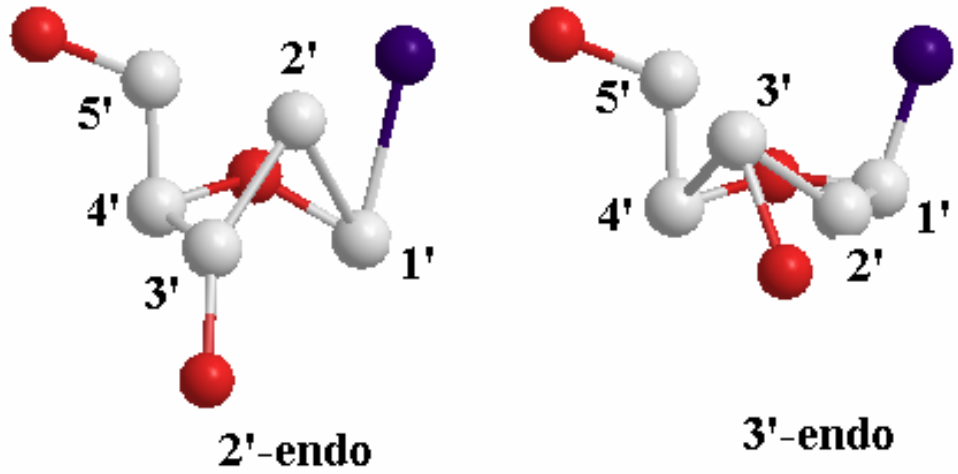

Figure 1.3: 2'-deoxyribose sugar puckering in DNA. White, red and blue balls represent carbon, oxygen and nitrogen respectively. Hydrogens are not shown in the picture.

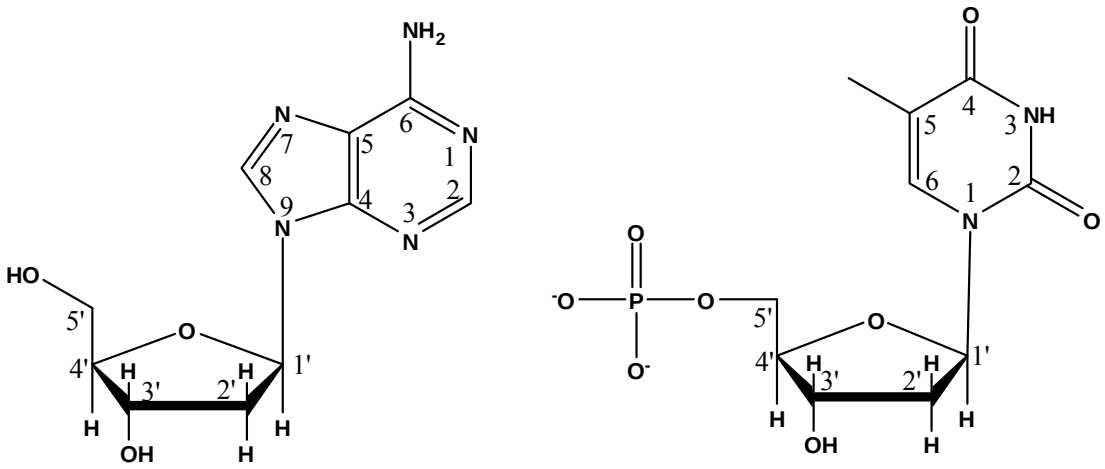

2'-Deoxyadenosine
(Nucleoside)

Thymidine monophosphate
(Nucleotide)

Figure 1.4: Nucleoside and nucleotide

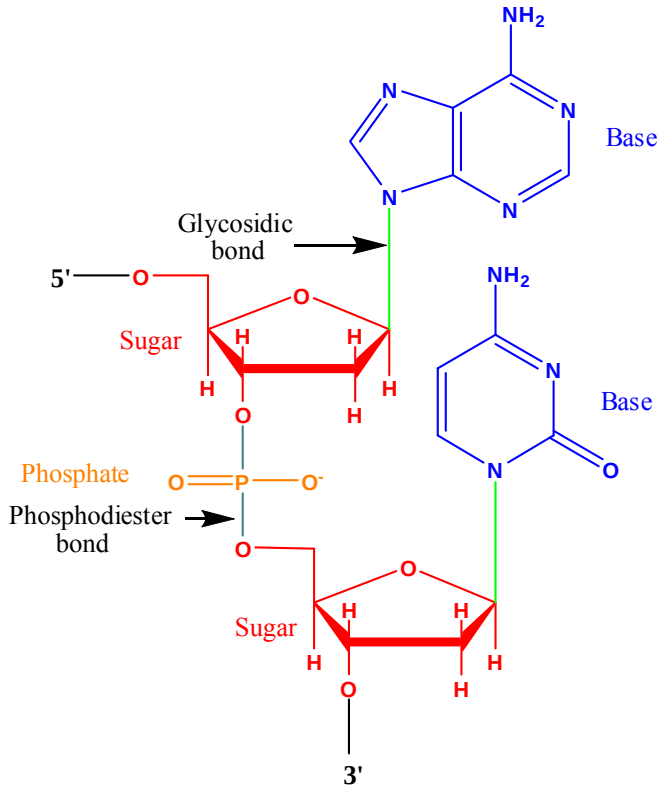

Figure 1.5: Different components of DNA shown in a dinucleotide portion. Bases, sugars and phosphate are shown in blue, red and orange respectively.

1.1.2 DNA Duplex

Two complementary DNA strands are bind to each other to form the double stranded DNA or DNA duplex. Hydrogen bondings between the bases are responsible for the complementarity and help to form the helical DNA duplex structure.

Base pair:

In DNA the purine bases and pyrimidines bases are paired to each other, but more specifically adenine pairs to thymine and guanine pairs with cytosine (Figure 1.6). There are two hydrogen bonds between A and T, while G and C are held together by three hydrogen bonds. In A-T base pair, one H-bond is between the C6-NH2 of A and C4-O of T and one H-bond between N1 of A and N3-H of T. The G-C base pair has an H-bond between C6-O of G and C4-NH2 of C, an H-bond between N1-H of G and N3 of C, and an H-bond between C2-NH2 of G and C2-O of C. These base pairing plays the central role in the replication of DNA where an exact replica of each strand is created. The enzyme identifies the precise base and places the complement opposite that position. When both strands are copied a new duplex is formed which has exactly the same sequence as the parent one.

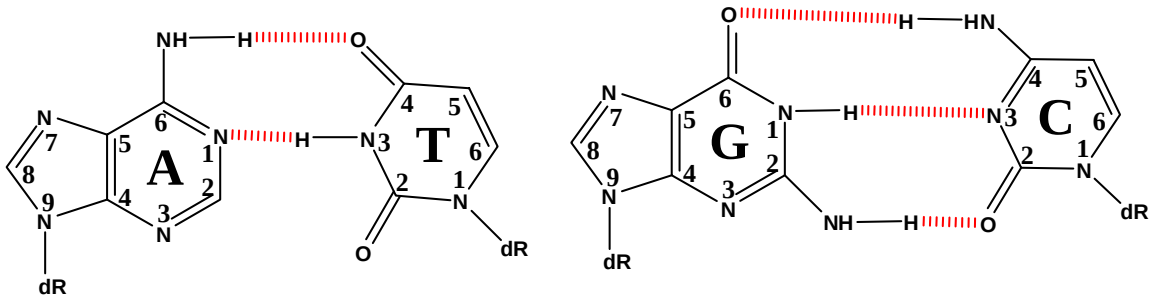

Figure 1.6: Watson and Crick base pairs. Hydrogen bonds are shown as red lines.

Double Helix:

The evidence that DNA is a helical molecule was first provided by an X-ray diffraction image of a fiber DNA taken by Rosalind Franklin[7,8]. The description of the image enabled Watson and Crick to deduce the double helical model of DNA[3]. Later investigations have confirmed the general accuracy of the Watson-Crick Model, although its details have been changed. The major features of double helical DNA structure are mentioned below:

- Two complementary polynucleotide chains wind around a common axis to form the DNA double helix (Figure 1.7).
- The two single strands of DNA are antiparallel (run in opposite directions), but each forms a right-handed helix.
- The bases occupy the core of the helix and sugar-phosphate backbone chains run along the periphery, thereby minimizing the repulsions between the charged phosphate groups. The surface of the double helix contains two grooves of unequal width. They are known as **major** and **minor grooves**.(Figure 1.7)

The double stranded DNA helix is stabilized and held together by several different forces. Hydrogen bonding between the bases on the complementary strands holds the DNA duplex, although, this force contributes a little to the stability of the double helix. The aromatic bases within the center of the helix stabilize the duplex through stacking interactions between the aromatic rings in adjacent bases[9]. (Figure 1.8) Also, the metal cations surround the negatively charged phosphate groups in the sugar-phosphate backbone and add more stability to the DNA duplex. Lastly, water molecules

cooperatively bind along the major and minor groove of the DNA[10] adding further stability to the duplex structure.

When a solution of DNA duplex is heated above a characteristic temperature, its native structure collapses and two complementary strands separate into single strands. This process is known as **denaturation** of DNA and the characteristic temperature is termed as the **melting temperature** or $\mathbf{T_m}$ of that strand.

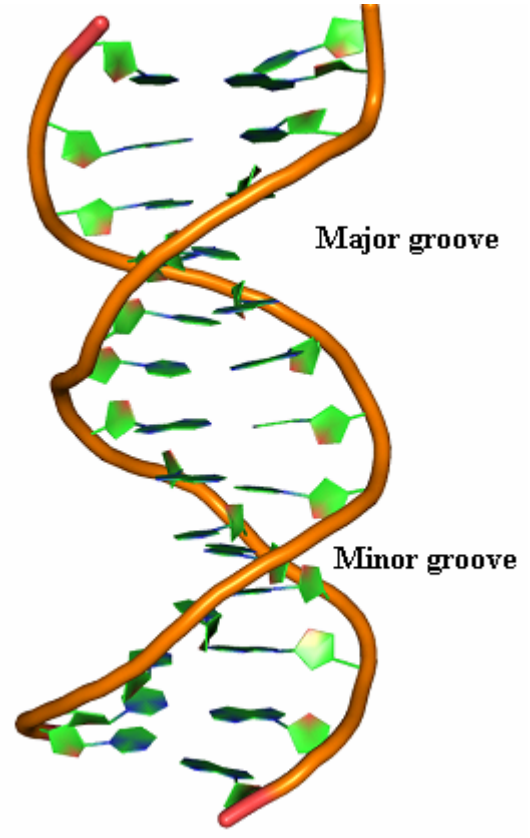

Figure 1.7: Cartoon representation of a segment of DNA double helix.

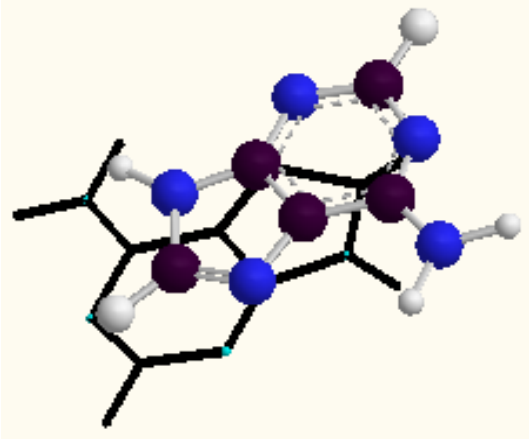

Figure 1.8: Stacking of two adenines. One of the adenines is represented as ball and stick model and other by black line model. (Black balls indicates carbon, blue indicates oxygen and white indicates hydrogen)

1.1.3 Conformations of DNA

DNA duplex assumes mainly three different conformations. These are known as A-form, B-form and Z-form of DNA. Characteristics of these three DNA conformations are listed in Table 1.1.

B-DNA:

B-DNA is the most common DNA conformation (Figure 1.9). The right handed helix of B-DNA has the bases along the axis and the sugar-phosphate backbone along the periphery. The base pairs in B form DNA (B-DNA) are relatively perpendicular to the helical axis, and approximately 3.4 angstroms apart from each other. The helical turn of B-DNA is extended over approximately 34 angstroms, which means, there are 10 base pairs per turn. Its glycosidic bonds form anti conformations, while its sugar puckers form C2'-*endo* conformations. In B-DNA, the major groove of is wider (12 v 6 Å) and deeper (8.5 v 7.5 Å) than the minor groove[12]

Table 1.1:[11] Parameters of different DNA Helices.

Properties	A-DNA	B-DNA	Z-DNA
Helix sense	Right-handed	Right-handed	Left-handed
Repeating helix unit	One base pair	One base pair	Two base pair
Rotation per base pair	33.6^0	$t_t = 38.0^0(4.4^0)$* $t_g = 35.9^0(4.2^0)$*	$-60^0/2$
Mean base pair per turn	10.7	10.0 (1.2)*	12
Inclination of base normals to helix axis	$+ 19^0$	$- 1.2^0$	$- 9^0$
Rise per base pair along helix axis	2.3 Å	3.32 Å (0.19Å)*	3.8 Å
Pitch per turn of helix	24.6 Å	33.2 Å	45.6 Å
Mean propeller twist	$+18^0$	$+16^0$ (7^0)*	0^0
Glycosyl angle conformation	*anti*	*anti*	*anti* at C, *syn* at G
Sugar pucker conformation	C3'-endo	O1'-*endo* to C2'-*endo*	C2'-*endo* at C C2'-*exo* to C1'-*exo* at G

* Mean and standard deviation over 36 bases or 33 base steps in three independently refined dodecamers: CGCGAATTCGCG with bent helix axis, and CGCGAATT^{Br}CGCG (where ^{Br}C is 5-bromocytosine) under conditions in which its axis is bent and straight. The quantity t_g is the global twist angle as measured from outside the helix, whereas t_t is the local value considering the two base pairs in isolation. They differ because the local helix axis frequently deviates from the best overall axis.

.

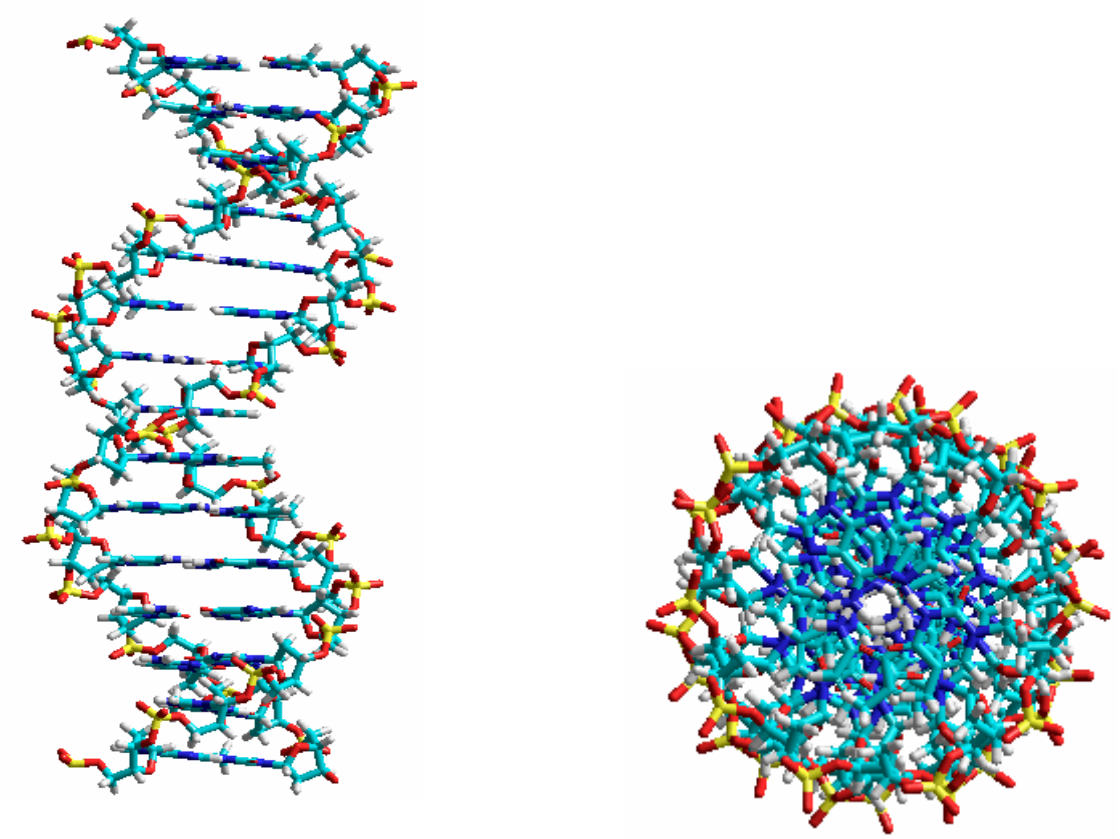

Figure 1.9: Hyperchem generated picture of a portion of B-DNA (side and top view). Light blue, dark blue, red and yellow indicate C, N, O and P respectively.

A-DNA:

The results of x-ray diffraction studies of dehydrated DNA fibers revealed the A-DNA (Figure 1.10), which appears when the relative humidity is reduced to less than about 75%. A-DNA is a right handed double helix made up of antiparallel strands held together by Watson-Crick base-pairing. The A helix is wider and shorter than B helix, and its base pairs are tiled to the axis. The sugar puckering is C3'-endo in case of A-DNA, and it leads to a 19^0 tilting of the base pairs away from the normal to the helix[12].

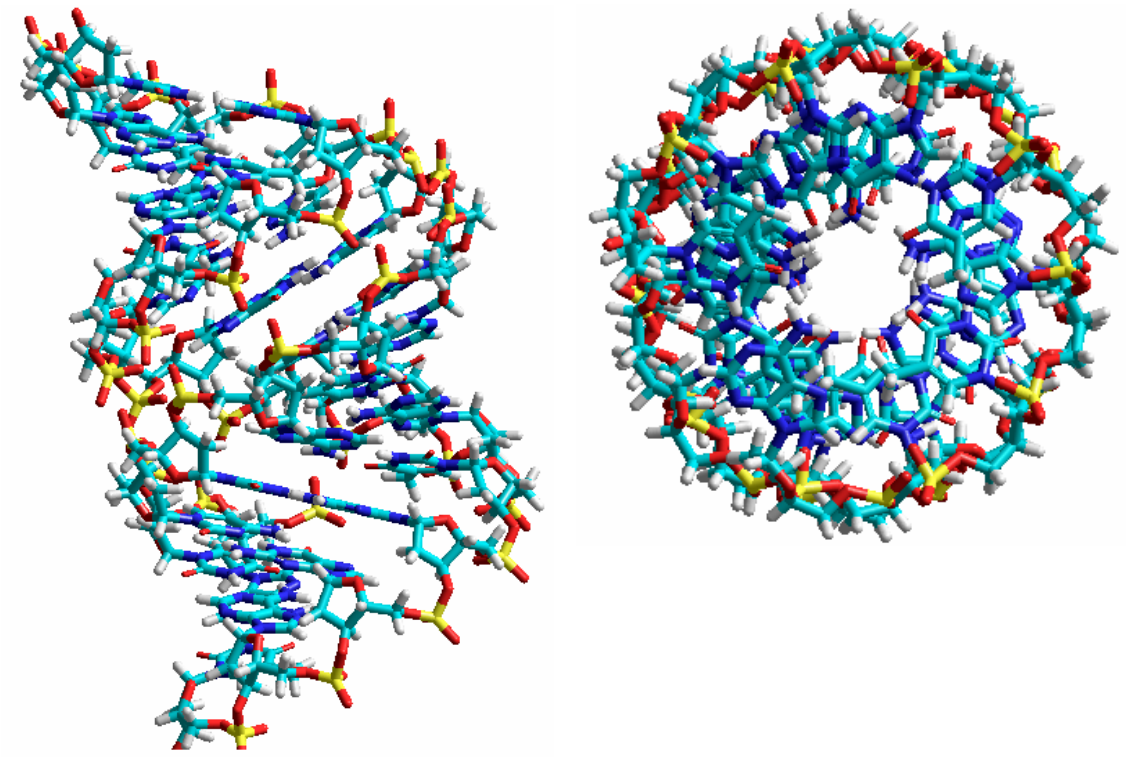

Figure 1.10: Hyperchem generated picture of a portion of A-DNA (side and top view) Light blue, dark blue, red and yellow indicate C, N, O and P respectively.

Z-DNA:

Z-DNA (Figure 1.11) was first observed when DNA tetramer CGCG was crystallized from high salt solution[13]. This tetranucleotide forms a duplex held together by Watson-Crick base pairing. However, the double helix is left-handed and the phosphates in the backbone are zigzagged. This form is adopted by short oligonucleotides that have sequences of alternating pyrimidines and purines. High salt concentrations are required to minimize electrostatic repulsion between the backbone phosphates, which are closer to each other than in other two conformations.

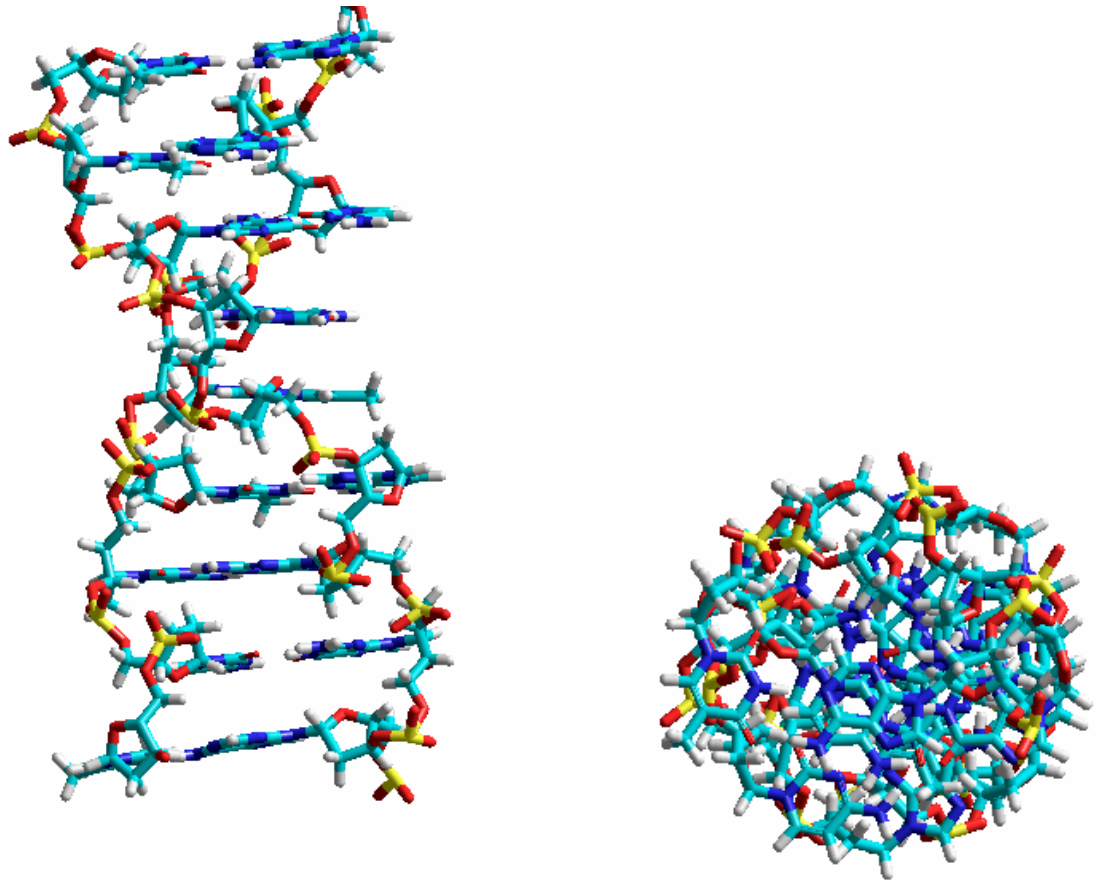

Figure 1.11: Hyperchem generated picture of a portion of Z-DNA (side and top view). Light blue, dark blue, red and yellow indicate C, N, O and P respectively.

1.2 DNA Damage and Repair

As mentioned earlier, DNA is the carrier of biological information and this information is transmitted by replication carried out by specific enzymes known as DNA polymerases. The accuracy of DNA replication carried out by these enzymes and their attendant proofreading functions is essential for the accurate transmission of genetic information during cell division. Yet errors occasionally occur during the enzyme activity and if not repaired, may alter the nucleotide sequences of genes. DNA can also be modified by environmental factors such as alkylating agents and ionizing radiation. Such

alterations can locally distort DNA's base paired structure, potentially interfering with transcription and replication.

1.2.1 Oxidative Damage

Oxidative stress is produced in cells by oxygen-derived species resulting from interaction with cells of exogenous sources such as redox-cycling drugs, carcinogenic compounds and ionizing radiations and from cellular metabolism. DNA damage caused by oxygen-derived species is known as oxidative DNA damage. Damage caused by oxygen-derived species including free radicals is the most frequent type encountered by aerobic cells. When this type of damage occurs to DNA, it is called oxidative DNA damage and it can produce a multiplicity of modifications in DNA including base and sugar lesions, strand breaks, DNA-protein cross-links and base-free sites[14-17]. Accurate measurement of these modifications is essential for understanding of mechanisms of oxidative DNA damage and its biological effects. Numerous DNA lesions have been identified in cells and tissues at steady-state levels and upon exposure to free radical-generating systems. Data accumulated over many years clearly show that oxidative DNA damage plays an important role in a number of disease processes. Thus, oxidative DNA damage is implicated in carcinogenesis and neurodegenerative diseases such as Alzheimer's disease[18-20]. There is also strong evidence for the role of this type of DNA damage in the aging process[21]. Oxidative damage to DNA is a result of interaction of DNA with reactive oxygen species (ROS), in particular the hydroxyl radical. Superoxide and hydrogen peroxide are normally not reactive towards DNA. However, in the presence of ferrous or cuprous ion (the Fenton reaction), both superoxide and hydrogen peroxide are converted to the highly reactive hydroxyl radical. Hydroxyl radical produces a

multiplicity of modifications in DNA. Oxidative attack by OH radical on the deoxyribose moiety will lead to the release of free bases from DNA, generating strand breaks with various sugar modifications and simple abasic (AP) sites. In fact, one of the major types of damage generated by ROS is AP site, a site where a DNA base is lost. AP sites are also formed at an appreciable rate from spontaneous depurination. It is estimated that at least 10,000 depurination events occur per cell per day under physiological conditions. A similar amount of AP site is thought to be generated by normal aerobic respiration. In addition to AP site, a wide spectrum of oxidative base modification occurs with ROS (fig 1.12). The C_4-C_5 double bond of pyrimidine is particularly sensitive to attack by OH radical, generating a spectrum of oxidative pyrimidine damage including thymine glycol, uracil glycol, urea residue, 5-OHdU, 5-OHdC, hydantoin and others. Similarly, interaction of OH radical with purines will generate 8-OHdG, 8-OHdA, formamidopyrimidines (fapy-dG, fapy-dA) and other less characterized purine oxidative products. It has been estimated that endogenous ROS can result in about 200,000 base lesions per cell per day [22].

The biological consequences of many of the oxidative products are known. For example, unrepaired thymine glycol is a block to DNA replication and is thus potentially lethal to cells. On the contrary, 8-oxoG, an abundant oxidative damage to dG, is readily bypassed by the DNA polymerase and is highly mutagenic. Unrepaired 8-oxoG will mispair with dA, leading to an increase in G to T transition mutations. Apart from several biological processes leading to oxidative damage to DNA, there are three known chemical sources resulting from photosensitization that can oxidize DNA: **hydrogen atom abstraction** from an intermediate free radical[23], **singlet oxygen** or hydroxyl radical

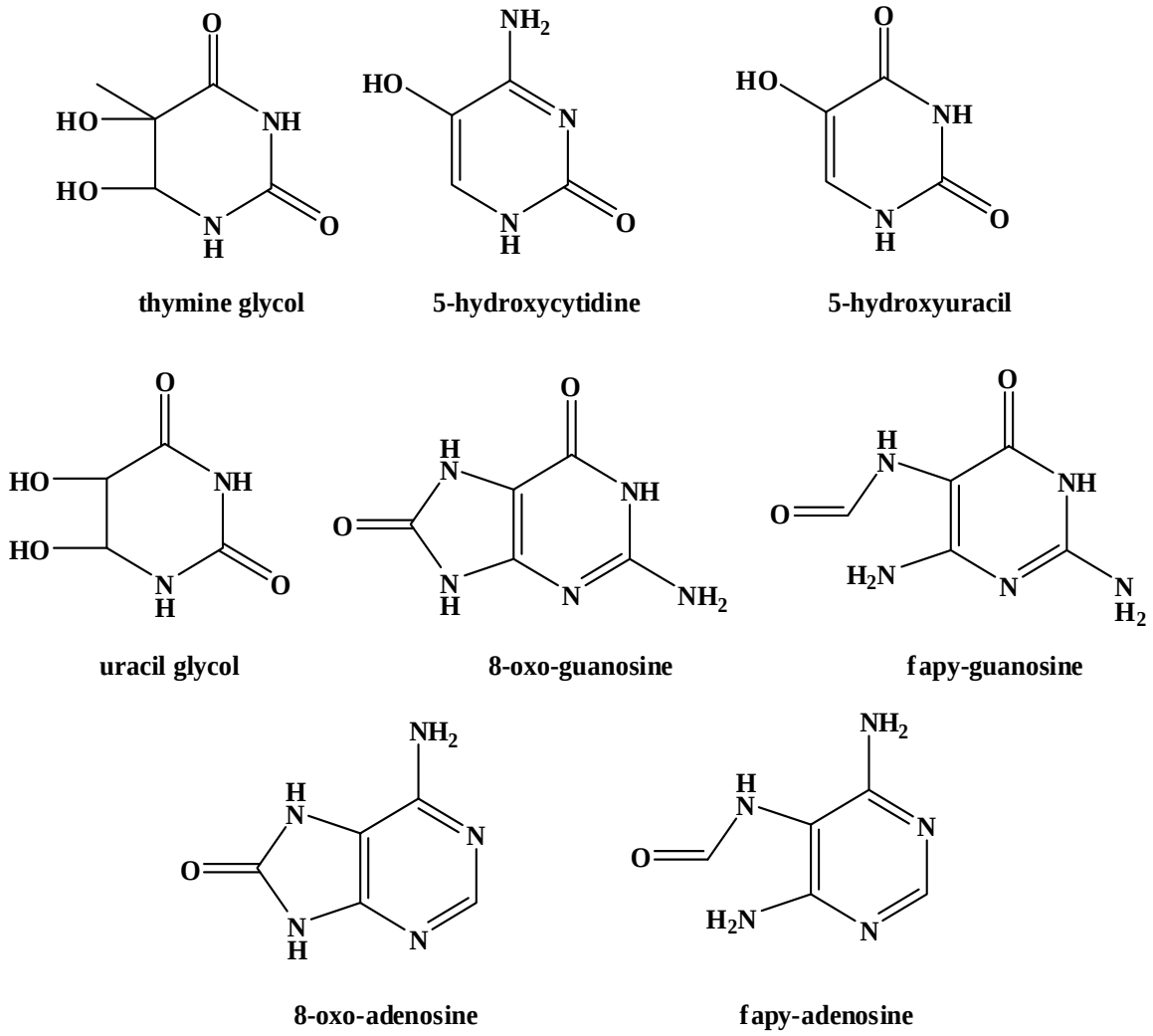

Figure 1.12: Some of the modified bases generated from oxidative DNA damage

generated from an excited photonuclease[24], and **electron transfer** from a nucleobase generating a radical cation[25].

During hydrogen abstraction process, by irradiation of a photosensitizer in the presence of hydrogen donating substrate, hydrogen is transferred from the donating substrate to the excited photosensitizer[26]. This type of reactions results in the formation of radical pair. The deoxyribose sugar moiety of DNA often can act as the hydrogen

donating substrate as it has multiple hydrogen donating sites[14]. After formation of sugar radicals by hydrogen abstraction it can rearrange and eventually leads to strand cleavage of DNA. Some examples of photosensitizers that cleave DNA through hydrogen abstraction are activated bleomycin[27], photoactive rhodium (III) complexes[28] and cationic metal porphyrins [29].

Singlet oxygen is the lowest excited state of molecular oxygen and it is highly reactive[14]. Energy transfer from an excited photosensitizer to ground state molecular oxygen generally leads to the formation of singlet oxygen[30], provided the excited photosensitizer have high enough triplet energy to generate singlet oxygen. It preferentially reacts at the guanine (G) residues in DNA[31]. Porphyrins[32], ruthenium (III) complexes[33], and Vanadium (V) complexes[34] are examples of photosensitizers that have been found to induce oxidative damage through singlet oxygen generation.

During the electron transfer process in DNA, a base donates an electron to an excited photosensitizer producing a radical cation on the base and a radical anion on the photosensitizer. Electron transfer is dependent on the reduction potential, and excited state energy of the photosensitizer, and the oxidation potential of the base[30]. Guanine has the lowest oxidation potential of the four bases[15]. As a result, guanine residues often undergo the most oxidative damage. Some examples of photosensitizers that induce oxidative damage through electron transfer are riboflavin[35] and anthraquinones[25].

1.2.2 Repair of DNA Damage

DNA damage is countered in cells by DNA repair, which is a basic and universal process to protect the genetic integrity of organisms. The genomes of organisms encode

DNA repair enzymes that continuously monitor chromosomes to correct DNA damage. Multiple processes such as base- and nucleotide-excision pathways exist to repair the wide range of DNA damages. If left unrepaired, oxidative DNA damage can lead to detrimental biological consequences in organisms, including cell death, mutations and transformation of cells to malignant cells. Therefore, DNA repair is regarded as one of the essential events in all life forms. There is an increasing awareness of the importance of oxidative DNA damage and its repair to human health. Thus, it becomes exceedingly important to understand, at the fundamental level, the mechanisms of oxidative DNA damage, and its processing by DNA repair enzymes as well as how unrepaired DNA lesions may lead to cytotoxicity, mutagenesis and eventually to diseases and aging. More detailed knowledge of mechanisms of DNA damage and repair might allow us to modulate DNA repair. This could lead to drug developments and clinical applications including the improvement of cancer therapy by inhibiting DNA repair in drug- or radiation-resistant tumors and/or the increase in the resistance of normal cells to DNA damage by over-expressing DNA repair genes.

There are several mechanisms that lead to the DNA damage repair; **Direct chemical reversal** of the damage and **Excision Repair**, in which the damaged base or bases are removed and then replaced with the correct ones in a localized burst of DNA synthesis.

Cells are known to eliminate three types of damage to their DNA by chemically reversing it. These mechanisms do not require a template, since the types of damage they counteract can only occur in one of the four bases. Such direct reversal mechanisms are specific to the type of damage incurred. The formation of thymine dimers (a common

type of cyclobutyl dimer) upon irradiation with UV light results in an abnormal covalent bond between adjacent thymidine bases. The photoreactivation process directly reverses this damage by the action of the enzyme photolyase, whose activation is obligately dependent on energy absorbed from blue/UV light (300-500nm wavelength) to promote catalysis[36]. Another type of damage, methylation of guanine bases, is directly reversed by the protein methyl guanine methyl transferase (MGMT), the bacterial equivalent of which is called as ogt. This is an expensive process because each MGMT molecule can only be used once; that is, the reaction is stoichiometric rather than catalytic[37]. A generalized response to methylating agents in bacteria is known as the adaptive response and confers a level of resistance to alkylating agents upon sustained exposure[38]. The third type of DNA damage reversed by cells is certain methylation of the bases cytosine and adenine.

When only one of the two strands of a double helix has a defect, the other strand can be used as a template to guide the correction of the damaged strand. In order to repair damage to one of the two paired molecules of DNA, there exist a number of excision repair mechanisms that remove the damaged nucleotide and replace it with an undamaged nucleotide complementary to that found in the undamaged DNA strand[37].

1. Base excision repair (BER), which repairs damage due to a single nucleotide caused by oxidation, alkylation, hydrolysis, or deamination;
2. Nucleotide excision repair (NER), which repairs damage affecting longer strands of 2-30 bases. This process recognizes bulky, helix-distorting changes such as thymine dimers as well as single-strand breaks (repaired with enzymes such UvrABC endonuclease). A specialized form of NER known as Transcription-Coupled Repair

(TCR) deploys high-priority NER repair enzymes to genes that are being actively transcribed;

3. Mismatch repair (MMR), which corrects errors of DNA replication and recombination that result in mispaired nucleotides following DNA replication.

1.3 Charge Migration through DNA

As mentioned earlier DNA photosensitization leading to loss of electron from nucleosides affects the integrity of DNA duplex and results in oxidative DNA damage. To protect this type of DNA damage it is very essential to know how the photosenitizers inject the charge into the DNA, how these charges move through the DNA and eventually lead oxidative reaction at different nucleosides. Apart from its biological relevance, this process has been studied extensively also because of its potential application towards manufacture of new molecular electronic devices[39]. It has been reported that desiccated DNA can act as an efficient conductor[40]; on the other hand, some researchers showed contrary experiments implying DNA acts as insulator or semiconductor [41-43].

The electron loss from the nucleobase leads to the formation of radical cation and that moves through the DNA. The exact mechanism of this charge migration has been a subject of debate for long time. To asses the properties that dictate the charge movement through DNA, the main three steps of this process have been examined thoroughly over the years; these are (1) interaction of charge injector and nucleobase to form the nucleobase radical cation (2) migration of the radical cation through DNA and (3) reaction of the radical cation at the nucleobases resulting in DNA damage.

1.3.1 Charge Injection

To understand the charge injection process from the charge injector to the nearest nucleobases, different types of charge injectors have been used. Some of them are covalently linked to end nucleoside of DNA strand; some are intercalated between the base-pairs or bound in the major or minor grooves. Barton and coworkers have used rhodium and ruthenium metallointercalators to introduce a photoexcited hole into a DNA π–stack in order to evaluate oxidative DNA damage[44,45]. The most important charge injectors developed by them bis(phenanthrenequinone diamine)(4,4'-dimethylbipyridine)rhodium(III) and bis(phenanthroline) (dipyrido-phenazine) ruthenium(II) (1 and 2, respectively, in Figure 1.13). These injectors are attached to one of the nucleobases of DNA and believed to intercalate between the π–stack of the nucleobases. However, it has been reported that with such injectors aggregation can take place and that will make the interpretation of the results complicated[46,47].

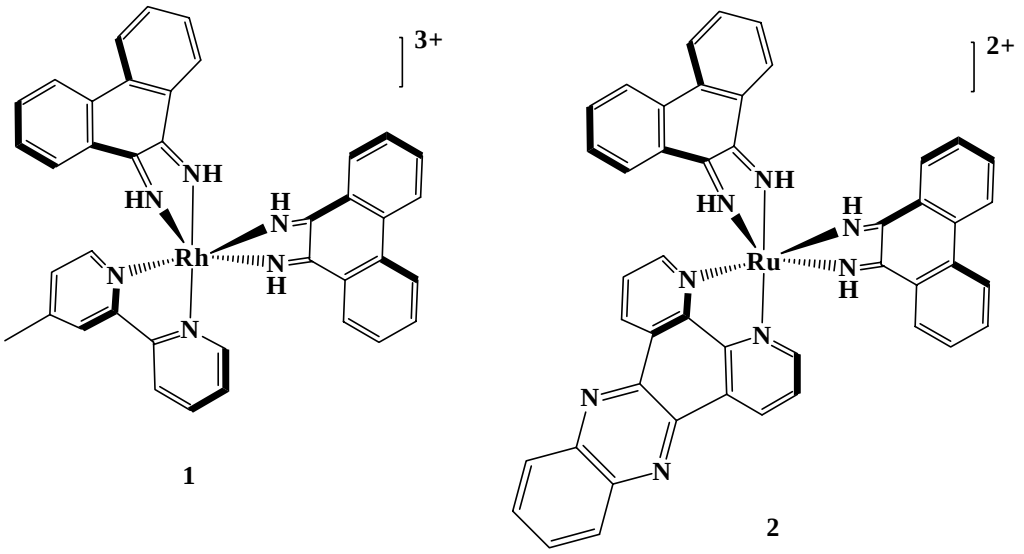

Figure 1.13: Rhodium and ruthenium complexes used as charge injectors

In 1995, Letsinger and Wu reported the formation of exceptionally stable synthetic DNA hairpins possessing a stilbene-4,4'-dicarboxamide (Sa) linker (Figure 1.14) connecting complementary oligonucleotides[48] and later was used by Lewis and Wu as photosensitizer for charge injection[49,50]. But, this system is efficient for short range charge migration only. Similarly, trioxatriangulenium ion (Figure 1.14) is an intercalator with a preferential binding site of G/C base pairs that has been shown to be a relatively inefficient sensitizer[51].

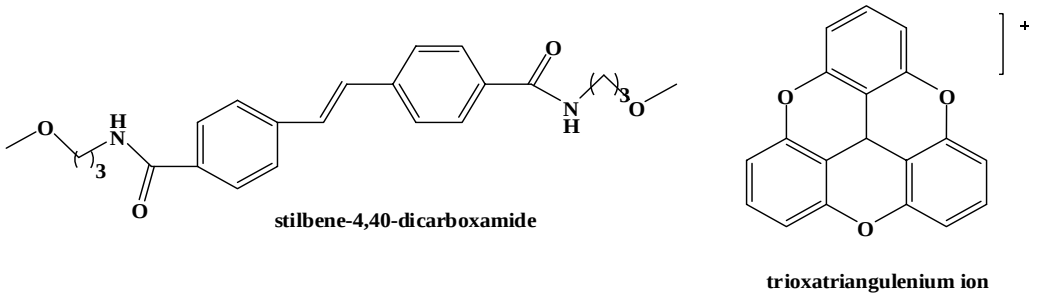

Figure 1.14: Stilbene derivative and trioxatriangulenium ion charge injectors

Bernd Giese and coworkers used the higher oxidation potential of the enol ether radical cation compared to the guanine radical cation to inject radical cation into DNA (Figure 1.15). The generation of an enol ether radical cation 5, which can be used for hole transfer experiments in DNA, starts from the modified nucleotide 3, whose photolysis forms the nucleotide radical 4. In double and single stranded oligomers radical 5 leads radical cation 6 in high yields as long as radical traps like O_2 are absent[52-54].

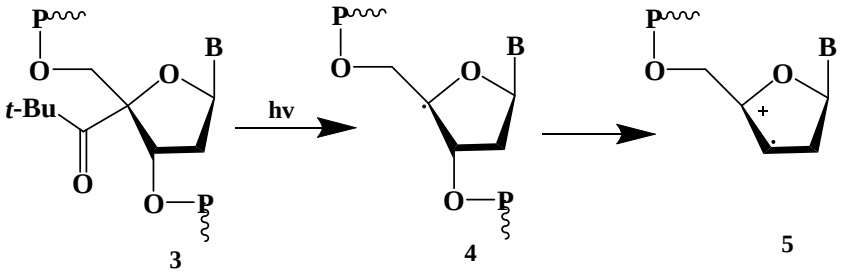

Figure 1.15: Generation of radical cation by photolysis of modified nucleotide

Apart from these, modified nucleosides such as p-cyanobenzophenon [55,56] and pyrene (Py)[57] containing uridine have been used charge injectors. We have focused our attention on charge injection by anthraquinone derivatives.

Anthraquinones are nearly perfect charge injectors for the one-electron oxidation of DNA. They absorb light in the near-UV spectral region around 350 nm where DNA is essentially transparent. This allows excitation of the anthraquinone without the any light absorption by DNA, which would complicate chemical and mechanistic analyses. Initially, a singlet excited state is generated by absorption of a photon by an anthraquinone molecule; however, through rapid intersystem crossing, within a few picoseconds of excitation a triplet state of the anthraquinone is normally formed, (Fig 1.16)[23]. Application of the Weller equation[58] indicates that both the singlet and the triplet

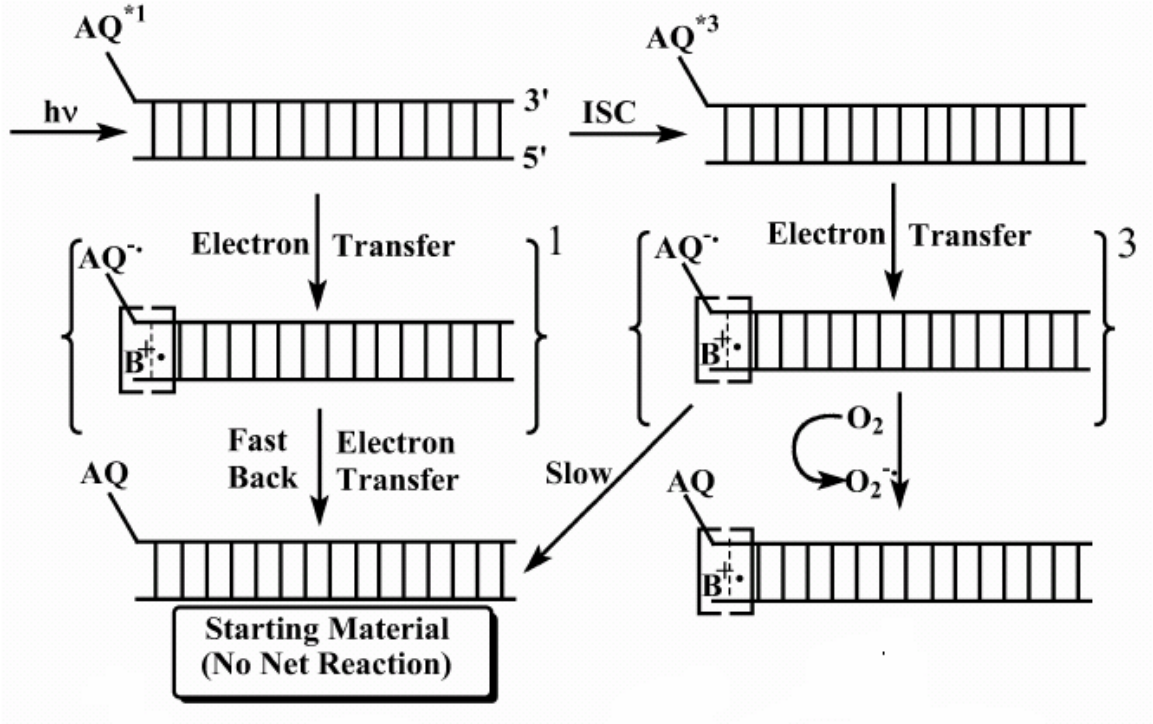

Figure 1.16[59]: Charge injection by Anthraquinone

excited states of anthraquinones are capable of the exothermic one-electron oxidation of any of the four DNA bases to form the anthraquinone radical anion ($AQ^{-\cdot}$) and a base radical cation ($B^{+\cdot}$). The Anthraquinone radical anion reacts with oxygen and forms anthraquinone again. This way a radical cation is inserted into nucleobases of DNA and no radical anion is formed. Anthraquinone is linked to the DNA by carboxamide linker. The electronic configuration of the reacting excited state is dependent on the direction of the carboxamide linker attached to the anthraquinone chromophore. It has been shown that the desired linker should have the chromophore linked to the carbonyl followed by the amine group as this orientation gives the lowest excited state for charge-transfer character[25]. This charge injector can be tethered to the DNA via standard phosphoramidite chemistry as shown in Figure 1.17. This anthraquinone moiety (AQ)[60] can be attached to the 5'-terminus of a DNA single-strand or it can be also attached to 3'-oxygen of uridine nucleoside (UAQ)[61] at anywhere within the DNA (Figure 1.18). It has been indicated by molecular modeling, chemical quenching studies, and spectroscopic analyses that the end-linked AQ derivative is associated with the DNA by end-capping of the final base pair, as shown in Figure1.19. End-capping allows the relatively efficient oxidation of the DNA by the anthraquinone at a known initial site and it does not disrupt the base stacking that result from intercalated charge injectors. It has been shown that when the AQ is end-capped, efficiency of charge injection depends on the sequence of bases near the AQ. Maximum efficiency is observed when there is no G/C base pair within the three base pairs closest to the AQ[62]. The anthraquinone group of the UAQ sensitizer is intercalated on the 3'-side of its linkage site[63]. Use of UAQ permits assessment of the directionality of long-range radical cation migration.

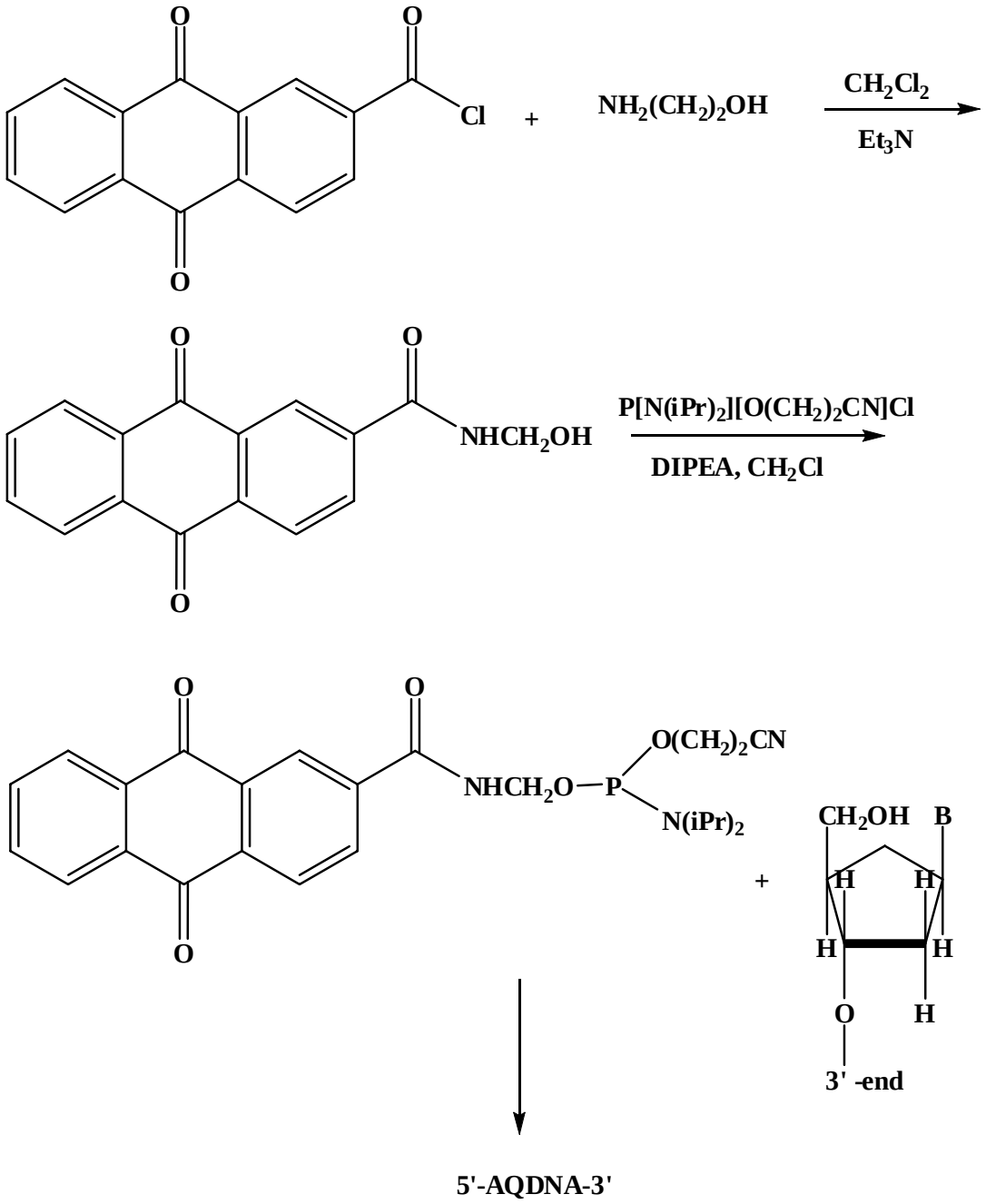

Figure 1.17: Synthetic scheme for attachment of AQ with DNA

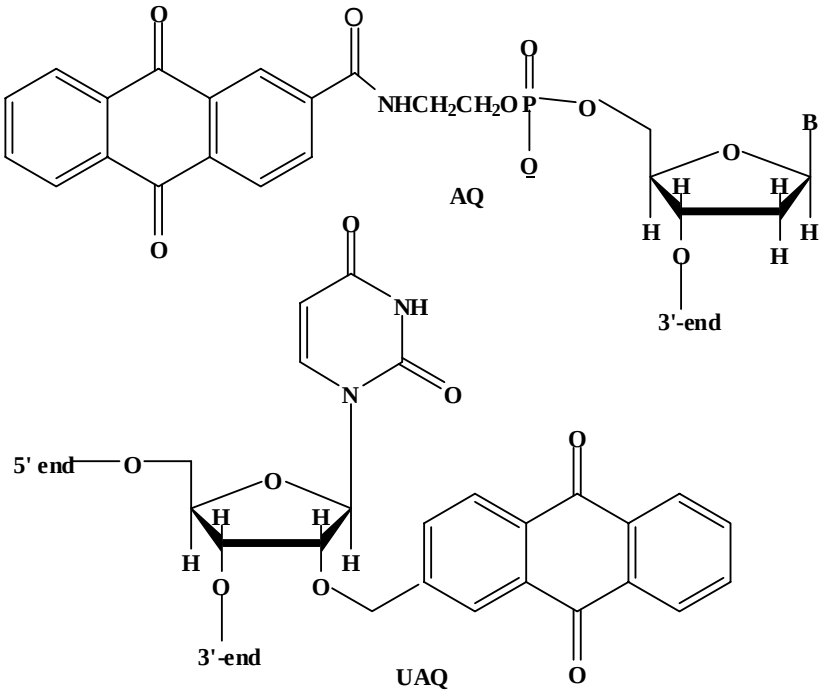

Figure 1.18: AQ and UAQ attached to DNA

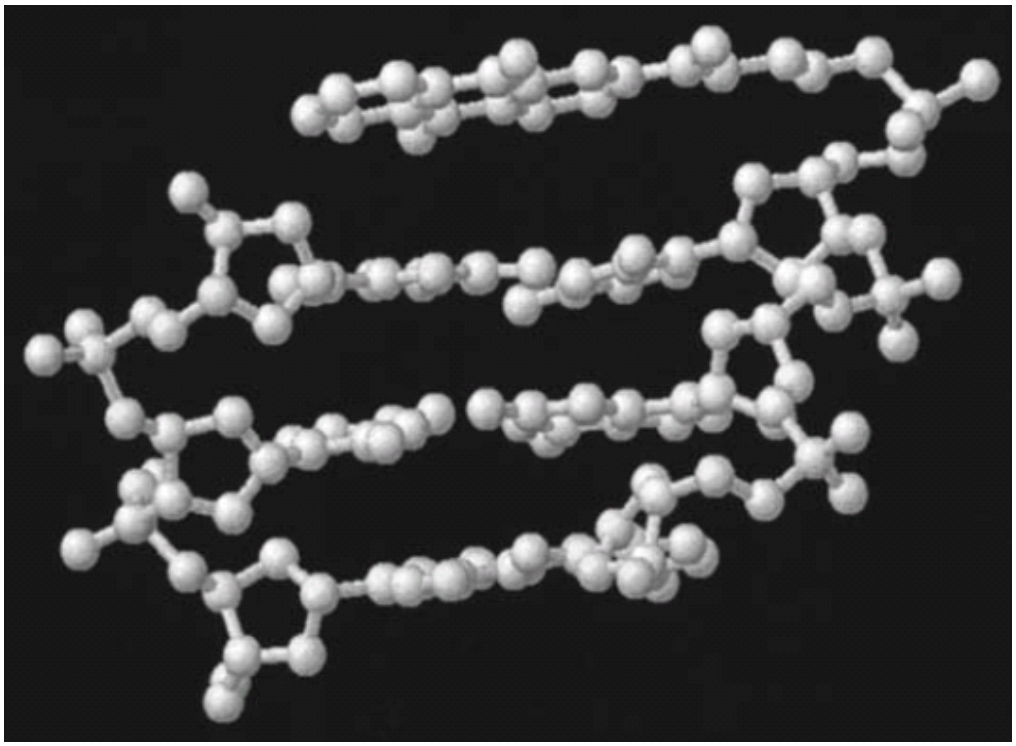

Figure 1.19[64]: Molecular modeling showing AQ end-capping the DNA duplex

1.3.2 Charge Migration

Migration of a radical cation through the DNA results in one-electron oxidation at the nucleobases, especially at guanines(G) and oxidative damage to guanine yields a piperidine labile product. Treatment with hot piperidine yields strand scission at the damaged site of DNA, providing a basis for studying the mechanism of charge migration through DNA. While charge transport through DNA is well accepted experimentally, the mechanism of charge migration through DNA proceeds is still not fully established.

A very fast electron transport from a donor to an acceptor mediated by the π-stacking of the DNA base pairs has been indicated by the initial studies, which was referred to as a "π-way"[65]. This fast electron transfer was attributed to a coherent, rapid, single-step charge transfer from the donor to the acceptor. Subsequent investigations have resulted in contradicting reports that include several possible mechanisms for charge migration. Those include mechanisms involving superexchange and tunneling[66,68-72], as well as different hopping mechanisms[67,73]. Two limiting mechanisms of charge transport in DNA may be considered. In the first, DNA behaves like a wire having a continuous, delocalized molecular orbital. In this orbital, each base pair is in electronic contact with every other, and charge transport occurs by superexchange[74]. The second model is discrete hopping, which presumes that the radical cation is localized on one base and has no significant electronic overlap with adjacent bases. The localized radical cation migrates (hops) by a thermally activated process to adjacent bases[64]. Giese and Jortner and coworkers have advanced arguments that superexchange and multistep charge transport will operate in separate energetic systems. They observed a very efficient charge transfer even when the charge donor ($G^{+\cdot}$) and the accepters (GGG) are separated

by 15 base pairs[75]. This DNA strand contains 8 G's between the first $G^{+\cdot}$ and the GGG unit. It has been assumed that these intervening G's can be oxidized by the donor; thus, they act as relay stations for the charge on the way to the GGG unit (Figure 1.20). As a result, the charge transport from the first $G^{+\cdot}$ to the GGG occurs through a multistep reaction rather than a single step one. Such situation can be correlated by the following equation[76],

$$\ln E \, \alpha \, -\ln N$$

where a charge migrates by a random walk through DNA. *E* is the efficiency of the charge transport expressed as the ratio between the trapped GGG sequence and the single G's and the number of the equidistant hopping steps is *N*. This correlation has been proved in experiments with four different double strands, where the number (*N*) of the electron-transfer steps, each of them over a distance of 10 Å, increased from 1 to 4[77].

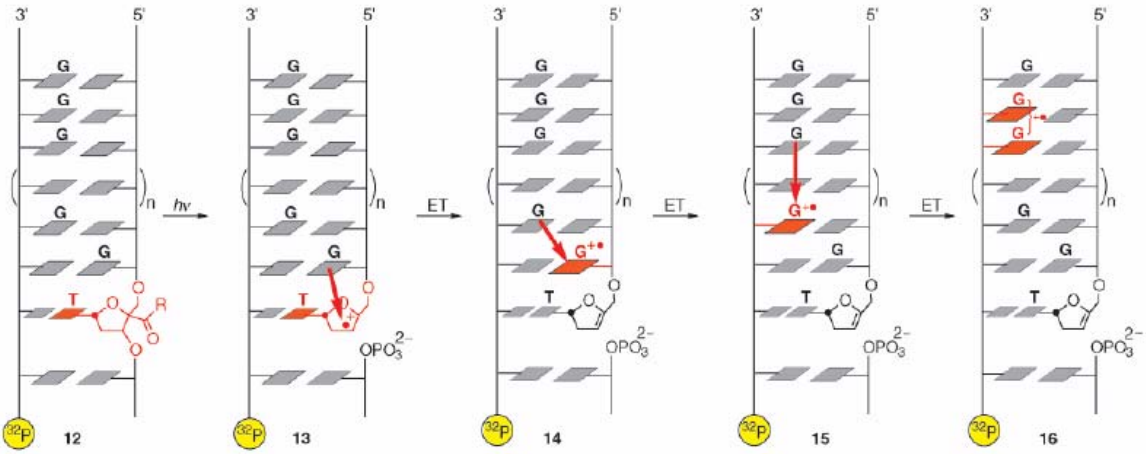

Figure 1.20[69]: Charge injection into a single G (12 to 14), charge transport to the complementary, strand (14 to 15), and charge transport from a single $G^{+\cdot}$ to a GGG sequence (15 to 16)

When the distance between donor and acceptor is short, the electron tunnels in a single-step reaction between the guanines, and the A/T base pairs do not act as charge carriers. On the other hand, if the distance is long, then the G·+ oxidizes the adjacent adenine and it very rapidly travels to the next G (Figure 1.21). Kinetic analysis conducted by Jortner and Bixon et al.,[71] supported the hopping model where the hopping process was treated as a sequential reaction which is characterized by the rates of the electron-transfer steps and the trapping steps. However, this theory does not offer any explanations on how the thermal motions of non-static DNA molecule influence the charge migration.

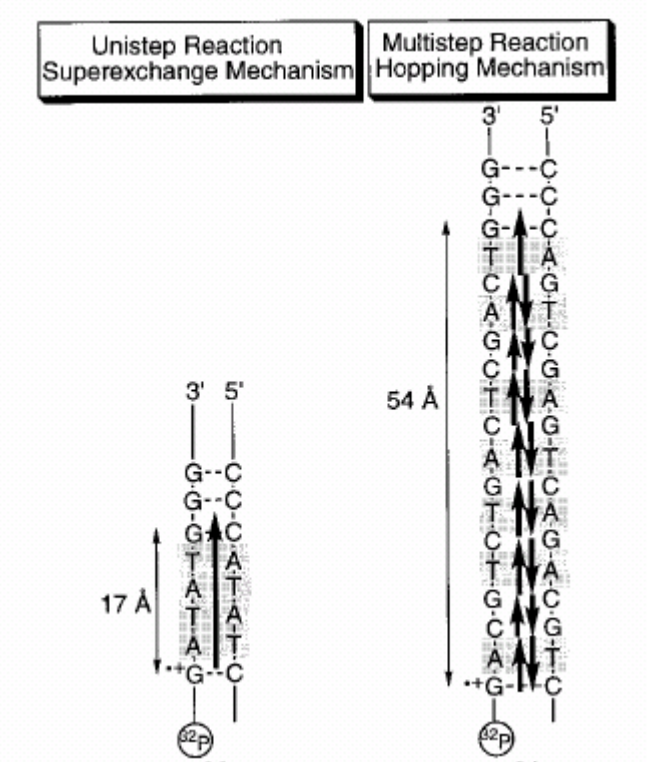

Figure 1.21[74]: Charge transfer in a unistep and a multistep reaction over 17 and 54 Å

In contrast to theories that involve superexchange, there are two theories involving the delocalization of the radical cation over several bases centered on guanine

and the charge transfer from one site to the other is postulated to be hopping initiated by thermal motions of the DNA and its environment. The first one of these is described as conformationally gated hopping through stacked domains[73,78]. This theory is presented in Figure 1.22. According to this theory, on the timescale of electron transfer, assemblies of a heterogeneous distribution of base conformations make the DNA solution. In some of these assemblies, the donor, the acceptor, and the DNA bridge (if present), are in such

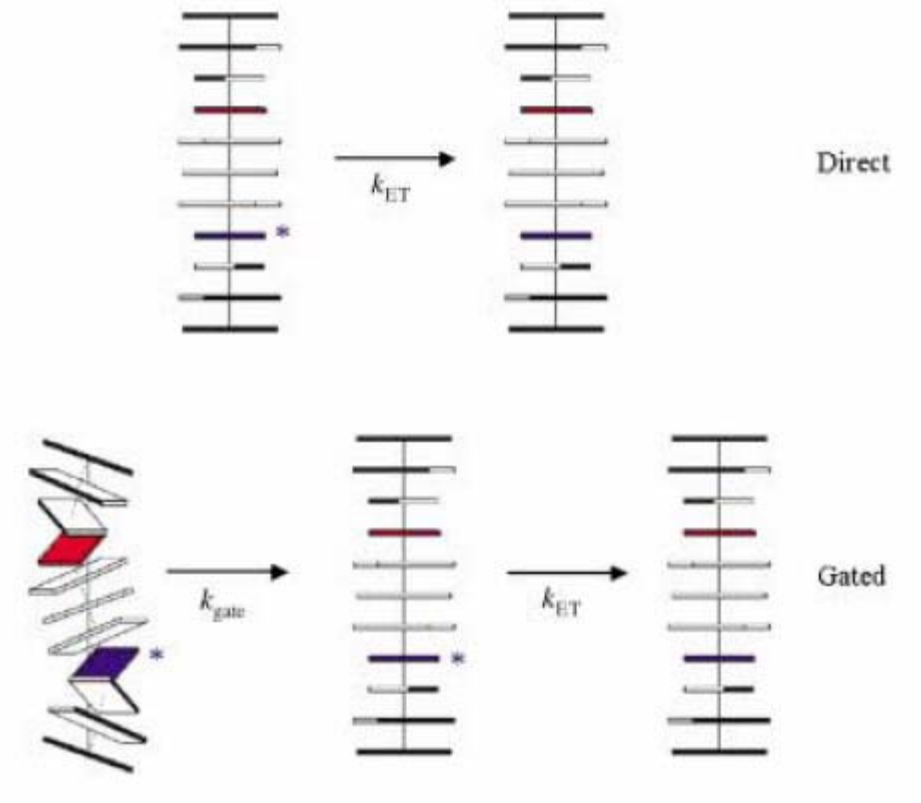

Figure 1.22[78]: Schematic representation of conformationally gated hopping theory

conformations that immediate electron transfer (ET) is facilitated upon excitation. This has been termed as direct ET. Other DNA assemblies do not adopt this type of conformations at the time of excitation, but can undergo significant base motions, and

that might lead to conformational reorganization, during the lifetime of the excited state of the 2-aminopurine charge injector (Ap*). Some of these assemblies may not assume ET-active conformations and, in that case, Ap* decays through non-ET pathways. On the other hand, some DNA assemblies do adopt ET-active conformations within the lifetime of Ap*; in those assemblies Ap* decays through ET that is gated by initial reorganizational motion. DNA dynamics have the most profound impact on ET for this population of assemblies. Bruinsma and coworkers reported a theoretical study that is consistent with this model[79].

The second theory involves delocalization of the radical cation, and then a hopping mechanism where the charge does reside on the barrier or "bridge", while migrating from one guanine to the other. This theory is termed phonon assisted polaron hopping[64,80,81]. According to this theory, injection of charge into DNA will cause its dynamic structure to change. As the base radical cations are electron deficient, DNA will rapidly distort its local structure to relieve this deficiency. The radical cation will be stabilized by its delocalization onto adjacent bases. Rapid distortion may result in a change in the normal inclination angle of neighboring bases, which will bring them closer to the radical cation, thus delocalizing and stabilizing it. Also, the radical cations may be delocalized by unwinding of the DNA which may increase the π-electron overlap with neighboring bases. The acidity of the partially charged bases of a delocalized radical cation will be more acidic than their uncharged forms as the normal base radical cations are more acidic than the unchanged forms[82]. This might lead to shifts of proton in the hydrogen bonds forming the base pairs and that is another likely structural distortion caused by radical cation injection. A polaron is defined as a radical ion self-trapped by

structural distortion of its containing medium[83]. The base radical cation, which is surrounded by the distorted section of duplex DNA, may be considered a polaron-like species (Figure 1.23). It is not strictly a polaron because the detailed properties of the distortion will depend on base sequence. The polaron is not extended through the whole length of DNA. It can extend to that point where the energy required to distort the DNA will just balance the stabilization.

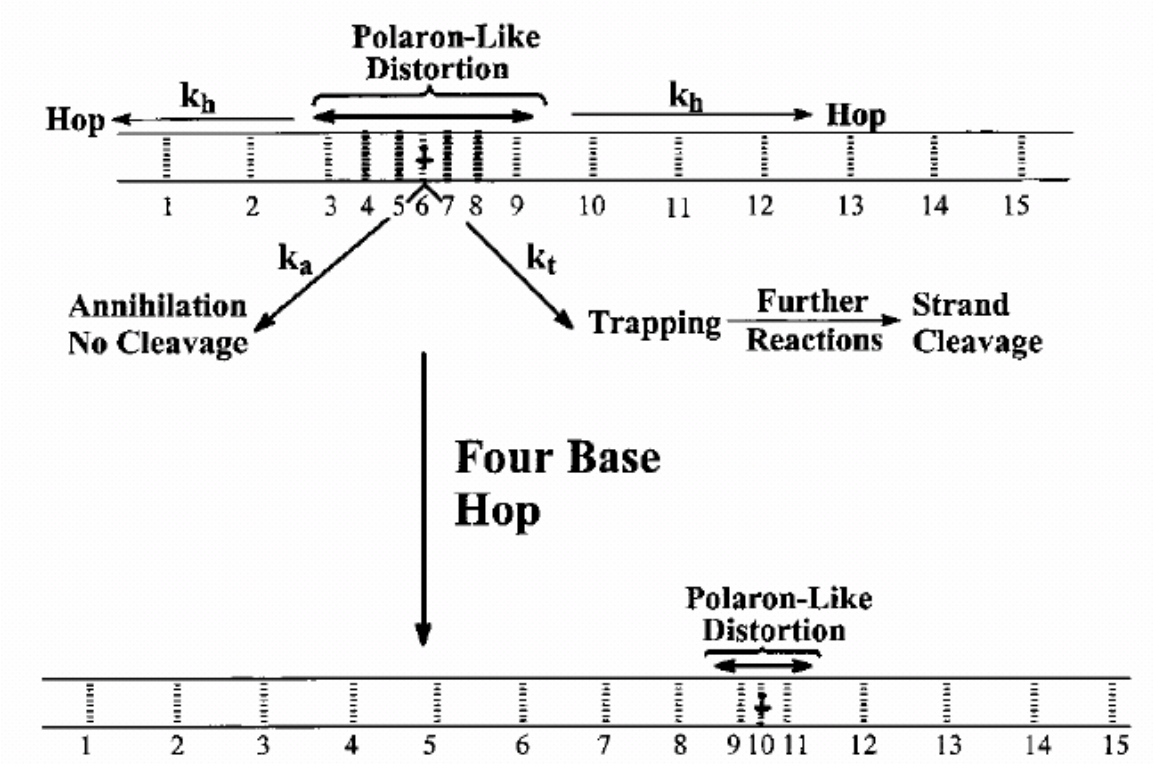

Figure 1.23[64]: Schematic representation of phonon assisted radical cation hopping. The vertical lines represent the base pairs and the horizontal lines stand for the sugar-phosphate backbone. The upper structure shows a 15-mer containing a radical cation delocalized as a polaron distortion over seven base pairs (3-9). The polaron may be consumed by annihilation (k_a), by reaction leading to strand cleavage (k_t), or by (phonon assisted) hopping (k_h). four-base hop is depicted in the Figure, with the lower structure showing a polaron delocalized over three base pairs (9-11) of the 15-mer.

The polaron hopping model differs from the superexchange model in the location of the radical cation when it is transferred from one guanine to the nearest low energy site across the bridge. The superexchange model describes a tunneling phenomenon where

the charge only virtually exists in the orbitals of the bridge bases. On the other hand, the polaron hopping model suggests that the radical cation exist as a detectable entity during migration through the bridge. Dohno and coworkers have studied the charge transfer using 2'-deoxy- N6-cyclopropyl-adenosine located between the charge injection site and a distal guanine site[83]. They were able to detect reactions between the radical cation and the cyclopropyl moiety of the modified adenosine, indicating the charge indeed resides on the bridge and this experiment support the polaron hopping. Further kinetic studies on charge migration support the phonon-assisted polaron hopping mechanism[67,84,85].

1.3.3 Charge Trapping

The most important outcome of the radical cation migration through DNA strands is chemical reactions at some of the nucleobases. From biological point of view, these reactions may lead to mutations and eventually can result in DNA damage. So, it is very important to Figure out the products and the mechanisms involved in these reactions. On the other hand, these reactions are used to actually monitor the charge transfer process. As mentioned earlier, during the hopping through the DNA radical resides at G_n (n=1-3) because of G has the lowest oxidation potential among the nuclobases[86,87] and forms guanine radical cation. The radical cation then can react with H_2O and/or O_2 to form 8-oxoguanine (8-oxodG) and other products[15] (Figure 1.24). This process is known as charge trapping. The overall rate of charge migration depends on two factors: Rate of hopping (k_{hop}) and rate of trapping (k_{trap}). Ratio of these two factors is termed as k_{ratio} and it is indicator of the overall rate of charge transfer. When the rate of hopping is much greater than rate of trapping (high k_{ratio}) the charge migration is very little affected by

trapping reactions and all the G_n steps have almost equivalent amount of damage. However, if the rate of hopping is not much higher than rate of trapping, the trapping reactions do affect the charge migration and the damage decreases as the distance from AQ charge injector increases. And, if the rate of hopping is equal to rate of trapping (k_{ratio}=1), only the guanines near the AQ are damaged. Liu et al showed that k_{ratio} is highly dependent on the nature and number of bases between the G_n steps[67]. For example, hopping is much faster than trapping in an oligomer composed of (AAGG) repeats, and the amount of reaction at each GG step is essentially the same, but trapping is faster than hopping for DNA composed of (ATTAGG) repeats, and in this case, GG steps react with much greater efficiency if they are closer to the site of one-electron oxidation adjacent to the AQ. However, the real picture is not so simple when DNA sequences are examined which do not have so regular sequences. In that case the reactivity of a nucleobases must be understood considering all other nucleobases present in the system. The complex relationship between reactivity and sequence can be simplified by consideration of relative potential energy "landscapes" as shown in Figure 1.25[88]. Although, the reaction at guanines is well studied and understood, there is no report of systematic study of charge migration and reaction in A-T rich sequences or sequences that do not have any guanine.

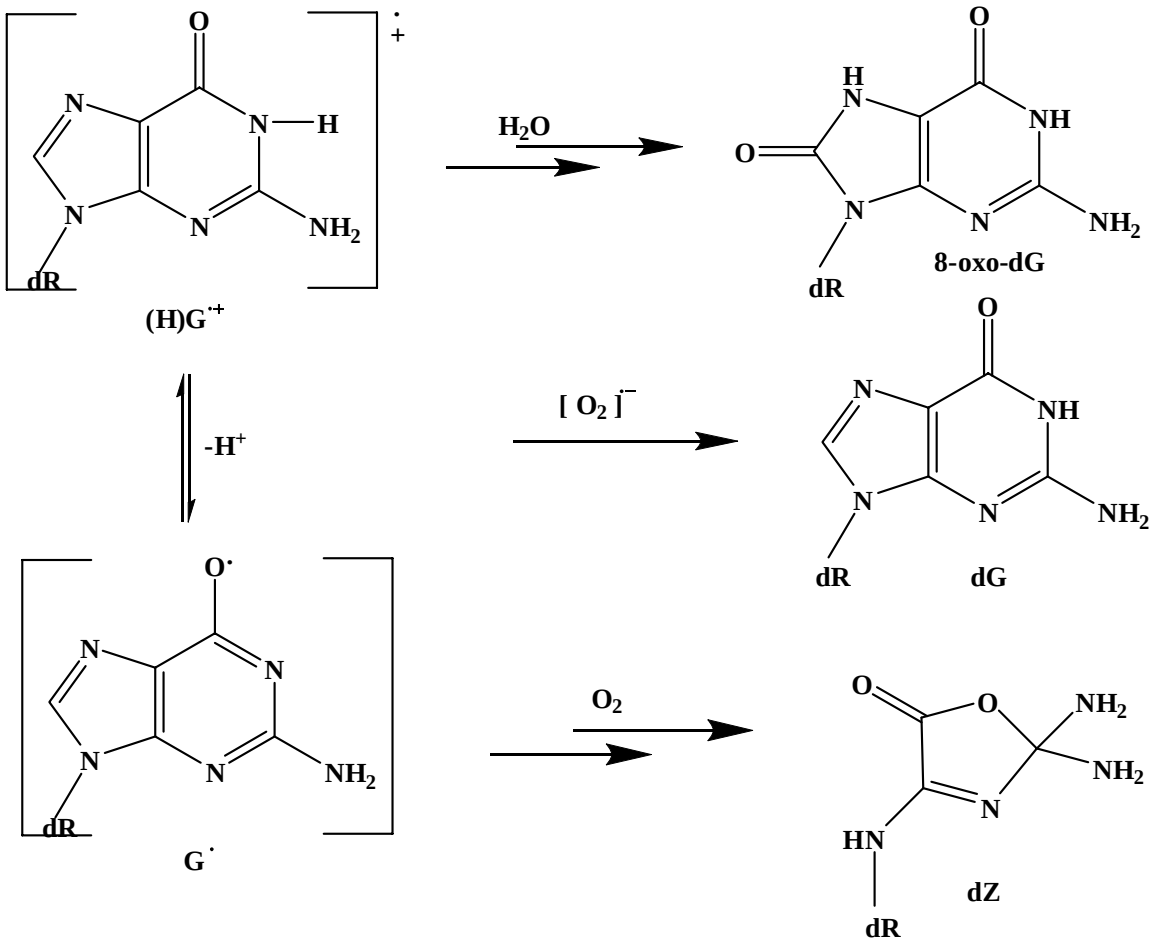

Figure 1.24: Reaction of guanine radical cation with water and oxygen

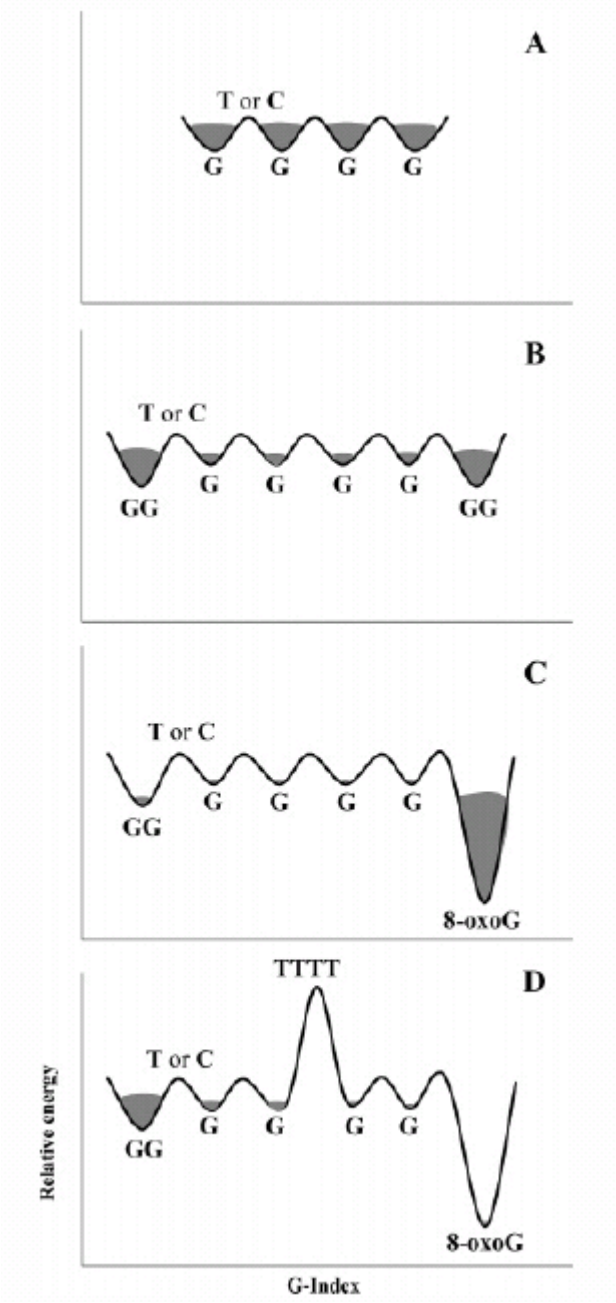

Figure 1.25: schematic representation of the potential energy landscapes for DNA oligomers. A "G" represents an "isolated" guanine in a TGT or CGC sequence. A "GG" represents two adjacent guanines in a GG step. The "T" or "C" represents thymine or cytosine nucleobases that separate G or GG steps from one and other. And "TTTT" represents four thymines. The shading represents the relative amount of strand cleavage observed at each site after irradiation of a piperidine treatment. The *X*-axis (G-index) is not drawn to scale and represents the position of guanines, GG steps, and 8-oxoG along the DNA oligomer; the intervening barriers may be one base pair or several.

REFERENCES

1. Voet, D.; Voet, J.G.; Pratt, C. W. *Fundamentals of Biochemistry* **2002**, Upgraded Ed., John Wiley & Sons, Inc.
2. Avery, O. T.; MacLeod, C. M.; McCarty, M. *The Journal of Experimental Medicine* **1944**, 79, 137-158.
3. Watson, J. D.; Crick, F. H. C., *Nature* **1953**, 171, 737-738.
4. Sinden, R. R. *DNA Structure and Function* **1994**, Academic Press
5. Campbell, M. K. *Biochemistry* **1995,** 2nd Ed., Saunders College Publishers
6. Bresler, S. E. *Introduction to Molecular Biology* **1971**, Academic Press.
7. Franklin, R. E.; Goslin, R. G. *Nature* **1953**, 172, 156.
8. Franklin, R. Elsie.; Goslin, R. G., *Acta Crystallography* **1953**, 6, 673.
9. Stewart, R.F.; Jensen, L. H., *J. Chem. Phys*. **1964**, 40, 2071
10. Drew, H. R.; Dickerson, R. E. *Journal of Molecular Biology* **1981**, 151, (3), 535.
11. Dickerson, R. E.; Drew, H. R.; Conner, B. N.; Wing, R. M.; Fratini, A. V.; Kopka, M. L. *Science* **1982**, 216, (4545), 475.
12. Berg, J. M.; Tymoczko, J.L.; Stryer, L. *Biochemistry* **2002**, 5th addition, W. H. Freeman and Company, New york.
13. Drew, H.; Takano, T.; Tanaka, S.; Itakura, K. & Dickerson, R. E. *Nature* **1980**, 286, 567
14. Armitage, B. *Chem. Rev.* **1998**, 98, (3), 1171-1200.
15. Burrows, C. J.; Muller, J. G. *Chem. Rev.* **1998**, 98, (3), 1109-1152.
16. Sancar, A. *Annual Review of Biochemistry* **1996**, 65, (1), 43-81.
17. Kow, Y. W. *Annals of the New York Academy of Sciences* **1994**, 726, 178-180.

18. Kanvah, S.; Schuster, G. B. *J. Am. Chem. Soc.* **2004**, 126, (23), 7341-7344.

19. Demple, B.; Harrison, L. *Annual Review of Biochemistry* **1994**, 63, 915-948.

20. Poulsen, H. E.; Prieme, H.; Loft, S. *European Journal of Cancer Prevention* **1998**, 7, (1), 9-16

21. P. Hasty; J. Vijg *Science* **2002**, 296, 1250-1251.

22. Liu, P. K.; Hsu, C. Y.; Dizdaroglu, M.; Floyd, R. A.; Kow, Y. W.; Karakaya, A.; Rabow L. E.; Cui, J. K. *The Journal of Neuroscience* **1996**, 16(21):6795–6806

23. Armitage, B.; Yu, C.; Devadoss, C.; Schuster, G. B. *J. Am. Chem. Soc.* **1994**, 116, (22), 9847-9859.

24. Macgregor, R. B. *Analytical Biochemistry* **1992**, 204, (2), 324-327.

25. Breslin, D. T.; Schuster, G. B. *J. Am. Chem. Soc.* **1996**, 118, (10), 2311-2319.

26. Turro, N. J. *Modern Molecular Photochemistry* **1978**, Benjamin/Cummings Publication Co., Inc.,California,

27. Burger, R. M. *Chem. Rev*. **1998**, 98, 1153-1170

28. Chow, C. S.; Barton, J. K. *Methods Enzymol.* **1992**, 212, 219-242

29. Pratviel, G.; Pitie, M.; Bernadou, J.; Meunier, B.; *Angew. Chem. Int. Ed. Engl.* **1991**, 30, 702-704

30. Kochevar, I.; Dunn, D. A. *Biorg. Photochem.* **1990**, 1, 273-315

31. Lee, C. C.; Rodgers, M. A. *Photochem. Photobiol.* **1987**, 45, 79-86

32. Croke, D. T.; Perrouault, L.; Sari, M. A.; Battioni, J. P.; Mansuy, D.; Helene, C.; Le Doan, T.; *J. Photochem. Photobiol.B* **1993**, 18, 41-50

33. Mei, H.; Barton, J. K.; *Proc. Natl. Acad. Sci. U.S.A.* **1988**, 85, 1339-1343

34. Hiort, C.; Goodisman, J.; Dabriowiak, J. C. *Biochemistry* **1996**, 35, 12354-12362

35. Ito, K.; Inoue, S.; Yamamoto, K.; Kawanishi, S. *J. Biol. Chem.* **1993**, 268, 13221-13227

36. Sancar, A. *Chem Rev* **2003**, 103(6):2203-37.

37. Watson, J.D.; Baker, T.A.; Bell, S.P.; Gann, A.; Levine, M.; Losick, R.; *Molecular Biology of the Gene* **2004** Peason Benjamin Cummings; CSHL Press. 5th ed.

38. Volkert. M. R, *Environ Mol Mutagen* **1988** 11(2):241-55.

39. Di Ventra, M.; Zwolak, M. *DNA Electronics*: **2000** Nalwa, H. S., Ed.; American Scientific Publishers: Stevenson Ranch, CA

40. Fink, H. W.; Schonenberger, C. *Nature* **1999**, 398, 407-410

41. Porath, D.; Bezryadin, A.: De Vries, S.; Dekker, C. *Nature* **2000**, 403, 635-638

42. Cai, L. T.; Tabata, H.; Kawai, T. *Appl. Phys. Lett.* **2000**, 77, 3105-3106

43. Storm, A. J.; van Noort, J.; de Vries, SS.; Dekker, C. *Appl. Phys. Lett.* **2001**, 79, 3881-3883

44. Hall, Daniel B.; Holmlin, R. Erik; Barton, Jacqueline K. *Nature* **1996**, 382, (6593), 731-735.

45. Murphy, C. J.; Arkin, M. R.; Ghatlia, N. D.; Bossmann, S.; Turro, N. J.; Barton, J. K. *Proc. Natl. Acad. Sci. U.S.A.* **1994**, 91, (12), 5315-5319.

46. Fahlman, R. P.; Sharma, R. D.; Sen, D. *J. Am. Chem. Soc.* **2002**, 124, (42), 12477-12485.

47. Olson, E. J. C.; Hu, D.; Hormann, A.; Barbara, P. F. *J. Phys. Chem. B* **1997**, 101, (3), 299-303.

48. Letsinger, R. L.; Wu, T. *J. Am. Chem. Soc.* **1995**, 117, 7323-7329

49. Lewis, F. D.; Liu, X.; Wu, Y.; Miller, S. E.; Wasielewski, M. R.; Letsinger, R. L.; Sanishvili, R.; Joachimiak, A.; Tereshko, V.; Egli, M. *J. Am. Chem. Soc.* **1999**, 121, 9905-9912

50. Lewis, F. D.; Letsinger, R. L.; Wasielewski, M. R. *Acc. Chem. Res.* **2001**, 34, (2), 159-170.

51. Krebs, F. C.; Laursen, B. W.; Johannsen, I.; Faldt, A.; Bechgaard, K.; Jacobsen, C. S.; Thorup, N.; Boubekeur, K. *Acta Crystallographica Section B* **1999**, 55, (3), 410-423.

52. Marx, A.; Erdmann, P.; Senn, M.; Korner, S.; Jungo, T.; Petretta, M.; Imwinkelried, P.; Dussy, A.; Kulicke, K. J.; Macko, L.; Zehnder, M.; Giese, B. *Helv Chim Acta* **1996**, 79, 1980-1984

53. Giese, B.; Dussy, A.; Meggers, E.; Petretta, M.; Schwitter, U. *J. Am. Chem. Soc.* **1997**, 119, 11130-11135

54. Meggers, E.; Dussy, A.; Schofer, T.; Giese, B. *Chem Eur J.* **2000**, 6, 485-489

55. Nakatani, K.; Dohno, C.; Saito, I. *J. Am. Chem. Soc.* **1999**, 121, 10854–10855

56. Nakatani, K.; Dohno, C.; Saito, I. *J. Am. Chem. Soc.* **2002,** 124, 6802–6803

57. Kawai, K.; Takada, T.; Tojo, S.; Ichinose, N.; Majima, T. *J. Am. Chem. Soc.* **2001**, 123, 12688-12693

58. Rehm, D.; Weller, A. *Israel J Chem* **1970**, 8, 259-264

59. Schuster, G. B. *Longe-Range Charge Transfer in DNA I*, Springer Berlin, **2004**.

60. Gasper, S. M.; Schuster, G. B. *J. Am. Chem. Soc.* **1997**, 119, 12762-12766

61. Ly, D.; Sanii, L.; Schuster, G. B. *J. Am. Chem. Soc.* **1999**, 121, 9400-9404

62. Sanii, L.; Schuster, G. B. *J. Am. Chem. Soc.* **2000**, 122, 11545-11549

63. Deshmukh, H.; Joglekar, S. P.; Broom, A. D *Bioconjugate Chem* **1995**, 6, 578-581

64. Schuster, G. B. *Acc. Chem. Res.* **2000**, 33, (4), 253-260.

65. Murphy, C. J.; Arkin, M. R.; Jenkins, Y.; Ghatlia, N. D.; Bossmann, S. H.; Turro, N. J.; Barton, J. K. *Science* **1993**, 262, (5136), 1025-1029.

66. Lewis, F. D.; Liu, J.; Weigel, W.; Rettig, W.; Kurnikov, I. V.; Beratan, D. N. *Proc. Natl. Acad. Sci. U.S.A.* **2002**, 99, (20), 12536-12541.

67. Liu, C. S.; Hernandez, R.; Schuster, G. B. *J. Am. Chem. Soc.* **2004**, 126, (9), 2877-2884.

68. Shao, F.; Augustyn, K.; Barton, J. K. *J. Am. Chem. Soc.* **2005**, 127, (49), 17445-17452.

69. Giese, B. *Acc. Chem. Res.* **2000**, 33, (9), 631-636.

70. Armitage, N. P.; Briman, M.; Grüner, G. *physica status solidi (b)* **2004**, 241, (1), 69-75.

71. Bixon, M.; Giese, B.; Wessely, S.; Langenbacher, T.; Michel-Beyerle, M. E.; Jortner, J. *Proc. Natl. Acad. Sci. U.S.A.* **1999**, 96, (21), 11713-11716.

72. Berlin, Y. A.; Burin, A. L.; Ratner, M. A. *Chemical Physics* **2002**, 275, (1-3), 61-74.

73. O'Neill, M. A.; Barton, J. K. *J. Am. Chem. Soc.* **2004**, 126, (37), 11471-11483

74. Turro, N. J.; Barton, J. K. *J. Biol. Inorg. Chem.* **1998**, 3, 201-209.

75. Meggers, E.; Michel-Beyerle, M. E.; Giese, B. *J. Am. Chem. Soc.* **1998**, 120, 12950-12955.

76. Jortner, J.; Bixon, M.; Langenbacher, T.; Michel-Beyerle, M. E. *Proc. Natl. Acad. Sci. U.S.A.* **1998**, 95, 12759-12765.

77. Giese, B.; Wessely, S.; Spormann, M.; Lindemann, U.; Meggers, E.; Michel-Beyerle, M. E. *Angew. Chem., Int. Ed.* **1999**, 38, 996-998.

78. O'Neill, M. A.; Becker, H.; Wan, C.; Barton, J. K.; Zewail, A. H. *Angewandte Chemie International Edition* **2003**, 42, (47), 5896-5900.

79. Bruinsma, R.; Gruner, G.; D'Orsogna, M. R.; Rudnick, J. *Phys. Rev. Lett.* **2000**, 85, 4393-4397

80. Henderson, P. T.; Jones, D.; Hampikian, G.; Kan, Y.; Schuster, G. B. *Proc. Natl. Acad. Sci. U.S.A.* **1999**, 96, (15), 8353-8358.

81. Barnett, R. N.; Cleveland, C. L.; Joy, A.; Landman, U.; Schuster, G. B. *Science* **2001**, 294, (5542), 567-571.

82. Steenken, S. *Free Rad. Res. Commun.* **1992**, 16, 349-379.

83. Dohno, C.; Ogawa, A.; Nakatani, K.; Saito, I. *J. Am. Chem. Soc.* **2003**, 125, (34), 10154-10155.

84. Giese, B.; Spichty, M. *ChemPhysChem* **2000**, 1,(4), 195-198.

85. Takada, T.; Kawai, K.; Fujitsuka, M.; Majima, T. *Proc. Natl. Acad. Sci. U.S.A.* **2004**, 101, (39), 14002-14006.

86. Steenken, S.; Jovanovic, S. V. *J. Am. Chem. Soc.* **1997**, *119*, 617-618.

87. Senthilkumar, K.; Grozema, F. C.; Guerra, C. F.; Bickelhaupt, F. M.; Lewis, F. D.; Berlin, Y. A.; Ratner, M. A.; Siebbeles, L. D. A. *J. Am. hem. Soc.* **2005**, *127*, 14894-14903.

88. Joseph, J.; Schuster, G. B. *J. Am. Chem. Soc.* **2006***,* 128 (18), 6070 -6074

CHAPTER 2

THE ROLE OF N1 IMINO PROTON IN CHARGE MIGARTION THROUGH DNA

2.1 Introduction

Intensive investigation of the oxidation of duplex DNA has shown that loss of an electron generates a radical cation ("hole") that migrates by a hopping mechanism until it is trapped irreversibly in a chemical reaction with H_2O or O_2, which usually occurs at a guanine or a G_n (n > 1) sequence, because guanines have the lowest oxidation potential of the four natural bases (Table 2.1)[1-6].The relevance of these processes to genetic mutation and to the potential applications of DNA in molecular electronics has fueled interest in understanding the detailed mechanisms of the hopping and trapping reactions.[7].

The DNA double helix is made of two sugar-phosphate backbones wrapped around a central helical axis with heterocyclic base pairs in the middle of the axis (Figure1.9). The A-T and G-C base pairs form the complementary duplex, which is held together in part by hydrogen bonds (H-bonds). The G-C base pair is characterized by three hydrogen bonds between the C6-O, N1-H, and C2-NH2 of G paired with the C4-NH2, N3, and C2-O of C, respectively (Figure 1.6). During the charge migration a radical cation is formed at guanine and it reacts with H_2O or O_2 leading damage at that position. Solution studies indicate different reaction pathways depending on the structure of the oxidized guanine, where the N1 proton of G, which is hydrogen bonded with N3 of C, plays the critical role.[8-10] However, the exact role played by this proton during the charge migration remains unknown.

2.2 Proton Coupled Charge Transfer?

Conversion of 2'-deoxyguanosine to its radical cation causes an enormous increase in its acidity.[11] On the basis of solution-phase pK_a data, Steenken[12] concluded that oxidation causes the proton on N1 of guanine in a DNA G/C base pair to shift spontaneously to N3 of the cytosine. This is a very favorable process with a K_{EQ} of $10^{0.4}$ and a ΔG of -1.5 kcal/mol at room temperature (Figure 2.1).

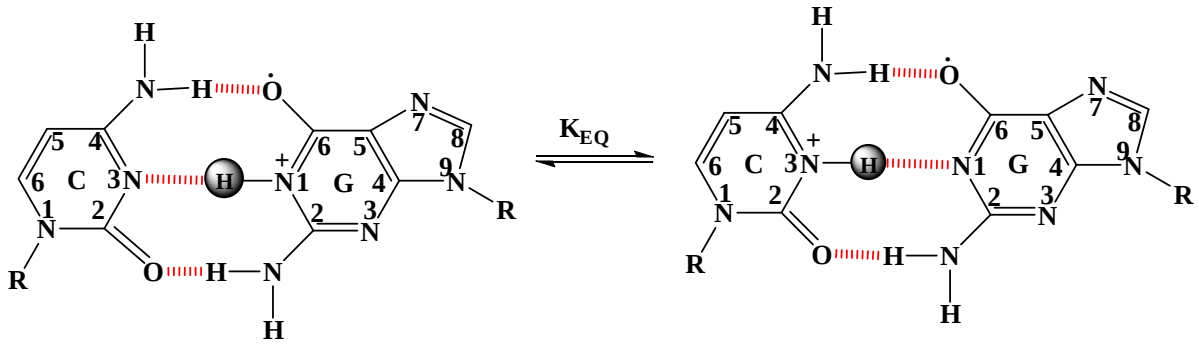

Figure 2.1: Imino proton transfer between C and G

However, DFT calculations in the gas phase, which is suggested to be a realistic model of stacked base pairs in DNA (where solvent is excluded), indicate that the structure with a proton on guanine N1 [C/(H)G$^{\cdot+}$] is more stable than [C$^+$(H)/G$^{\cdot}$] by 1.4 kcal/mol.[13] In contrast, first-principles calculations on a partially hydrated G/C base pair in DNA indicate that the proton transferred form [C$^+$(H)/G$^{\cdot}$] has an energy that is 4.0 kcal/mol below that of [C/(H)G$^{\cdot+}$].[14] Furthermore, an extensive calculation on a related system indicates that charge transfer in oxidized duplex DNA is coupled with proton transfer from guanine to cytosine.[15] This conclusion is consistent with experiments carried out in D_2O that reveal a kinetic isotope effect for guanine oxidation[16] and for charge transfer in DNA,[17] both of which implicate a concerted proton coupled electron transfer involving the guanine N1 proton, and with experiments that show inhibition of

charge transfer when proton loss from guanine is facilitated.[18] So, it is not clear from these studies that if the proton transfer from guanine radical cation to cytosine is coupled with the charge migration through DNA.

2.3 N1 Imino proton in Reaction of Guanine

The N1 proton is also thought to play the deciding role in the chemical reactions of oxidized guanines.[8-10] In solution, rapid loss of this proton and subsequent reaction of the resulting guanine radical with O_2 leads eventually to an oxazolone (dZ, see Figure2.2). However, proton loss from a guanine radical cation is slowed when it is part of a base pair with cytosine in DNA, and in this form it reacts with H_2O to form 8-oxo-7,8-dihydroguanine (8-oxoG).

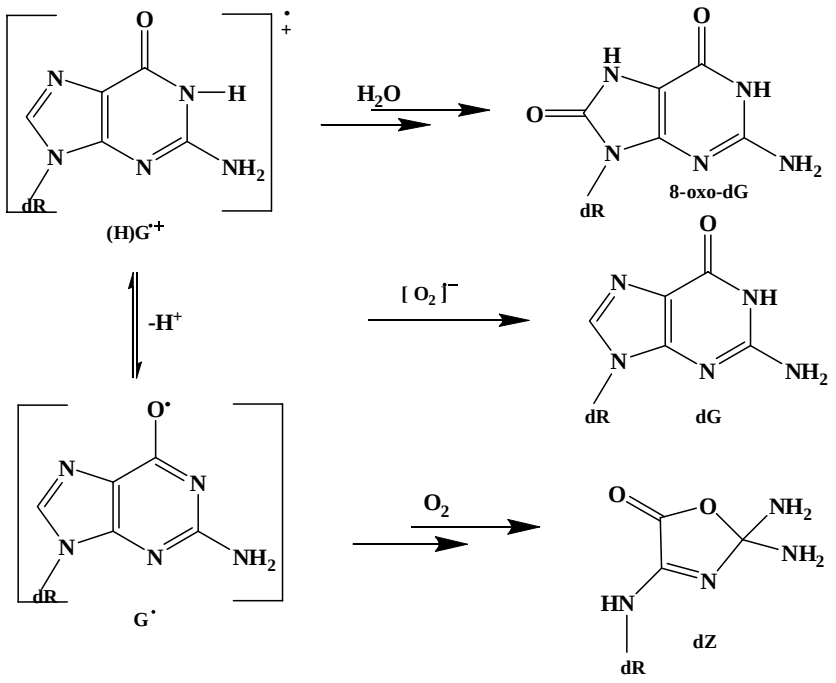

Figure 2.2: Role of Guanine N1 imino proton in reaction of guanine radical cation

2.4 Hypothesis: Perturbing the Proton Transfer

To investigate the correlation between proton transfer from guanine radical cation to cytidine and the charge migration through DNA, we attempted to perturb the proton transfer and study its effect on charge migration. One way to alter the proton transfer reaction between N1 of guanine radical cation and N3 of cytidine is changing the acidity of either of these donor and accepter nitrogens. On the basis of this strategy we decided to put 5-fluoro2'-deoxycytidine (F^5dC) instead of 2'-deoxycytidine (dC) opposite to 2'-deoxyguanosine (dG) (Fig. 2.3).

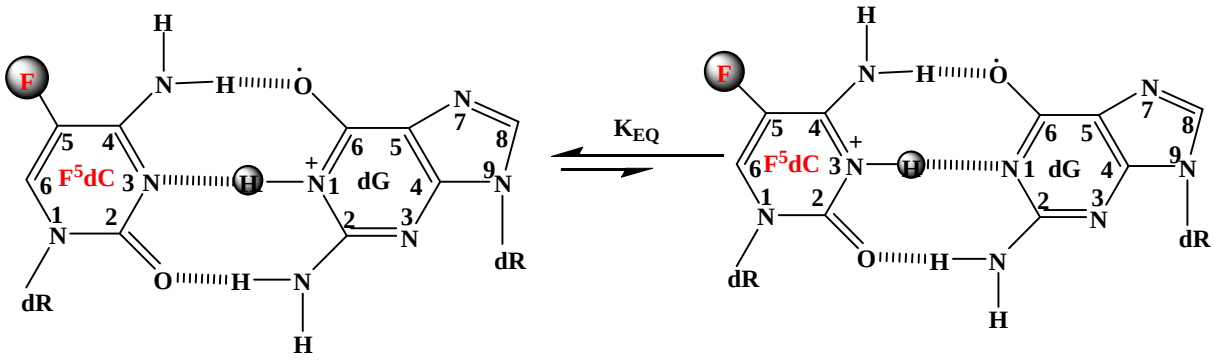

Figure 2.3: Proton transfer is prohibited in presence of 5-fluoro-2'-deoxycytidine (F^5dC)

Fluorine at C5 position of cytosine is expected to drive away electron density from N3. That will make the N3 of F^5dC weaker base (pK_a less) than the same nitrogen of dC. As a result, affinity of N3 nitrogen of F^5dC towards the N1 imino proton of the dG hydrogen bonded to it will be less than normal dC. So, In the presence of F5dC, the proton transfer from N1 of dG radical cation to N3 of dC is expected to be inhibited.

2.5 Testing the Hypothesis

Our experimental strategy is based on the assumption that pK_a of F^5dC is less than that of dC. To test this hypothesis 5-fluorocytidine (F^5C) is synthesized and pK_a of F^5C and dC is measured. For these experiments F^5C is used instead of F^5dC (Figure 2.4) because it is easy to synthesis and a hydroxyl group at 2' position should not effect the acidity of N3. We have also measured the pKa of 5-Bromo-2'-deoxycytidine (Br^5dC).

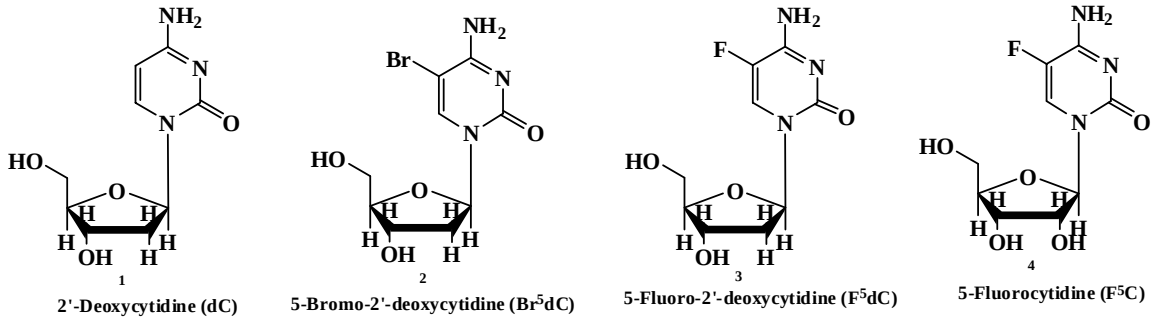

Figure 2.4: Normal and modified cytidines used in this work

2.5.1: <u>Synthesis of 5-Fluorocytidine</u>

The modified nucleoside 5-fluorocytidine (4) was synthesized from commercially available modified base 5-fluorocytosine (5) and protected sugar 1-acetyl-2,3,5-tribenzoyl-β-D-ribofuranoside (6) in an easy two step process (Figure 2.5). This synthetic pathway have been used in synthesis of 5-fluorouridine in literature, but, to our knowledge has not been used for 5-fluorocytidine before.

In the first step of the reaction the free amine group of 5-fluorocytosine is protected by HMDS and then coupled with the protected sugar using TMS-triflate. Then, deprotection of the product (7) gives the desired nucleoside (4). The final product has

been characterized by NMR and ESI mass spectrometry after proper purification and used for pK_a study.

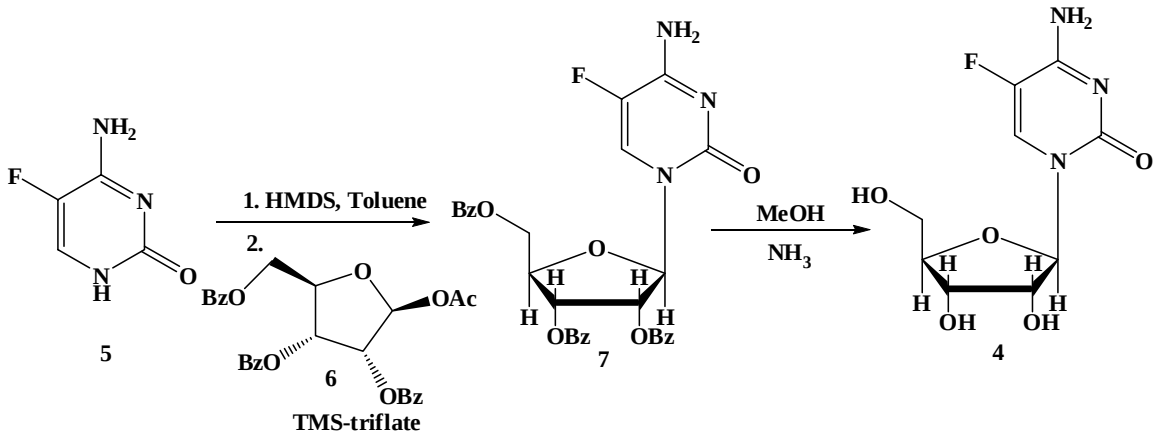

Figure 2.5: Scheme for synthesis of 5-fluorocytidine. Ac and Bz imply acetyl ($-COCH_3$) and benzoyl ($-COC_6H_5$) groups respectively.

In this reaction 2'-deoxysugar (9) has not been used as the 2'-benzoyl group of 5 plays a significant role in stereospecific generation of β anomer of the nucleoside. Due to the presence of bulky 2'-benzoyl group at the bottom side of the furanoside ring, the nucleophilic attack of the base only takes plays from up, resulting the β anomer only (Figure 2.6 A). If 2'-deoxysugar has been used, the 2'-deoxy-5-fluorocytidine could be synthesized. But, the final product would have been a mixture of α and β anomers (Figure 2.6 B), which are very difficult to separate.

A

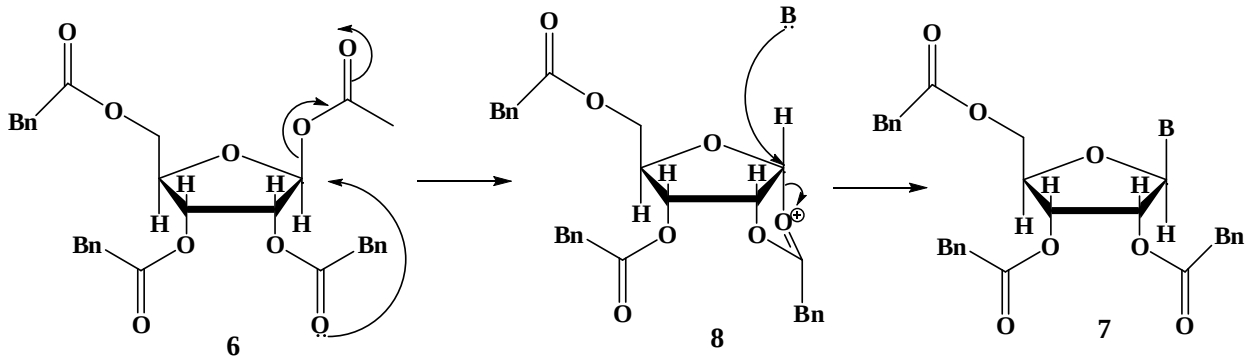

B

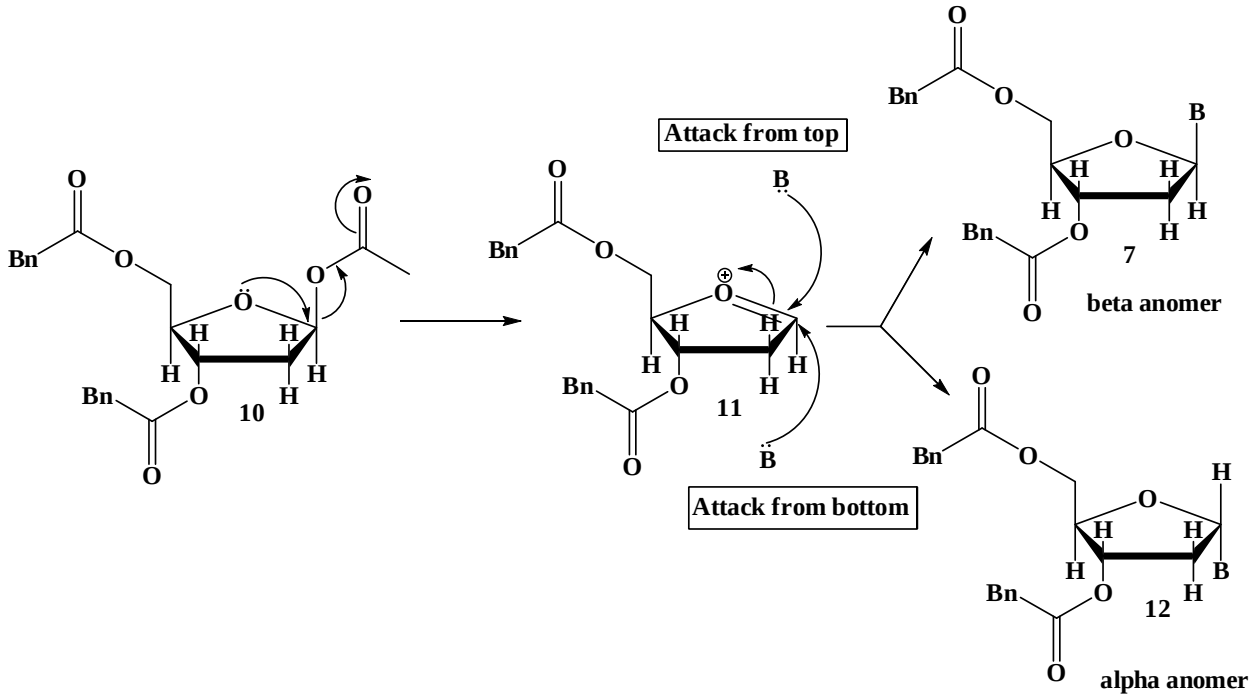

Figure 2.6: 2'-benzoyl group is essential for stereospecific synthesis of β anomer.
(A) Stereospecific attack of base results only β anomer **(B)** attack of base taking place from both sides resulting both anomers. Bn indicates benzene (-C_6H_5) group.

.

2.5.2 Measurement of pK_a

The UV absorption spectra of a solution of F^5C changes with treatment of H_2SO_4, as the N3 get protonated (Figure 2.7). This property is used to determine the pK_a of dC and F^5C.

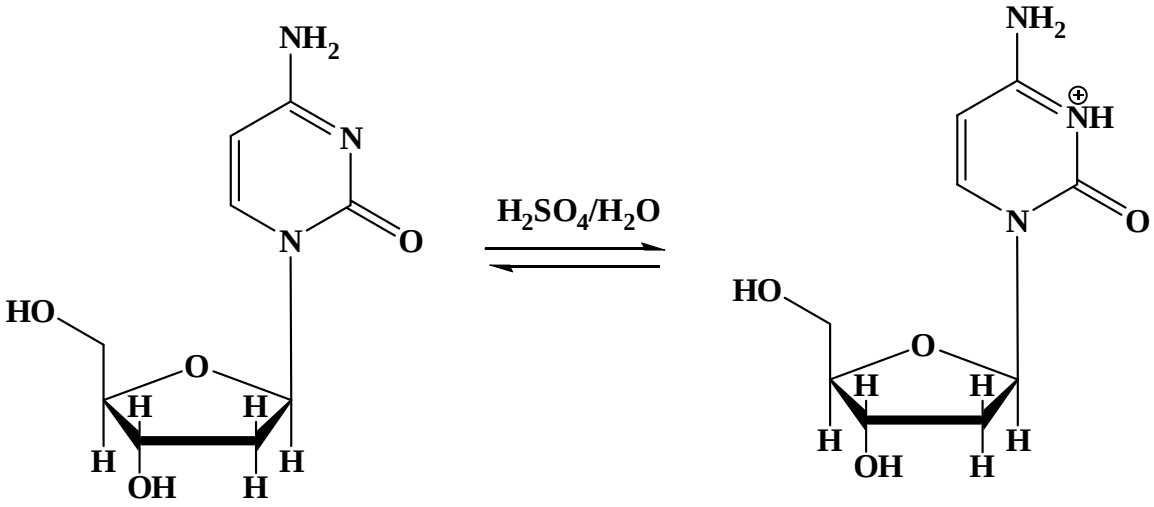

Figure 2.7: Protonation of N3 of 2'-deoxycytidine

The pK_a of dC and F^5C were determined by measuring the changes in their UV absorption spectra in water solution as a function of pH. Solutions (10^{-4} M) of cytidine and 5-fluorocytidine were prepared and aliquots of a dilute, standard H_2SO_4 solution were added. After each addition the pH of the solution was measured by Orion pHmeter (Model 250A) and the absorption spectra were recorded using HP spectrophotometer. The first derivative of absorbance was plotted against pH to obtain the pKa of the nucleobases (Figure 2.8, 2.9 and 2.10). The measured pKa values are reported in table 2.1.

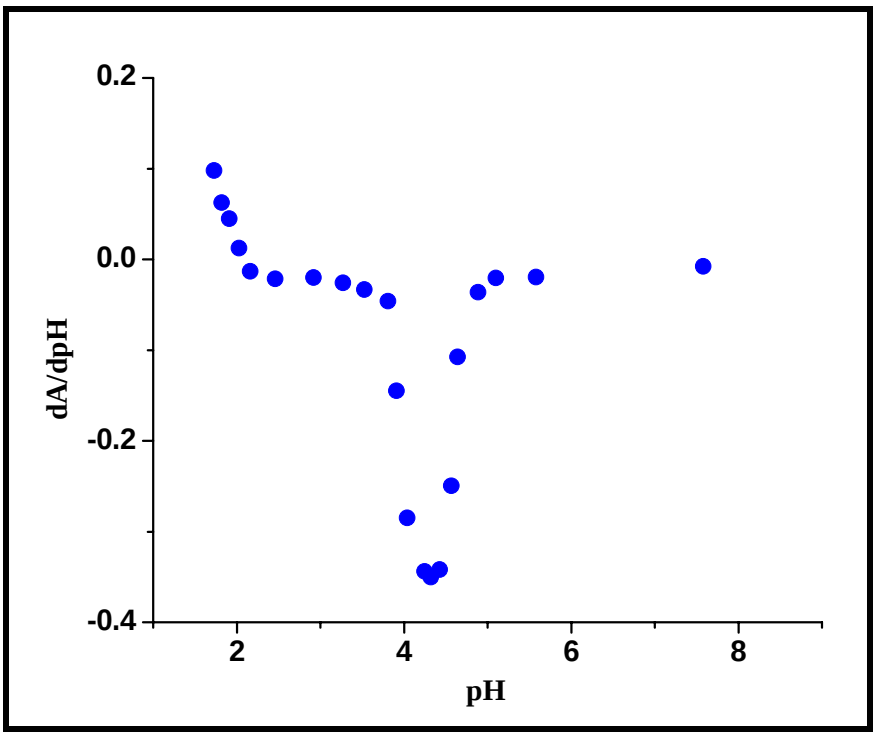

Figure 2.8: First derivative plot of the change in absorption for dC as a function of pH

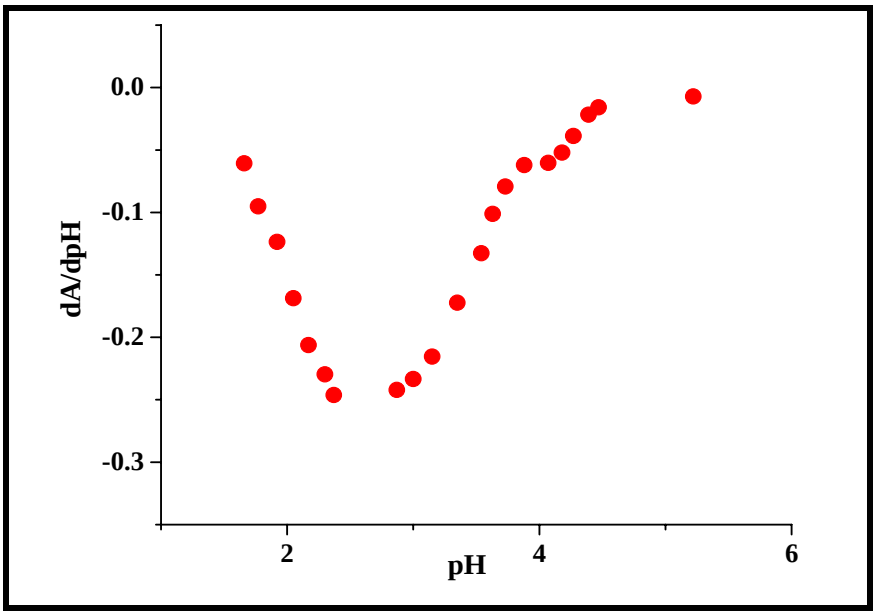

Figure 2.9: First derivative plot of the change in absorption for Br^5dC as a function of pH.

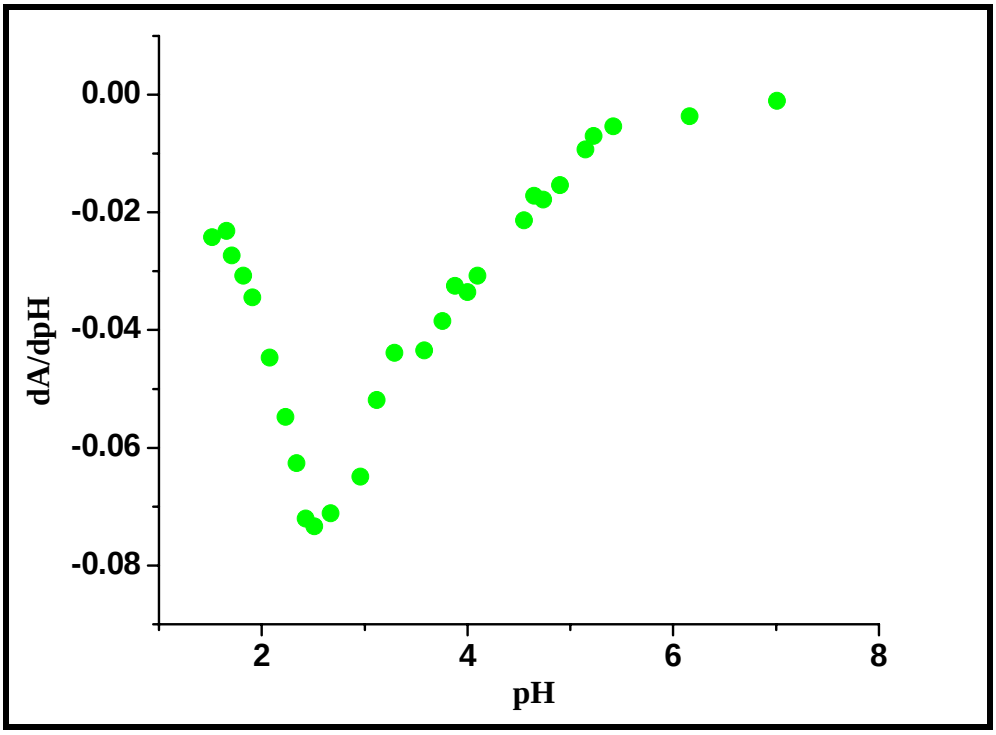

Figure 2.10: First derivative plot of the change in absorption for F^5dC as a function of pH

Table 2.1: pKa of modified and normal cytidines

Nucleoside	pKa (Measured)	pKa (Reported)
dC	4.3 ± 0.1	4.2 [19]
Br^5dC	2.9 ± 0.1	----
F^5C	2.6 ± 0.1	2.3 [19]

2.6 Designing the Strands

From the pK_a measurement experiments it is clear that pK_a of 2'-deoxy-5-fluorocytidine (F^5dC) is much less than that of 2'-deoxycytidine (dC). So, presence of F^5dC instead of dC, opposite to G is definitely going to affect the N1 imino proton transfer. To investigate the effect of this change in proton transfer rate on charge migration through DNA, we decided to put F^5dC opposite to some Gs in a multiple G containing strands.

The charge migration properties of $[GG(A)_nGG]_m$ and $[GG(T)_nGG]_m$ (n=2 to5, m=4 to 6) strands have been studied thoroughly.[19] The rate of hopping and rate of trapping are comparable in a $[GGTTGG]_6$ strand. This would be an ideal strand for our experiment as comparable hopping and trapping will allow us to investigate the effect of the modified cytidine on the charge migration and reaction at guanines. On the basis of this information, following DNA duplexes are planned to synthesize (Figure 2.11).

DNA 1	**5'-AQA A T T G G_1 T T G G_2 T T G G_3 T T G G_4 T T G G_5 T T G G_6 A T A T-3'**
	3'-T T A A C C A A C C A A C C A A C C A A C C A A C C T A T A-5'
DNA 2	**5'-AQA A T T G G_1 T T G G_2 T T G G_3 T T G G_4 T T G G_5 T T G G_6 A T A T-3'**
	3'-T T A A C C A A F F A A C C A A C C A A C C A A C C T A T A-5'
DNA 3	**5'-AQA A T T G G_1 T T G G_2 T T G G_3 T T G G_4 T T G G_5 T T G G_6 A T A T-3'**
	3'-T T A A C C A A F F A A C C A A F F A A C C A A F F T A T A-5'

Figure 2.11: DNA duplexes designed for the experiment. F indicates 5-fluoro-2'-deoxycytidine (F^5dC).

DNA1 has six dCdC (for simplicity has been referred as C in the figure) segments opposite to six GG segments. However, DNA 2 has F^5dC (referred as F) opposite to second GG step and DNA3 has F^5dC opposite to second, fourth and sixth GG steps. Charge injector anthraquinone (AQ) is attached to the 5' end of the GG containing strand.

2.7 Synthesis of F^5dC Phosphoramidite

The first approach to put F^5dC into the DNA strand was to synthesize the phosphoramidite of this modified cytidine (13) and incorporate it into the DNA.

5-Fluoro-2'-deoxycytidine phosphoramidite has been synthesized from 5-fluoro-2'-deoxyuridine in eleven steps before. We tried to synthesize it from 5-fluorocytosine directly to make the synthesis easy and short (figure 2.12). According to this scheme, 5-fluorocytosine (5) is coupled with the protected sugar (6) and the free amine is protected by acetyl group. After deprotection of sugar (15), 3' and 5' hydroxyl groups are protected by silyl (16) and the 2' hydroxyl is dehydroxylated by Barton dehydroxylation (18). Then deprotection (19) and DMT and phosphoramidite protection will give the desired compound (13). All the reagents for this proposed synthesis has been described in figure 2.12.

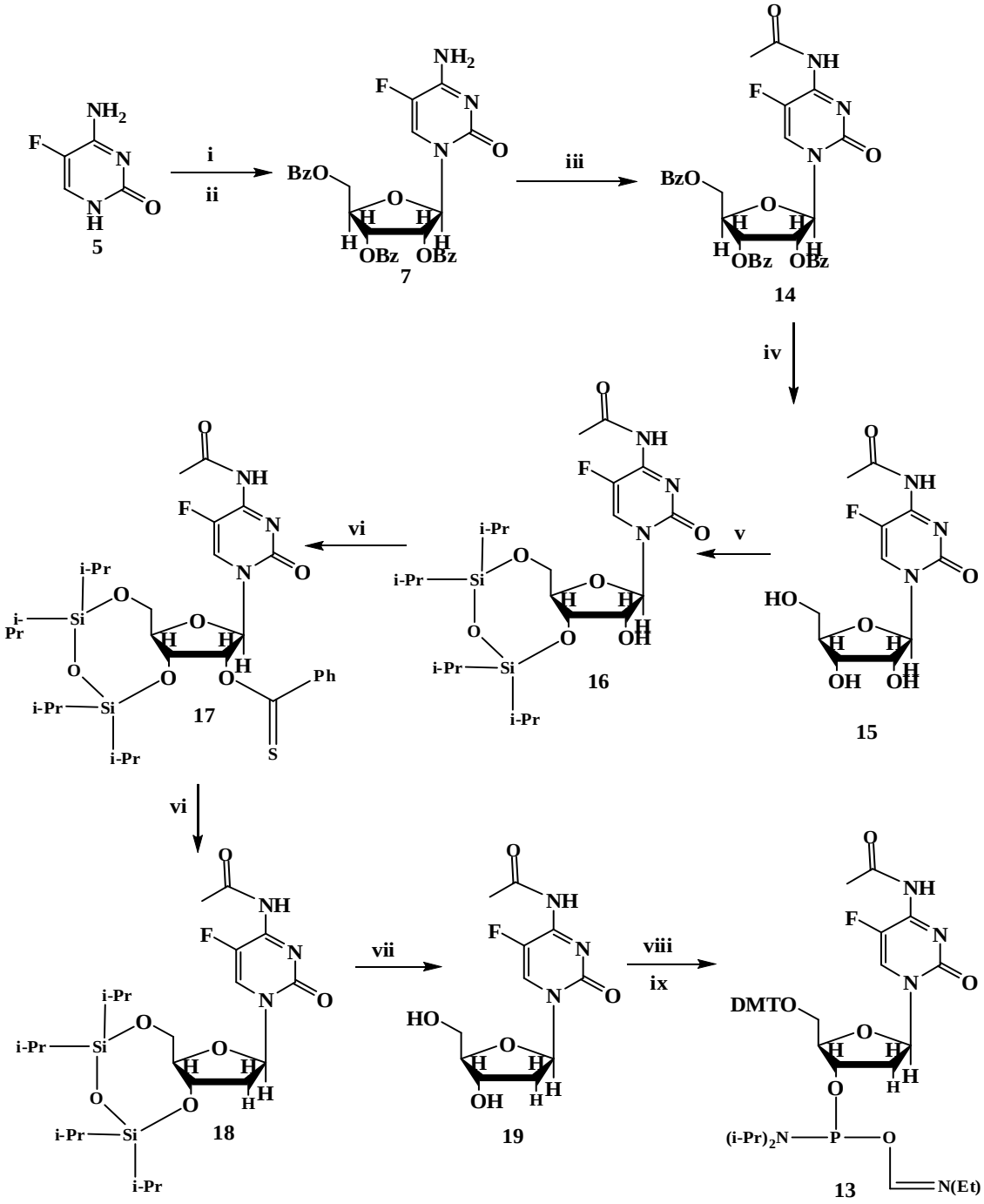

(i)HMDS/Toluene(ii) 1-acetyl-2,3,5-tribenzoyl-β-D-ribofuranoside,TMS-triflate (iii) Acetic anhydride, pyridine, DMAP (iv) NH3/MeOH (v) TPDS-Cl_2/Pyridine (v) PhOCSCl, DMAP, MeCN (vi) AIBN, TBTH, Toluene, 75^0 C (vii) TBAF, THF, 75^0 C (viii) DMT-Cl/pyridine, DMAP (*ix*) CNCH2CH2OP(Cl)N(*i*Pr)2,/CH_2Cl_2, DIEPEA

Figure 2.12: Scheme for synthesis of F^5dC phosphoramidite.

The first two steps of this scheme went on smoothly with an overall yield of 75%. However, the deprotection of sugar benzoyl groups did not work as expected and treatment with methanolic ammonia resulted in deprotection of acetyl group on cytidine amine too. To solve this problem, the scheme was changed a little. In the new scheme (Fig. 2.13) the amine is protected after deprotection of sugar benzoyl protecting group and silyl protection of 3' and 5'-OH. Rest of scheme remained same as the previous one.

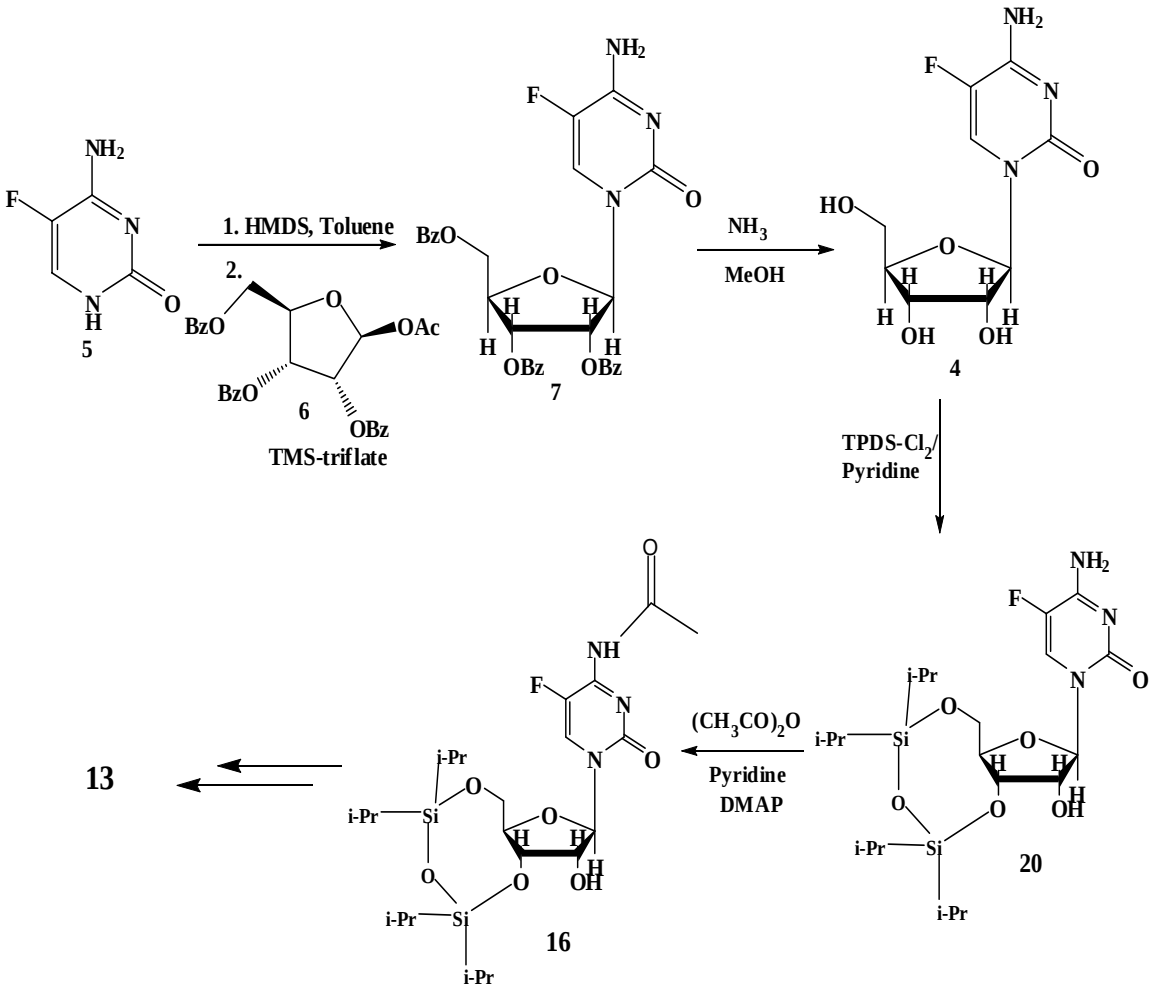

Figure 2.13: Modified scheme for synthesis of F^5dC phosphoramidite.

2.8 Experimental

2.8.1 Materials and Methods

All the chemicals and solvents for F^5dC synthesis were purchased from Sigma Aldrich and Fisher Scientific. All synthetic DNA oligonucleotides were synthesized in our laboratory by Dr. Sriram Kanvah on an Applied Biosystems Inc. Expedite DNA Synthesizer. Nucleotide phosphoramidites and *O*-TMP protected 5-fluoro-2'-deoxyuridine phosphoramidite were obtained from Glen Research and used as received. *O*-TMP protected 5-fluoro-2'-deoxyuridine was converted to 5-fluoro-2'-deoxycytidine (F^5dC) by heating the oligonucleotide overnight with ammonia at 60^0C. These synthetic DNA oligonucleotides were purified by HPLC on a Hitachi 7000 HPLC system set with a Varian Dynamax 25x21.4 mm reverse-phase C-18 column using 5-20% Acetonitrile in 0.5 M Triethylammonium Acetate and then desalted. UV/Vis studies on DNA oligonucleotides were conducted at 260 nm on a Hewlett-Packard Spectrophotometer. The extinction coefficients of the oligomers were calculated using a biopolymer calculator, and their concentrations were determined from the absorbance at 260 nm. An adenine is substituted for the anthraquinone group in the extinction coefficient calculation. The mass of each oligonucleotide was determined by a Micromass Quattro Electrospray Ionization (ESI) mass spectrometer. Radioactively labeled isotope (α-^{32}P) Adenosine triphosphate (ATP) and the enzyme terminal dinucleotide transferase (TdT) and its buffer were purchased from GE Healthcare. Formamidopyramidine glycosylase (Fpg enzyme) was purchased from Trevigen, Gaithersburg, MD. UV melting and cooling experiments were performed on a Cary 1E Spectrophotometer equipped with a multi-cell block, temperature controller and sample transport accessory. Circular Dichroism (CD)

measurements were conducted on a JASCO-720 instrument. Kodak film for PAGE analysis was purchased from Aldrich. The quantitative analysis of autoradiograms was performed on a FUJI 2340 BAS-Image system. The buffer used for all experiments was 10 mM sodium phosphate (NaPi) at pH 7.0.

2.8.2 Synthesis of 5-Fluorocytidine

1-(2,3,5-Tri-O-benzoyl-β-D-ribofuranosyl)-5-fluorocytosine (7)

5-fluorocytosine (5) (500 mg, 4 mmol) was suspended in toluene (20 mL) and hexamethyldisilazane (1 mL, 4 mmol) and the mixture was refluxed for 3 hours. Then it was cooled to room temperature and evaporated to dryness. The residue was dissolved in dry dichloroethane (20 mL) and was added 1-acetyl-2,3,5-tribenzol-β-D-ribofuranose (6, 1.24 gms, 2.5 mmol) and TMS-triflate (0.72 mL, 3.96 mmol). It was stirred for 8 hours at room temperature. Then, chloroform (100 mL) was added to the reaction mixture and it was washed with 5% $NaHCO_3$ solution, dried over Na_2SO_4, filtered, evaporated to have a white crystalline compound. It was purified by column chromatography (0-10% methanol in dichloromethane) to obtain pure **7** (1.3 gms) with 91% yield.

^{1}H NMR ($CDCl_3$): δ 8.2 (d, 1H, H-6), 8.1-7.3 (m, 15 H, 3 C_6H_5CO), 6.17 (dd, 1H, H-1'), 5.9-5.7 (m, 2H, H-2', H-3'), 4.85-4.75 (m, 3H, H-4', H-5', H-5'').

ESI (m/z): 1147 $(2M+H)^+$, 574 $(M+H)^+$, 504 $(8)^+$, 445 $(S)^+$.

5-Fluorocytidine (4)

1.0 gms (1.6 mmol) of 7 was dissolved in 40 mL of methanolic ammonia (7 N) and was stirred at room temperature for overnight. Then it was evaporated to dryness, coevaporated with methanol and the residue was dissolved in 100 mL of water. The water solution was washed with CH_2Cl_2 six times (100 mL each time) and evaporated to obtain

600 mg (90% from starting material) of white crystalline compound which was characterized by NMR and mass spectroscopy (Figure 2.14 and 2.15)

^{1}H NMR (D_2O): δ 7.9 (d, 1H, H-6), 5.7 (dd, 1H, H-1'), 4.1-3.6 (m, 5H, H-2', H-3', H-4', H-5', H-5'') .

^{1}H NMR (DMSO-d_6): δ 8.2 (d, 1H, H-6), 7.7-7.5 (broad d, 2H, -NH2), 5.7 (dd, 1H, H-1'), 5.4 (s, 1H, 2'-OH), 5.2 (s, 1H, 5'-OH), 5.0 (s, 1H, 3'-OH), 4.1-3.6 (m, 5H, H-2', H-3', H-4', H-5', H-5'') .

ESI (m/z): 523 $(2M+H)^+$, 262 $(M+H)^+$.

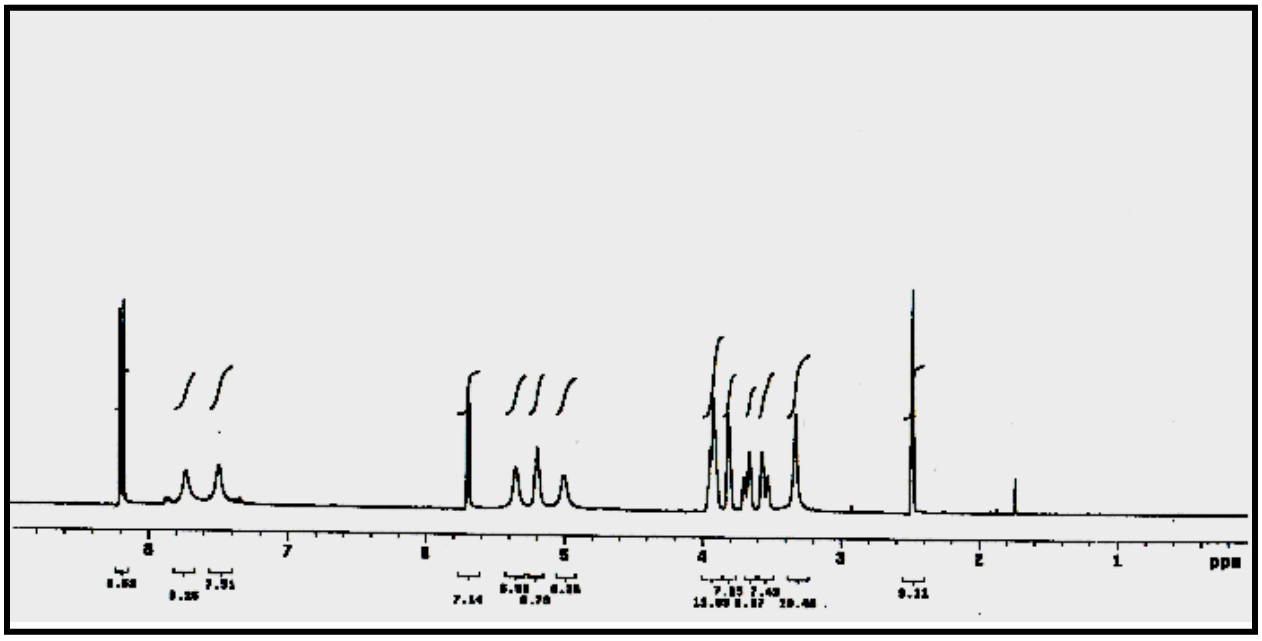

Figure 2.14: ^{1}H NMR spectrum of 4 in DMSO-d_6

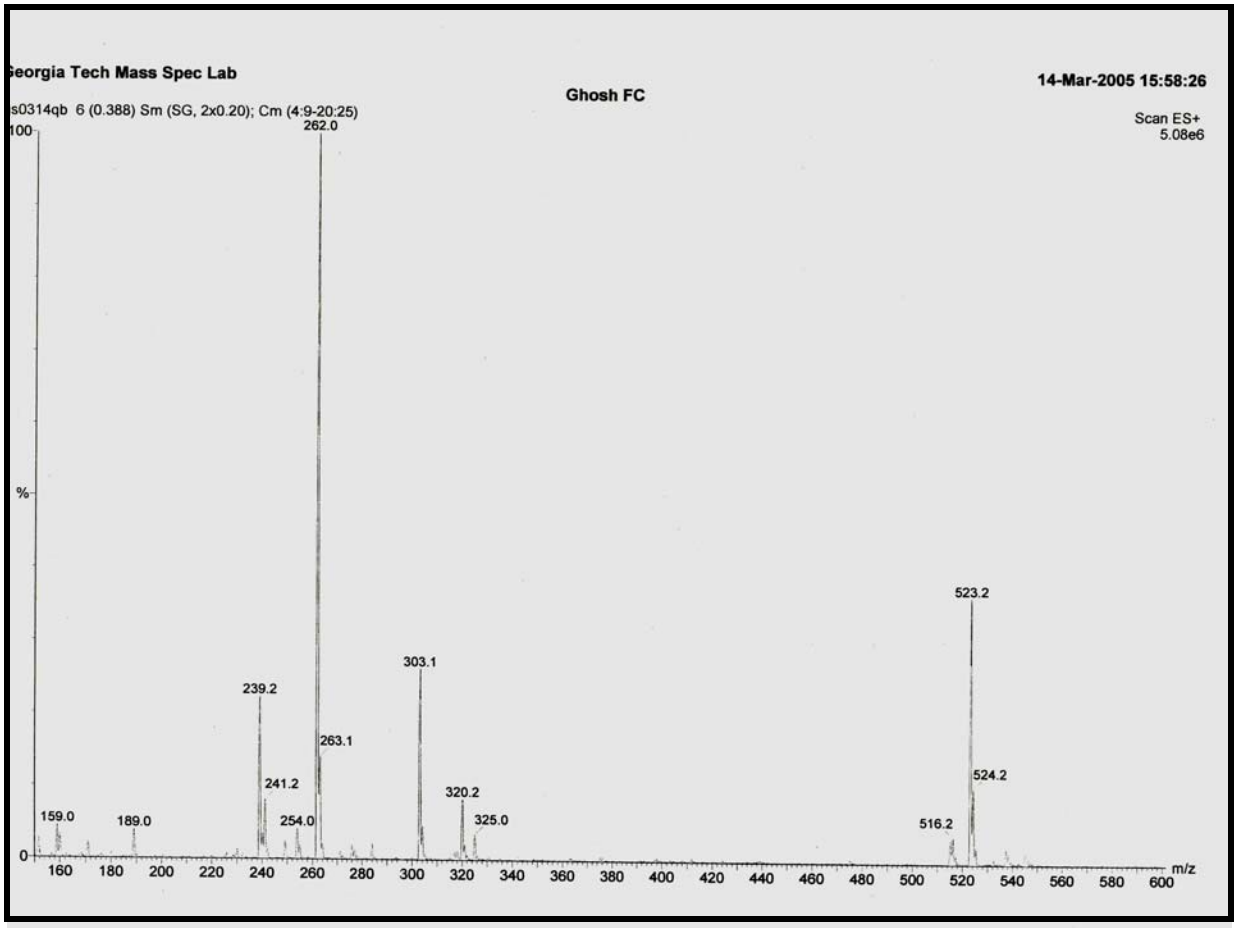

Figure 2.15: Low resolution ESI spectra of 4

2.8.3 Synthesis of 5-Fluoro-2'-deoxycytidine phosphomidite

4-N-Acetyl-1-(2,3,5-tri-O-benzoyl-β-D-ribofuranosyl)-5-fluorocytosine (14)

1.2 gms (2 mmol) of 7 was dissolved in 20 mL of pyridine and catalytic amount of DMAP and acetic anhydride (0.5 mL, 5 mmol) was added dropwise. The mixture was stirred for overnight, evaporated, phase separated between water and CH_2Cl_2. The organic layer was washed with water, 1 M HCl solution, water, dried over Na_2SO_4, filtered and evaporated. Residue was purified by column chromatography (0-10% methanol in CH_2Cl_2) to get 1.0 gm (81%) of 14 as yellow oil.

^{1}H NMR ($CDCl_3$): δ 8.65 (d, 1H, H-6), 8.1-7.3 (m, 15 H, 3 C_6H_5CO), 6.4 (dd, 1H, H-1'), 5.9-5.7 (m, 2H, H-2', H-3'), 4.85-4.75 (m, 3H, H-4', H-5', H-5''), 2.4 (s, 3H, CH_3CO).

ESI (m/z): 1120.5 $(2M+H)^+$, 616.3 $(M+H)^+$, 445.3 $(S)^+$.

4-N-Acetyl-5-fluorocytidin (15)

1.0 gms (1.6 mmol) of 14 was dissolved in 40 mL of methanolic ammonia (7 N) and was stirred at room temperature for overnight. Then it was evaporated to dryness, coevaporated with methanol and the residue was dissolved in 100 mL of water. The water solution was washed with CH_2Cl_2 six times (100 mL each time) and evaporated to obtain 400 mg of a yellow oil, which was characterized by NMR and mass spectroscopy.

^{1}H NMR (D_2O): δ 7.9 (d, 1H, H-6), 5.7 (dd, 1H, H-1'), 4.1-3.6 (m, 5H, H-2', H-3', H-4', H-5', H-5''), 1.8 (s, 3H, CH_3CO).

ESI (m/z): 303 $(M)^+$, 262 $(M-CH_3CO+H)^+$.

We assumed that the peak at 1.8 was for the acetyl protons and the acetyl group was cleaving off during ESI to give the protonated mass for the non-acetylated product. ESI at lower temperatures and with lower ionization energies were checked and same result was obtain. Then, while checking the NMR of the side products of the reaction, we found that water soluble acetamide shows a signal at 1.8 ppm. We concluded that the acetyl group was cleaved of during the debenzoylation process and water soluble side product acetamide was responsible for the acetyl peaks. So, this reaction did not work as expected and we went on with the modified scheme (Figure 2.13). At first 5-fluorocytidine was synthesized according to section 2.9.2 and then the following reactions were carried out.

3',5'-O-TPDS-5-fluorocytidine (20)

525 mgs (2mmol) of 4 was dissolved in 10 mL of pyridine and was added 0.32 mL (1.1 mmol) of TPDS-Cl_2. After 4 hours, pyridine was evaporated; residue dissolved in 100 mL of EtOAc, washed with water, 1 M HCl solution, water, 5% $NaHCO_3$ solution and brine respectively, dried over Na_2SO_4, filtered and solvent was evaporated to obtain 500 mg of a white crystalline product. This was purified by column chromatography (0-5% methanol in CH_2Cl_2) to obtain 750 mgs (74%) of **20**.

^{1}H NMR (CD_3OD): δ 8.0 (d, 1H, H-6), 5.6 (dd, 1H, H-1'), 4.3-4.0 (m, 5H, H-2', H-3', H-4', H-5', H-5''), 1.0 (m, 28H, TPDS-protons)

^{1}H NMR (DMSO-d_6): δ 7.8 (d, 1H, H-6), 7.8-7.5 (broad d, 2H, -NH2), 5.7 (dd, 1H, H-1'), 5.5 (s, 1H, 2'-OH), 4.2-3.8 (m, 5H, H-2', H-3', H-4', H-5', H-5''), 1.0 (m, 28H, TPDS-protons)

ESI (m/z): 504 $(M+H)^+$.

4-N-Acetyl-3',5'-O-TPDS-5-fluorocytidine (16)

750 mg (1.5 mmol) 17 was dissolved in DMF (10 mL). Acetic anhydride (2.5 mL, 2.3 mmol) was added to it dropwise. After 5 hrs, methanol (2mL) was added to quench the reaction. The reaction mixture was concentrated and purified by silica gel column chromatography (0-5% MeOH in CH_2Cl_2) to obtain a white foam of **16** (650 mg, 80%).

^{1}H NMR ($CDCl_3$): δ 8.2 (d, 1H, H-6), 5.75 (dd, 1H, H-1'), 4.3-3.9 (m, 5H, H-2', H-3', H-4', H-5', H-5''), 2.6 (s, 3H, N-acetyl), 1.0 (m, 28H, TPDS-protons) [peaks for EtOAc are present in the spectra]

^{1}H NMR (DMSO-d_6): δ 8.1 (d, 1H, H-6), 5.8 (dd, 1H, H-1'), 5.5 (s, 1H, 2'-OH), 4.2-3.9 (m, 5H, H-2', H-3', H-4', H-5', H-5''), 2.2 (s, 3H, N-acetyl), 1.0 (m, 28H, TPDS-protons).

ESI (m/z): 1091 $(2M+H)^+$, 546 $(M+H)^+$.

4-N-Acetyl-2'-O-phenoxythiocarbonyl-3'-5'-O-TPDS-5-fluorocytidine (17)

550 mg (1 mmol) of 12 was dissolved in 20 mL dry acetonitrile, and 1gm (8 mmol) DMAP was added. The solution was cooled in ice-water and 0.2 mL (1.1 mmol) of PTC-Cl was added. The mixture was stirred at 0-5^0 C for 1 hour. After the standard processing, the residue was subjected to column chromatography (0-2% MeOH in CH_2Cl_2). After analyzing the product spot by NMR it seems that it contains atleast two compounds. In ESI some other significant signals apart from the expected product signal (682) has been obtained.

After several tries we were not able to this step work and we have used an alternative method to put 2'-deoxy-5-fluorocytidine in DNA. This has been described in next chapter.

2.8.4 Synthesis of DNA Single Strands

5-Fluoro-2'-deoxycytidine can be synthesized from 5-fluoro-2'-deoxyuridine. In this method, commercially available protected fluorouridine derivative *O*-TMP-F-dU-CE Phosphoramidite (20 in Figure 2.16) is incorporated into the DNA along with other protected normal nucleoside phosphoramidites. After synthesis of DNA, for deprotection, it is treated with ammonia at 60^0 C for overnight. During this process an amine group

replaces the O-TMP of 5-fluoro-2'-deoxyuridine and converts it to 5-fluoro-2'-deoxycytidine.

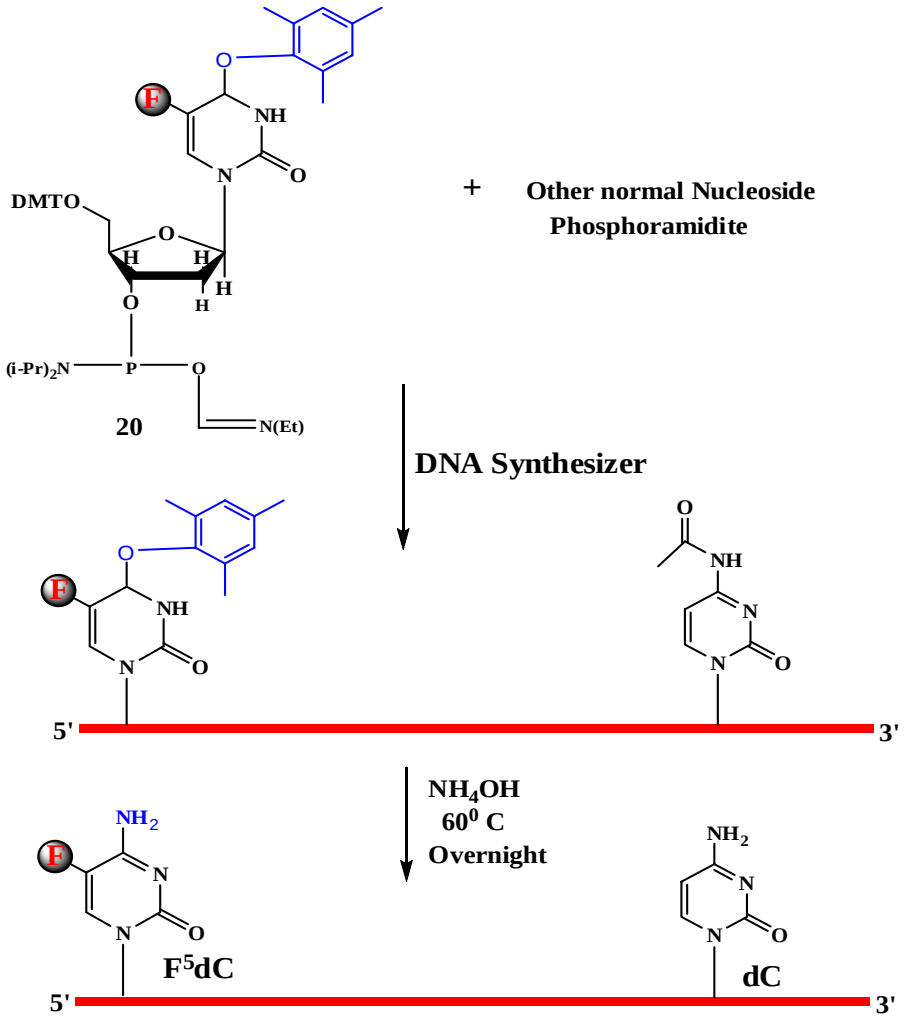

Figure 2.16: Incorporation of F^5dC in DNA

Applying this method two modified single strands were synthesized along with two normal strands (Figure 2.17) to get our designed DNA duplexes (Section 2.6). These single strand DNA's were purified by HPLC, desalted and then characterized by ESI mass spectrometry. The mass spectrometry results are summarized in table 2.2 and it shows that we were able to synthesize the modified and unmodified strands successfully.

S1	**5’-AQAATTGGTTGGTTGGTTGGTTGGTTGG ATAT-3’**
S2	**5’-ATATCCAACCAACCAACCAACCAACCAATT-3’**
S3	**5’-ATATCCAACCAACCAACCAAFFAACCAATT-3’**
S4	**5’-ATATFFAACCAAFFAACCAAFFAACCAATT-3’**

Figure 2.17: Modified and unmodified DNA single strands

Table 2.2: Mass spectrometry results of DNA strands S1-S4

DNA strand	Expected Mass	Observed Mass
S1	**9757**	**9758**
S2	**9009**	**9010**
S3	**9045**	**9046**
S4	**9117**	**9118**

2.8.5 Characterization of DNA Duplexes

Thermal Denaturation

The thermal denaturation properties of DNA duplexes (DNA 1, 2 and 3) were characterized by UV absorption at 260 nm. The first derivative of the absorbance vs. temperature curve gives the melting temperature of the DNA duplex. The DNA samples (5 μM DNA in 10 mM NaPi solution at pH 7.0) are placed in a UV transparent quartz cell with a 1 cm path length and placed inside the Cary 1E Spectrophotometer. To verify the reversibility of the thermal transitions several temperature ramps from 15 to 90 ºC were investigated.

The results (Figure 2.18) show that the modified and unmodified duplexes have similar melting temperature and F^5dC does not affect the stability of double stranded DNA.

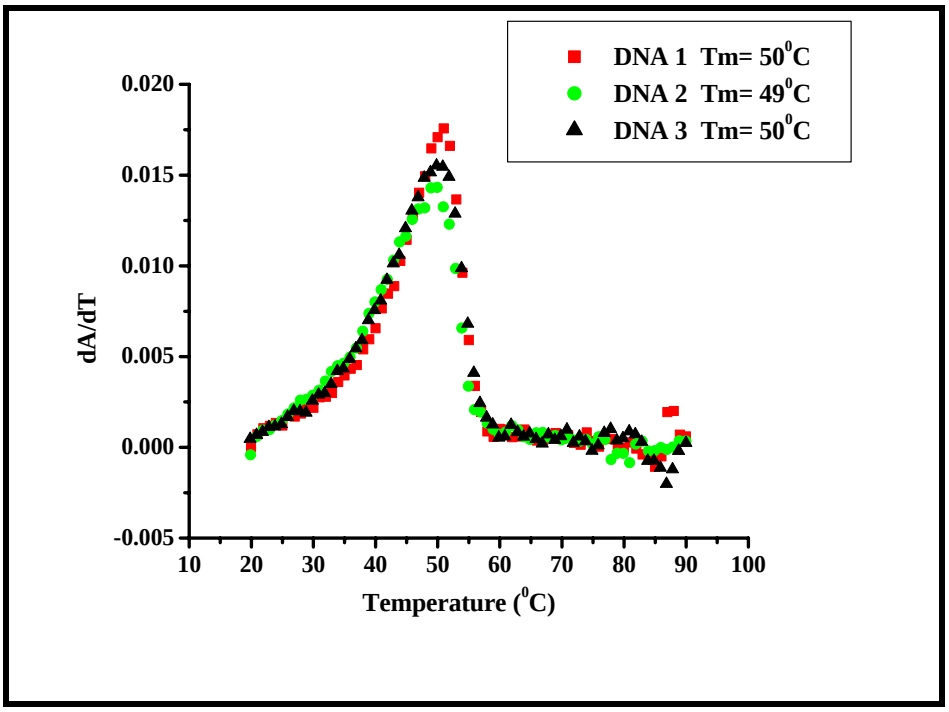

Figure 2.18: Plot of first derivative of absorbance against temperature for DNA 1-3.

Circular Dichroism

The secondary structure of DNA duplexes (1-3) were confirmed by circular dichroism (CD) experiment at room temperature. The exact samples used for the thermal denaturation experiments discussed above were used for the CD experiments. Introduction of two or six F^5dC is not expected to change the B-DNA conformation of the duplexes. This is indeed the case for DNA (1-3), where under our experimental conditions there is no change in the shape of CD spectra and each DNA molecule resembles B-DNA with no significant structural distortions (Figure 2.19).

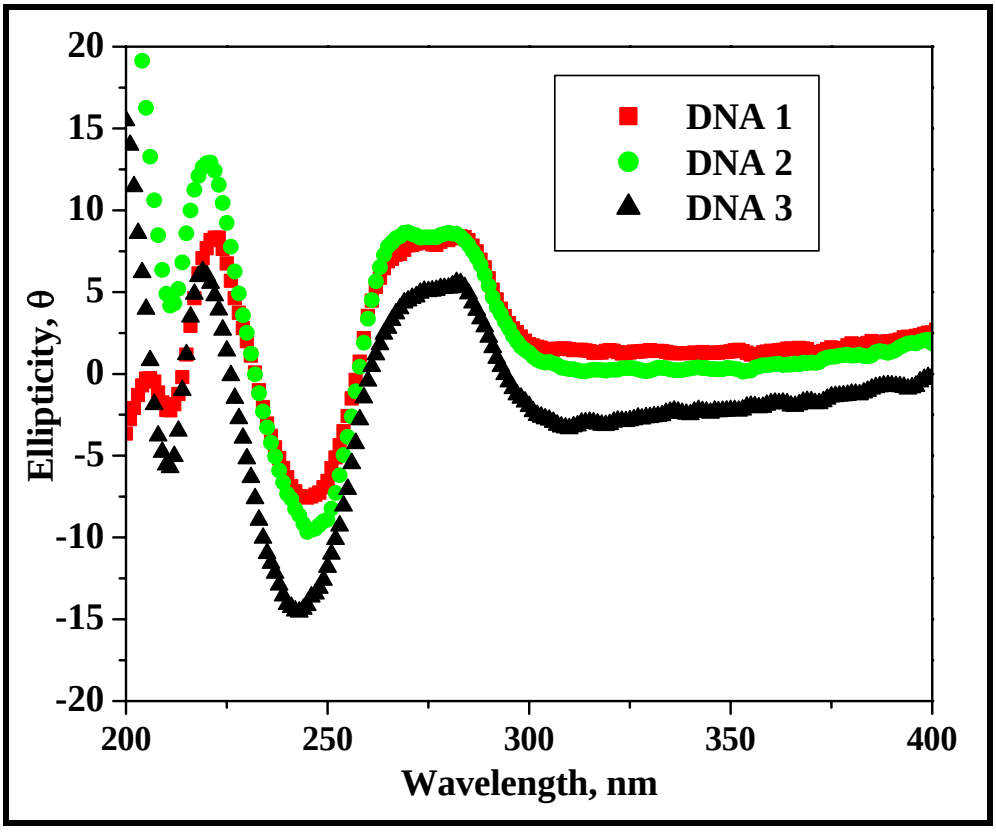

Figure 2.19: Circular dichroism spectra of DNA 1-3

2.8.6 Preparation of Radiolabeled DNA.

The DNA oligomer S1 was radiolabeled at the 3'-end using [α-^{32}P]ATP and TdT enzyme. A 5 μL sample of desired single stranded DNA was incubated with 1 μL of [α-^{32}P]ATP and 2 μL of TdT enzyme in a total volume of 20 μL at 37 ^{0}C for 45 min. After incubation, the DNA sample was suspended in a denaturing loading dye and was purified on a 20% denaturing polyacrylamide gel. The desired DNA band was excised from the gel and eluted with 800 μL of elution buffer (0.5 M NH_4OAc, 10 mM $Mg(OAc)_2$/1.0 mM EDTA/0.1% SDS) at 37 0C for 12 h. The DNA was precipitated from the supernatant by addition of 600 μL of cold ethanol and 2 μL of glycogen. The mixture was vortexed, placed on dry ice for about 60 min, and centrifuged at 13000 rpm for 45 min. The supernatant was removed, and the residual DNA was washed with 100 μL of 80% ethanol and air-dried. Suitable volumes of water were added for further experimentation.

2.8.7 UV Irradiation and Gel electrophoresis

Samples for irradiation were prepared by hybridizing a mixture of unlabeled (5.0 μM) and radiolabeled (10000 cpm) oligonucleotides with complimentary AQ-linked DNA in sodium phosphate buffer solution at pH 7.0. Hybridization was achieved by heating the samples at 90 ^{0}C for 10 min, followed by slow cooling at room temperature for 3 h. Samples were irradiated at ca. 30 ^{0}C in microcentrifuge tubes in a Rayonet Photoreactor (Southern New England Ultraviolet Co., Bransford, CT) equipped with two 350 nm lamps. For investigation of reaction in absence of oxygen, nitrogen gas was passed through the samples prior to the irradiation. After irradiation, the samples were precipitated once with cold ethanol (100 μL) and 2 μL of glycogen. The precipitated samples were washed twice with 100 μL of 80% ethanol and dried. To investigate the

piperidine labile damage these samples were treated with 50 μL piperidine and heated at 90 ^{0}C for 30 minutes. Then the piperidine was evaporated out and the samples were dissolved in denaturing loading dye and subjected to 20% 19:1 polyacrylamide gel electrophoresis. For Fpg labile damage investigation, the precipitated and dried samples were mixed with 3 μL of Fpg enzyme, 2 μL of buffer solution and diluted to 20 μL with nanopure water, heated at 37 ^{0}C for 2 h and then at 90 ^{0}C for 20 min. The samples were then reprecipitated with cold ethanol (100 μL) and 2 μL glycogen and the precipitated samples were washed with 100 μL of 80% ethanol. After evaporation of ethanol, the samples were dissolved in denaturing loading dye and subjected to 20% 19:1 polyacrylamide gel electrophoresis. The gels were dried, and the cleavage sites were visualized by autoradiography.

2.8.8 Quantitative Analysis through Phosphorimagery

Quantification of the amount of DNA damage at each GG step, which is relative to the efficiency of charge transfer through DNA, is accomplished by reading the gel image in a FUJI phosphorimager. The gel is exposed to a FUJI imaging plate, and read in the FUJI 2340 BAS-Image system. ImageGuage software is then used to determine the relative intensity of radiolabel at each GG step, revealed as dark spots in the autoradiogram. This relative intensity is directly related to the amount of DNA oligomer at the position on the gel.

2.9 Results

2.9.1 Fpg Labile Damage

The autoradiogram obtained from Fpg treated samples is shown in figure 2.20.

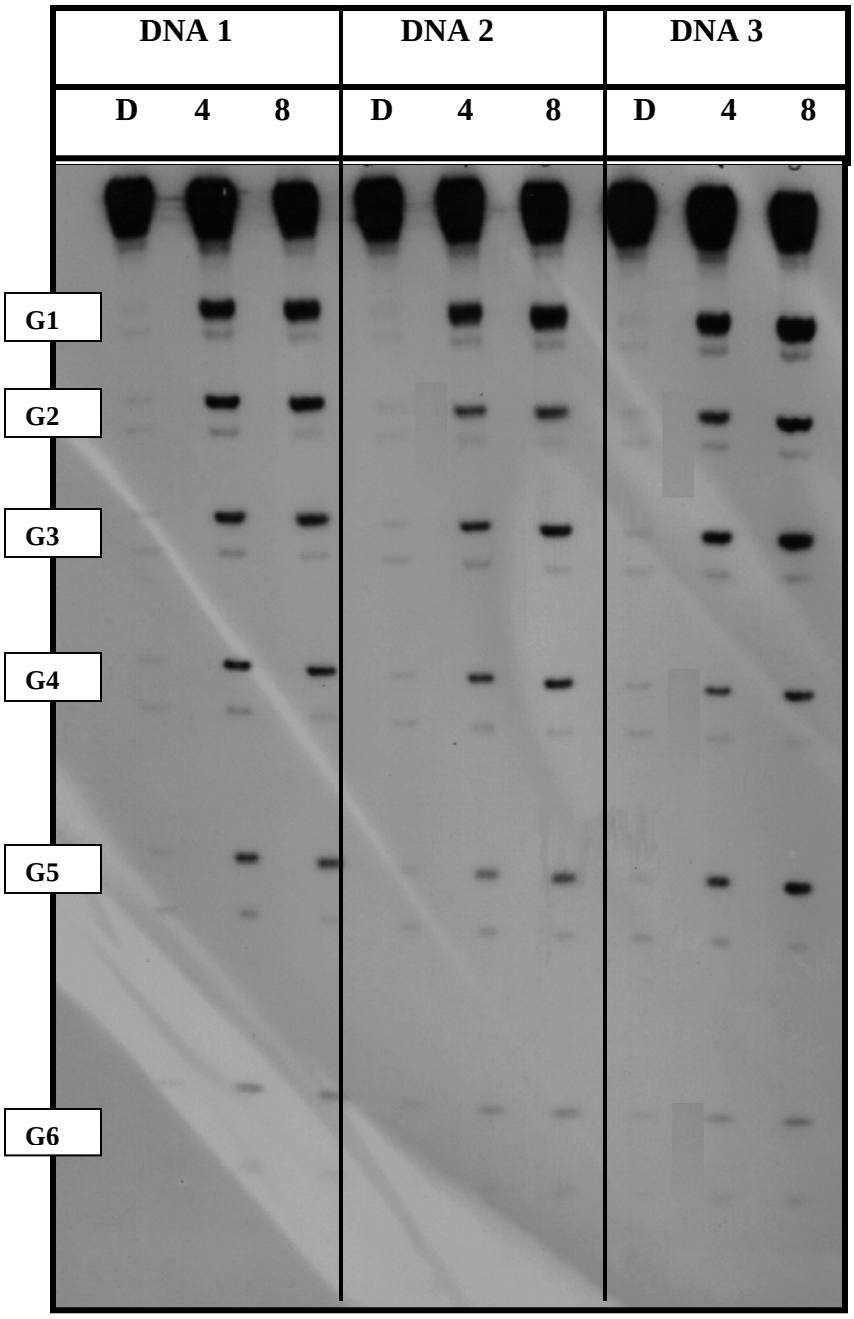

Figure 2.20: Autoradiogram of Fpg treated samples. D, 4 and 8 represents 0, 4 and 8 minutes of irradiation respectively. The six GG steps are indicated as G1-G6.

In this autoradiogram, damages at six GG steps are visible as bands in the irradiated samples and are indicated as G1-G6 in the figure 2.20. For all the GG steps in all three DNAs, damage at 5'-G is higher than the damage at 3'-G. Also, as expected[19], for DNA 1 the damage at GG steps decreases with increase in distance from AQ charge injector. However, for DNA 2 and DNA 3 the damage pattern is not so simple. For the guanines having F^5dC as complementary base, the damage is less than the guanines having a normal dC opposite to them. In case of DNA 2, the second GG step has F^5dC opposite to it, and it has less damage than the second GG step of DNA 1. The second, forth and sixth GG steps have F^5dC opposite to them and they all have less damage than the corresponding GG steps of DNA 1. These results were confirmed by quantitative analysis (Figure 2.21 and 2.22).

In Figure 2.21, the relative damages (ratio of damage at a particular GG step to total damage at all GG steps) of all GG steps of these three duplexes for 4 minutes of irradiation are shown as histograms. For DNA 1 (blue bars) the order of relative damage is 1>2>3>4>5>6, i.e., all GG steps have higher damage than the next ones. But, in DNA 2 (red bars) second GG step has less damage than the next one. And for DNA 3 (yellow bars), the second and forth GG steps have less damage than their next ones and the sixth GG step has less damage than the sixth GG steps of DNA 1 and DNA 2. The natural logarithm of relative damage is plotted against the distance from AQ in Figure 2.22. For DNA 1, the damage decreases almost linearly with distance. While, for DNA 2, all the points but the second one are in a straight line and for DNA 3, the second, fourth and sixth points are out of it.

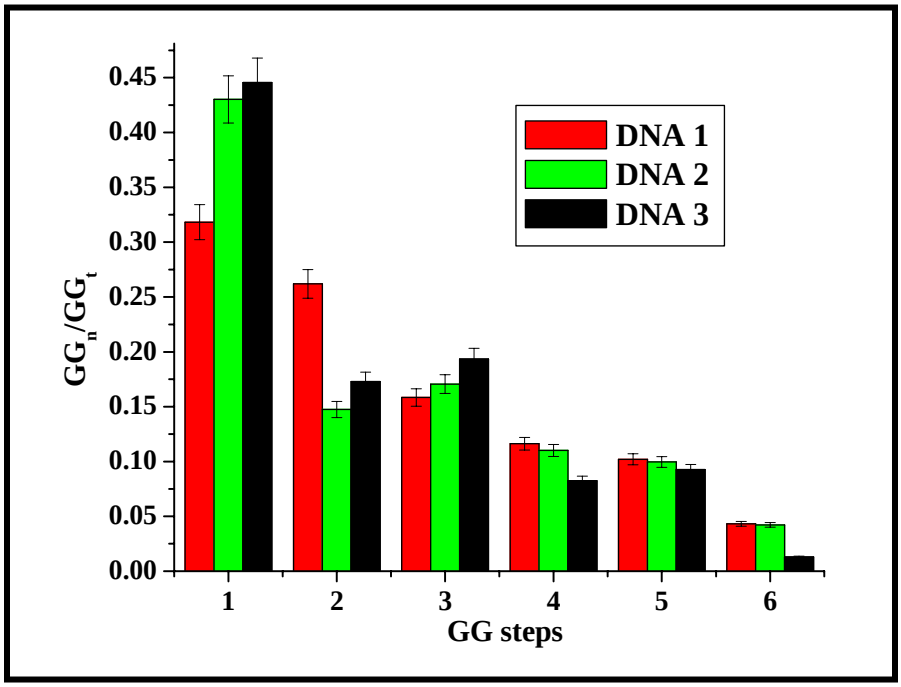

Figure 2.21: Histogram representing the quantitative analysis of autoradiogram. X-axis represents the GG steps and Y-axis represents the relative damage at each step.

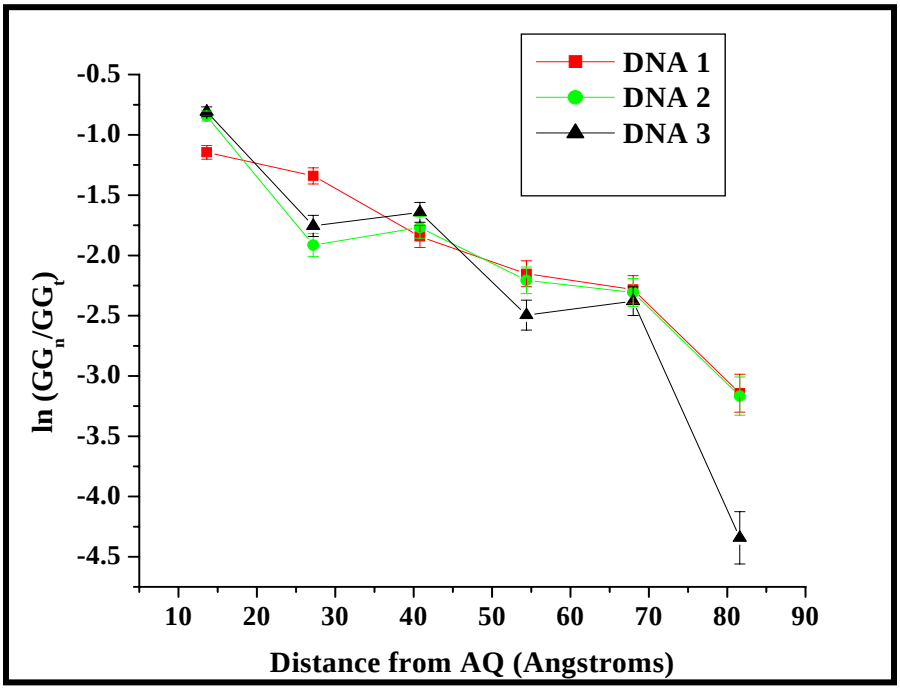

Figure 2.22: Plot of log of relative damage against the distance from AQ

2.9.2 Piperidine Labile Damage

The autoradiogram (figure 2.23) and quantitative analysis of PAGE results (figure 2.23) obtained from piperidine treated samples are similar to those obtained from Fpg treated samples.

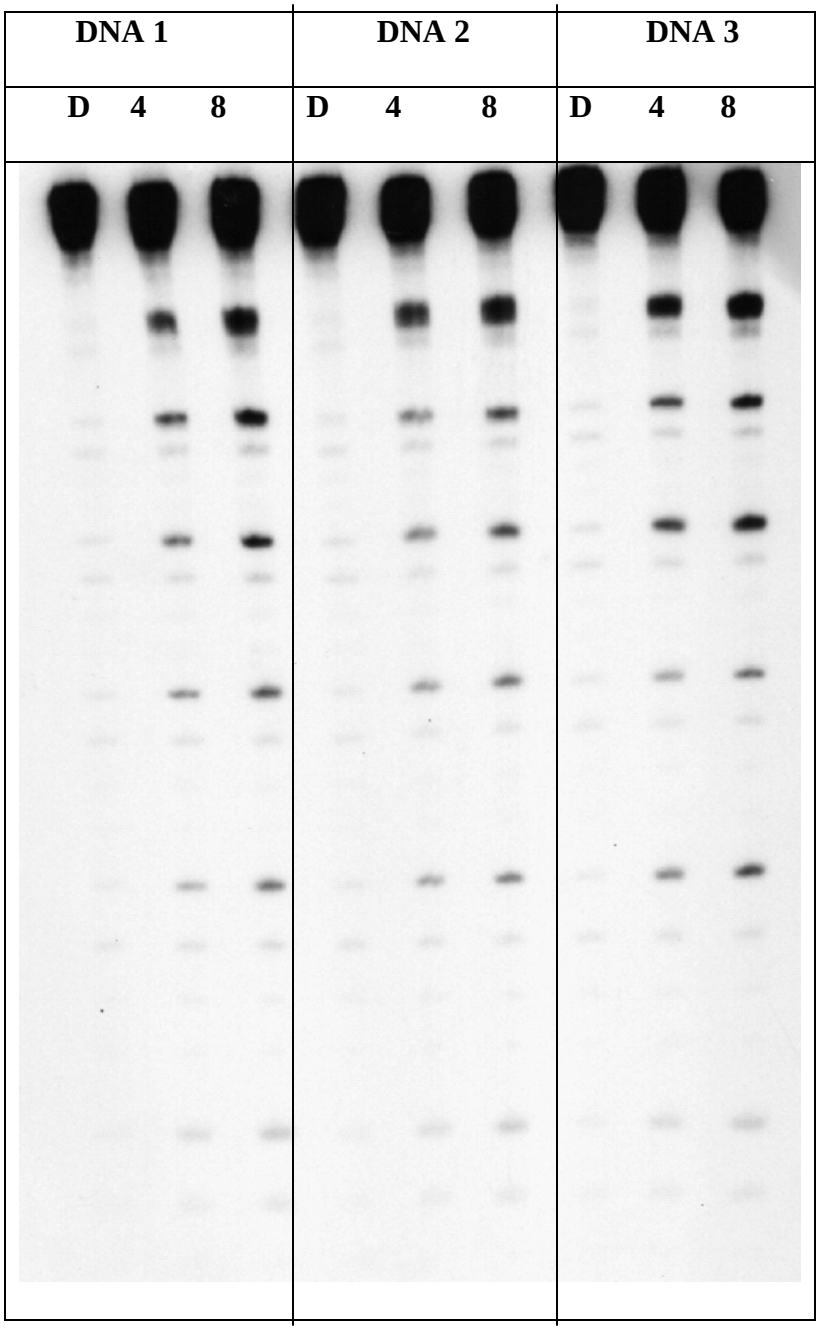

Figure 2.23: Autoradiogram obtained from PAGE of piperidine treated samples

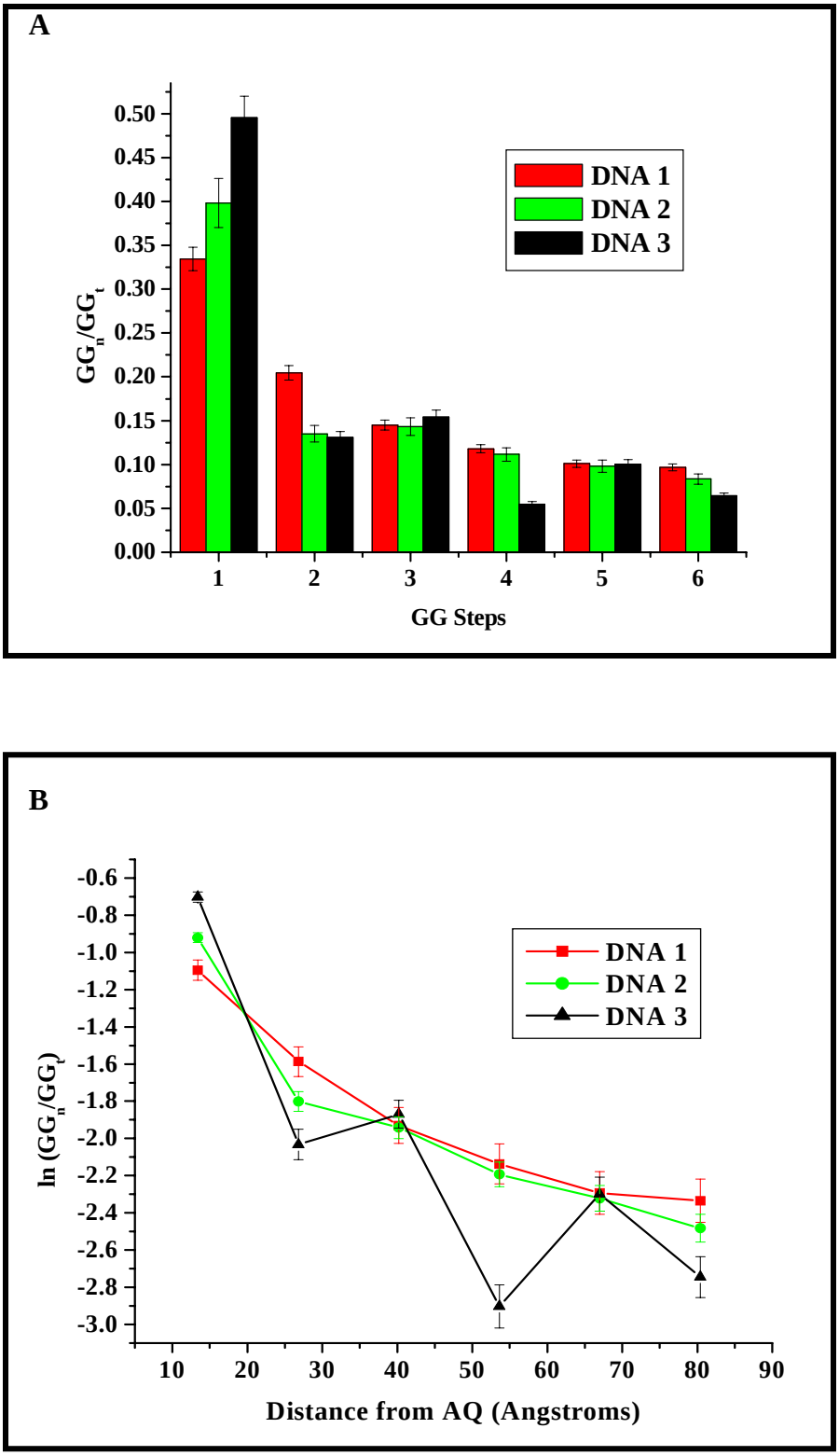

Figure 2.24: (A) Histogram representing the quantitative analysis of autoradiogram. X-axis represents the GG steps and Y-axis represents the relative damage at each step. (B) Plot of log of relative damage against the distance from AQ.

2.9.3 Fpg Labile Damage in Deoxygenated Condition

The deoxygenated condition was achieved by purging nitrogen through the samples for 30 minutes before irradiation. The autoradiogram (figure 2.25) and the quantitative analysis results (figure 2.26) are shown here.

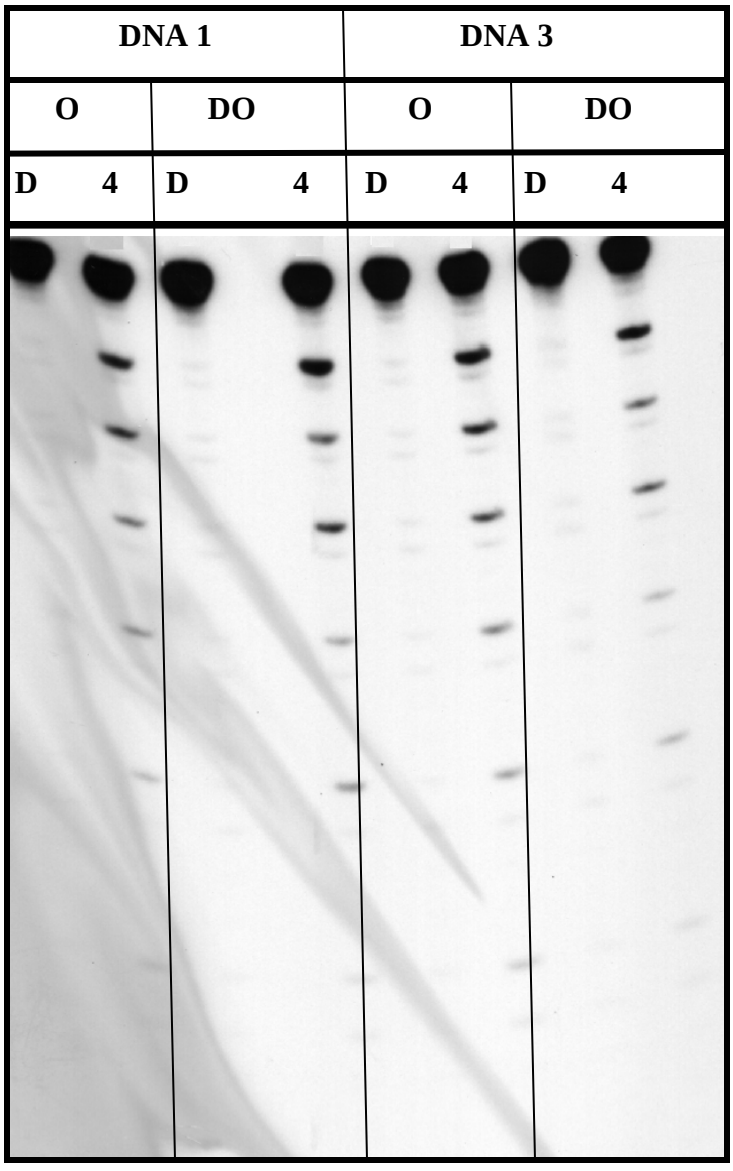

Figure 2.25: Autoradiogram obtained from Fpg treatment of deoxygenated samples. O and DO represents normal and deoxygenated samples respectively.

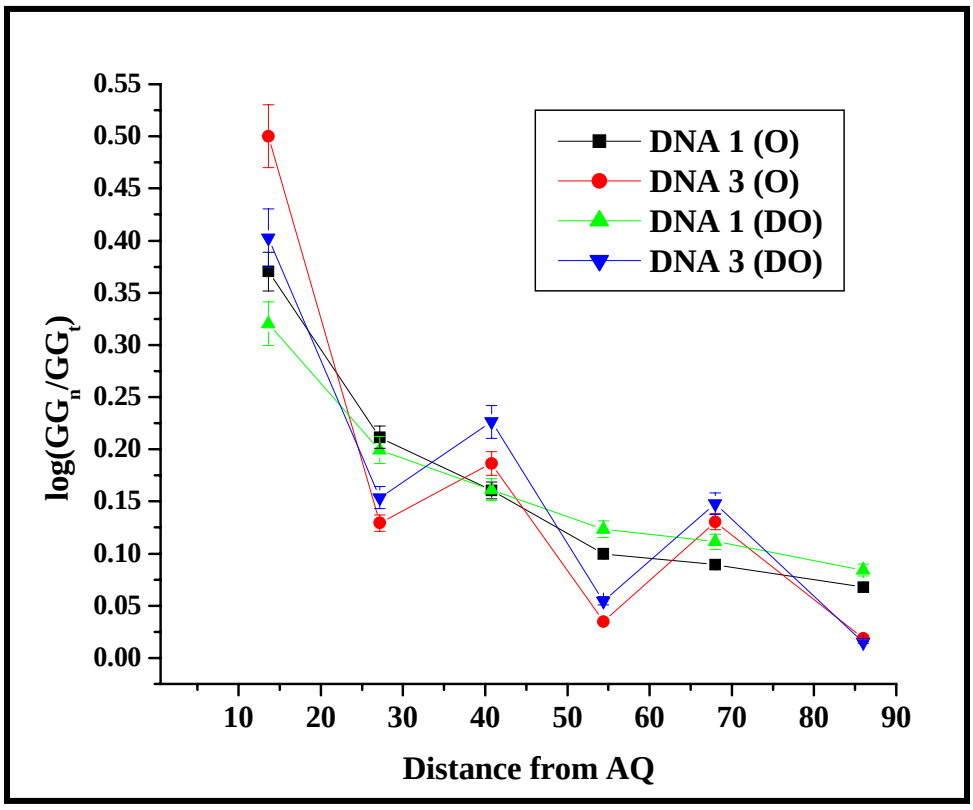

Figure 2.26: Plot of relative damage against the distance from AQ for DNA 1 and DNA 3 under normal and deoxygenated conditions. O and DO represents the normal and deoxygenated conditions respectively.

From the autoradiogram and the quantitative analysis it is clear that the pattern of guanine damage for these two duplexes are similar under normal and deoxygenated conditions. This indicates that the effect of F^5dC in reaction of guanine is independent of presence of oxygen.

2.9.4 Single Hit Condition

To make sure that the 4 and 8 minutes irradiations used in these experiments are within single hit condition (each base has been visited by radical cation only once), the relative damages at the six GG steps of DNA 1 for 4 and 8 minutes is plotted side by side. It is clear from this histogram that the relative damage at the GG steps does not depend

on the time of irradiation. This indicates that the experiments at 4 and 8 minutes irradiation are under single hit condition.

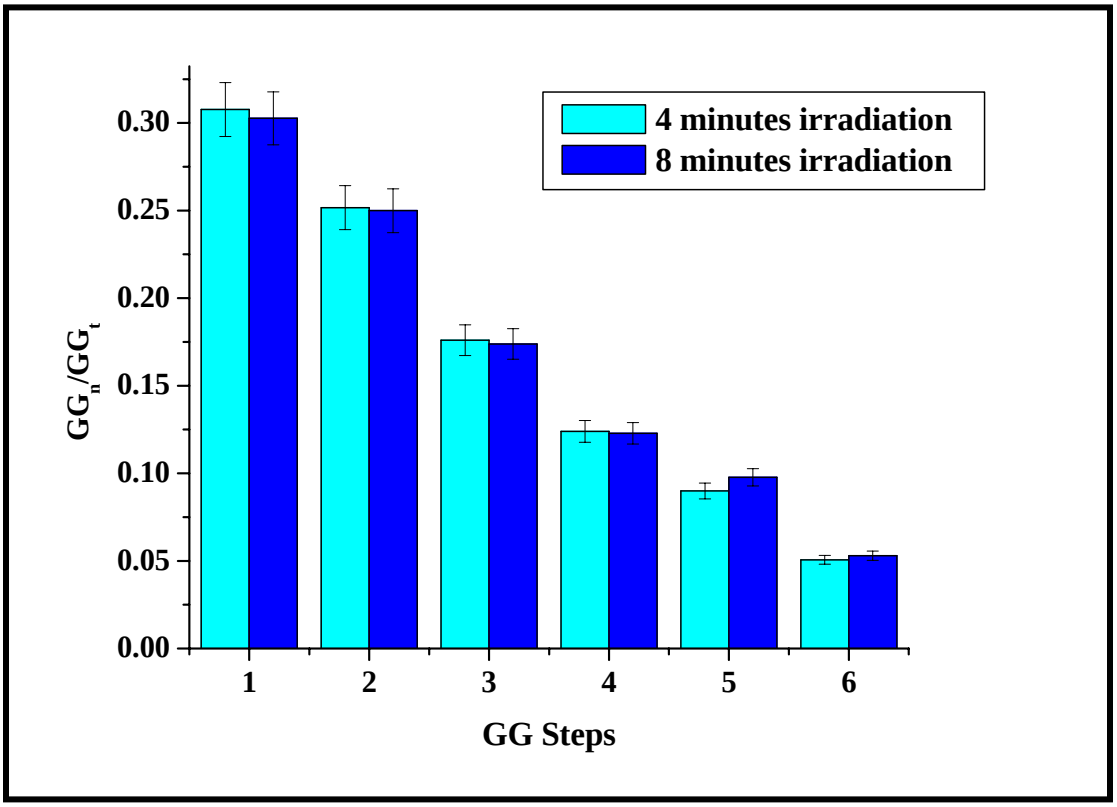

Figure 2.27: Histogram comparing the relative damage at the six GG steps of DNA 1 at 4 minutes and 8 minutes irradiation.

2.10 Discussion

The two most important observations from these experiments are (1) in F^5dC modified strands, presence of the modified base does not stop the migration of radical cation and (2) the guanine damage is decreased at the positions where there is F^5dC at the complementary strand.

DNA 2 has F^5dC opposite to the second GG step of the labeled strand. From the autoradiograms it is clear that the third, fourth, fifth and sixth GG steps are damaged.

And from the quantitative analysis it is evident that the relative damages at these GG steps are same as those for the unmodified duplex DNA 1, within experimental error. For DNA 3, there are F^5dC opposite to second, fourth and sixth GG steps and that do not change the damage at third and fifth GG steps compared to the unmodified strand.

These findings show that the efficiency of radical cation hopping from one GG segment to next is unaffected by the 50-fold decrease in basicity of cytosine that accompanies its fluorine substitution. On the other hand, the extent of damage at the GG steps, where there are F^5dC at the opposite strand, is decreased. So, this modification does influence the reactions of the complementary guanine radical cation with H_2O or O_2. These two observations have been summarized in figure 2.28.

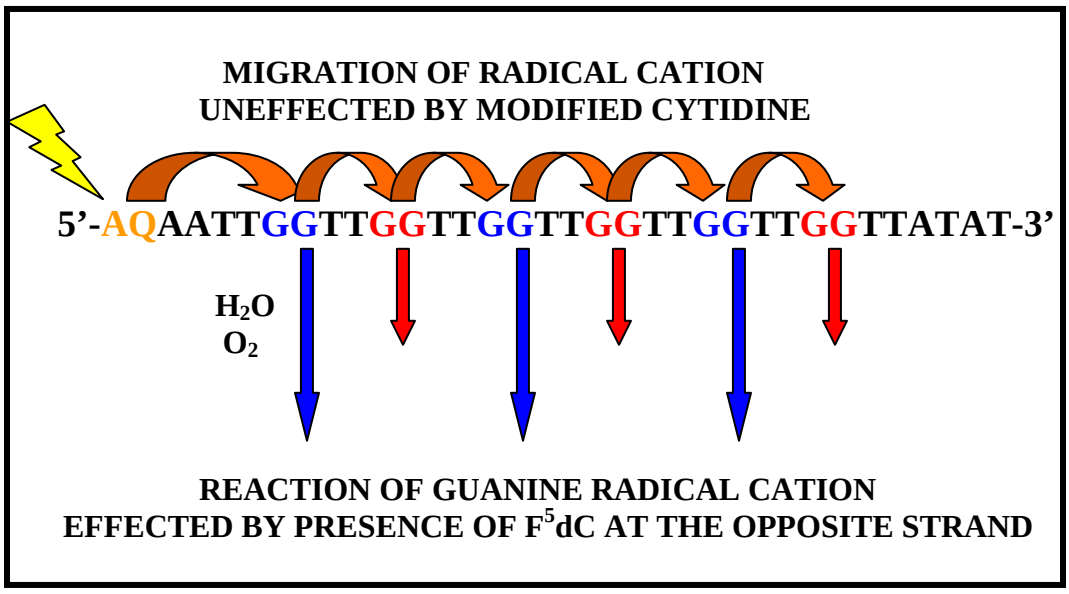

Figure 2.28: Effect of F^5dC on radical cation hopping and reaction of guanine radical cation with H_2O and O_2 in DNA 3. The guanines having F^5dC opposite to it are colored red, and the others are blue.

The role played by the imino N1 proton in charge migration in DNA and in reaction of the guanine radical cation is illuminated by these experiments. The reduced

basicity of F^5dC would inhibit hopping of the radical cation from one GG step to the next if this process is strongly coupled to proton transfer from guanine to cytosine. The experiments reported here show that substitution with F^5dC does not measurably affect the efficiency of hopping. This suggests that the N1 proton remains primarily on the guanine radical cation even in a normal G/C base pair, as was suggested by calculation.[13] In this case, the kinetic isotope effect observed in charge-transfer experiments carried out in D_2O solution[16] must involve other protons of the DNA or may be attributed to participation of water molecules tightly bound to the DNA.

In contrast, the Fpg induced strand cleavage at the damaged guanines is partially inhibited by the presence of F^5dC opposite to those guanines. There are two things that might lead to this inhibition of strand cleavage. First of all, the decreased basicity of F^5dC hydrogen bonded to those guanines may affect the reaction of guanine radical cation with H_2O and O_2. On the other hand, F^5dC may also influence the reactivity of Fpg, affecting the strand cleavage reaction. To investigate if the presence of modified cytidine affects the reactivity of Fpg, DNA1 and DNA 3 have been treated with equal amount of Fpg for 2, 4, 6 and 8 hours, after irradiation. The autoradiogram obtained from this experiment is shown in figure 2.29.Here, two samples are shown. The first is DNA1, which contains no modified 2'-deoxycytosine, the second is DNA3, which contains F^5dC at positions 2, 4 and 6 opposite the GG steps. Each sample (except for the dark controls, marked as D) was irradiated for 4 min (two lamps) under standard conditions. Following irradiation each sample was treated with an excess of Fpg. The samples were allowed to react at 37 °C in standard Fpg buffer solution and were stopped by denaturation at 90^o C after 2, 4, 6, and 8 h. High-resolution PAGE analysis (shown here) of each sample was carried out

according to the usual protocol. From the results it is evident that for all the six GG steps of both the strands, the amount of damage is same for all the time periods. This implies that the reaction of Fpg enzyme is complete within 2 hours for unmodified and modified strands and the presence of F^5dC does not affect the reactivity of Fpg.

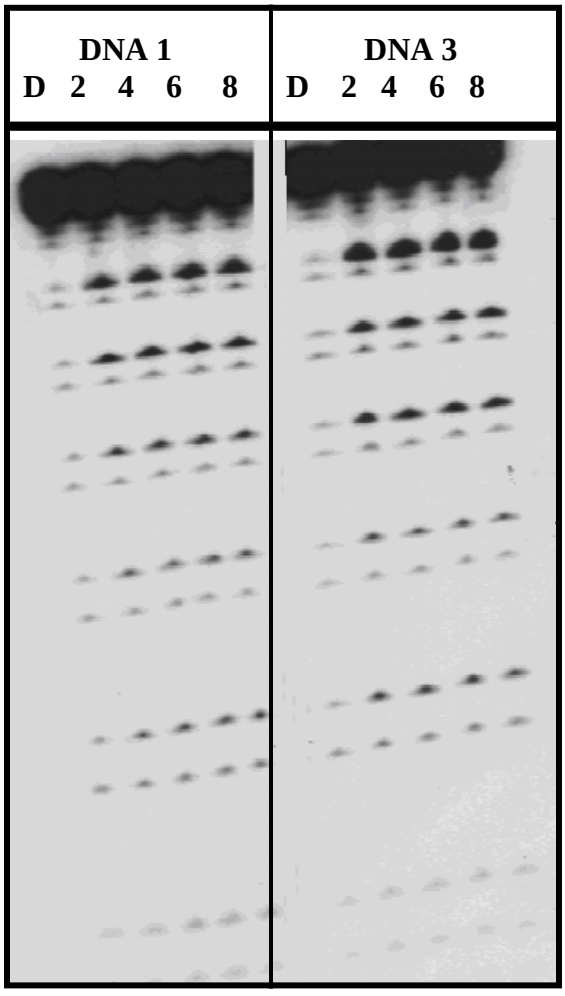

Figure 2.29: Autoradiogram showing F^5dC does not affect the reactivity of Fpg. D, 2, 4, 6 and 8 represent dark control and 2, 4, 6 and 8 hours of Fpg treatment.

It is clear that the presence of F^5dC affects the reaction of guanine radical cation with H_2O and O_2, not the reaction of Fpg with damaged nucleosides.. Apparently, proton transfer from the guanine radical cation to its cytosine partner plays an important role

when the DNA duplex and its immediate solvent environment are in a conformation that enables reaction to occur. Clearly, the decreased basicity of F^5dC shifts the equilibrium between the guanine radical cation and guanine radical and reduces the amount of guanine radical available for reaction with O_2 (figure 2.30), which may cause a concomitant reduction in the magnitude of trapping reaction, and thus a greater fraction of the radical cation will be consumed by the annihilation reaction (*k*a) that simply regenerates dG and reduces the amount of strand cleavage.

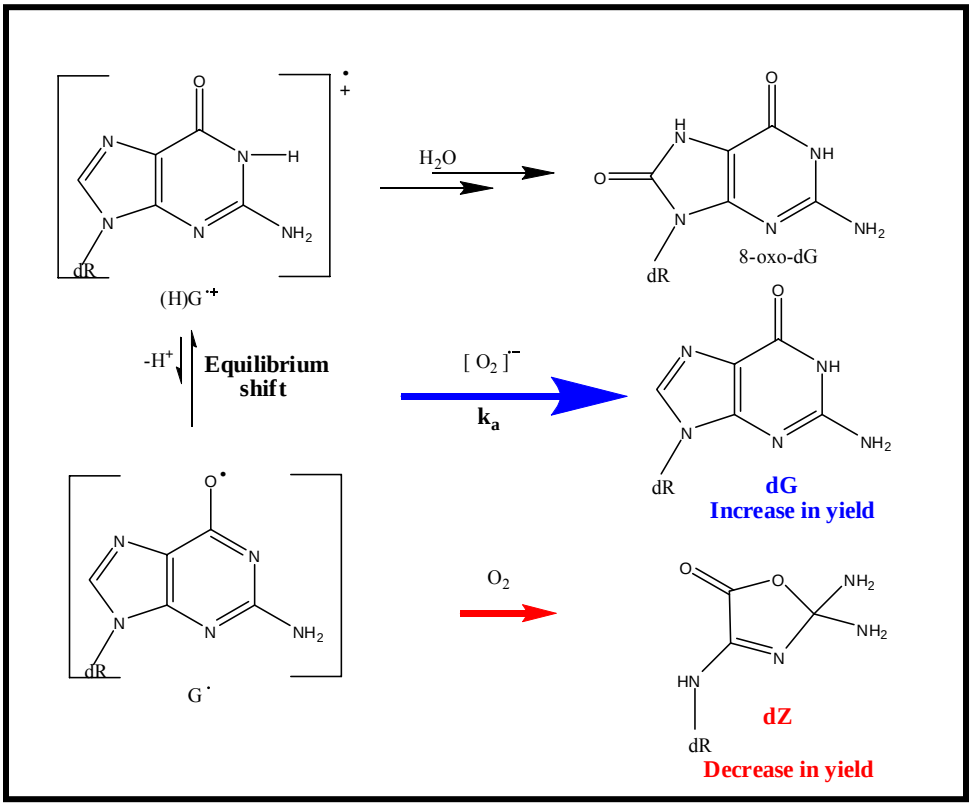

Figure 2.30: Equilibrium shift and decrease of Fpg labile damage in presence of F^5dC

2.11 Conclusion

It is well established that when a radical cation is generated in DNA, it migrates through the strands, leading the formation of guanine radical cations at the guanines.

These radical cations react with water or oxygen and leads to DNA damage. In this work, role of guanine N1 imino proton in the migration of radical cation and in the reaction of guanine radical cation has been examined.

The N1 imino proton of guanine radical cation is hydrogen bonded with N3 of cytidine and it can shift spontaneously to the cytidine N3. We investigated the effect of this proton transfer on charge migration and reactions by perturbing the proton transfer equilibrium. We have inserted 2'-deoxy-5-fluorocytidines (F^5dC) opposite to some guanines in a DNA duplex. The basicity of F^5dC is expected to be less than the normal cytidines and that will inhibit the proton transfer from guanine radical cation to cytidines.

We have chemically synthesized 5-fluorocytidine and by pK_a measurement proved that the basicity of this modified cytidine is much less than the normal cytidine. Although our effort to chemically synthesize F^5dC and insert that in DNA was not successful, we were able to insert *O*-TMP protected 5-fluorouracil into DNA and then convert it to F^5dC by simple ammonia treatment. These strands were purified by HPLC and characterized by Mass Spectroscopy.

Gel electrophoresis of UV irradiated and Fpg treated modified and unmodified DNA strands revealed very interesting results. First of all, presence of F^5dC opposite to certain guanines in the duplex does not stop the charge migration and it is evident from the observation that all the guanines in modified strands have been damaged. However, the extent of damage at the guanines having F^5dC opposite to them is affected. This observation implies that the F^5dC is affecting the reaction of guanine radical cation with water and oxygen.

From our experiments it is evident that the guanine N1 imino proton resides predominantly on guanine radical cation during the charge migration. On the other hand, decreased basicity of F^5dC changes the proton transfer equilibrium and decrease the amount of guanine radical available to react with oxygen to produce strand cleavage.[21]

The complexity of DNA is reflected in the analyses of the hopping and trapping reactions. For example, the replacement of normal cytidines by F^5dC may modify the base pair hydration environment or, operating through the hydrogen bonds, it may affect the electronic structure of the guanine.[22] However, neither of these effects is observed when 5-methyl-2'-deoxycytidines are paired with GG steps.[23] Clearly, the most significant consequence of replacing cytidines with F^5dC is the reduction in basicity, and the findings reported here are interpreted on this basis.

REFERENCES

1. Ly, D.; Kan, Y.; Armitage, B.; Schuster, G. B. *J. Am. Chem. Soc.* **1996**,*118*, 8747

2. Schuster, G. B. *Acc. Chem. Res.* **2000**, *33*, 253-260.

3. Giese, B.; Spichty, M.; Wessely, S. *Pure Appl. Chem.* **2001**, *73*, 449.

4. O'Neill, M. A.; Barton, J. K. *J. Am. Chem. Soc.* **2004**, *126*, 11471.

5. Lewis, F. D. *Photochem. Photobiol.* **2005**, *81*, 65.

6. Kawai, K.; Majima, T. *Pure Appl. Chem.* **2005**, *77*, 963.

7. Schuster, G. B. *Long-Range Charge Transfer in DNA I, II*; Springer-Verlag: Heidelberg, **2004**; Vol. 236, p 237.

8. Burrows, C. J.; Muller, J. G., *Chem. Rev.* **1998**, 98, (3), 1109-1152.

9. Kasai, Hiroshi; Yamaizumi, Ziro; Berger, Maurice; Cadet, Jean, *J. Am. Chem. Soc.* **1992**, 114, (24), 9692-9694.

10. Cadet, Jean; Douki, Thierry; Gasparutto, Didier; Ravanat, Jean-Luc, *Research/Fundamental and Molecular Mechanisms of Mutagenesis* **2003**, 531, (1-2), 5-23.

11. Candeias, L. P.; Steenken, S. *J. Am. Chem. Soc.* **1989**, *111*, 1094-1099.

12. Steenken, S. *Biol. Chem.* **1997**, *378*, 1293-1297.

13. Li, X.; Cai, Z.; Sevilla, M. D. *J. Phys. Chem. B* **2001**, *105*, 10115-10123.

14. Gervasio, F. G.; Laio, A.; Iannuzzi, M.; Parinello, M. *Chem. Eur. J.* **2004**, *10*, 4846-4852.

15. Gervasio, F. G.; Laio, A.; Parrinello, M.; Boero, M. *Phys. Re*V. *Lett.* **2005**, *94*, 158103.

16. Weatherly, S. C.; Yang, I. V.; Armistead, P. A.; Thorp, H. H. *J. Phys. Chem. B* **2003**, *107*, 372-378.

17. Shafirovich, V.; Dourandin, A.; Geacintov, N. E. *J. Phys. Chem. B* **2001**, *105*, 8431-8435.

18. Giese, B.; Wessely, S. *Chem. Commun.* **2001**, *2001*, 2108-2109.

19. Oeyelere et al; *J. Am. Chem. Soc.,.* **2000,** *122,* 10259

20. Liu, C.-S.; Hernandez, R.; Schuster, G. B. *J. Am. Chem. Soc.* **2004**, *126*, 2877-2884.

21. Ghosh, A. K.; Schuster, G. B *.J . Am. Chem. Soc.* **2006**, *128*, 4172-4173

22. Kawai, K.; Wata, Y.; Hara, M.; Tojo, S.; Majima, T. *J. Am. Chem. Soc.* **2002**, *124*, 3586-3590. These authors report a slightly accelerated rate constant for electron-transfer quenching in CH2Cl2 solution by a modified Br^5C/G base pair compared with C/G, which is attributed to a reduced E_{ox} for G in Br^5C/G. The p*K*a of C is reduced by bromine substitution.

23. Kanvah, S.; Schuster, G. B. *J. Am. Chem. Soc.* **2004**, *126*, 7341-7344.

CHAPTER 3

ONE ELECTRON OXIDATION OF DNA OLIGOMERS THAT LACK GUANINE

3.1 Introduction

Damage to DNA is caused by oxidative processes that result in loss of an electron and the concomitant generation of a radical cation that migrates through the nucleobases of the duplex by a hopping mechanism.[1-4] The radical cation is eventually trapped in a reaction with H_2O or O_2 that results in the conversion of a base to a mutated form. A defining characteristic of the one-electron oxidation of duplex DNA is reaction at G_n (n = 1-3) sites that is detected as strand cleavage following chemical or enzymatic treatment. It has been generally agreed that reaction occurs primarily at guanines because they have low oxidation potentials (E_{ox}),[5,6] which causes the migrating radical cation to pause there briefly, and this facilitates trapping.

Although, the hole migration and reactions in guanine containing DNA duplexes has been studied thoroughly, [1-6] the same process in only adenine and thymidine containing strands has been ignored mostly. There are only few reports on reactions of radical cations in DNA occur at bases other than guanine.[7] Analysis of the benzophenone sensitized oxidation of calf thymus DNA by GC-MS showed that the yield of the adenine oxidation product, 7,8-dihydro-8-oxoadenine, is a few percent of the 7,8-dihydro-8-oxoguanine yield, and cytosine and thymine oxidation products are formed in trace amounts.[8] Similarly, oxidation of DNA by photoionization with 193 nm light results primarily in reaction at G, but in "guanine poor regions", reaction at adenine is also observed.[9] These findings are consistent with the idea that relative oxidation potential

determines the reaction site because the E_{ox} of adenine is somewhat greater than that of guanine,[5] and pyrimidines T and C are considerably more difficult to oxidize than are the purines.[10] Indeed thymine, which has an E_{ox} of ca. 2.1 V vs NHE,[11] is the nucleobases that is most difficult to oxidize. However, Wagner[12] and co-workers report that photosensitized oxidation of DNA by a menadione (2-methyl-1,4-naphthoquinone) group that is linked covalently at an internal position causes reaction at nearby bases, including T. These discrete studies are not enough to draw any conclusion on the hole migration through A and T containing strands. Here we report a systematic study of charge migration through DNA strands that do not contain any guanines.

3.2 Oxidation Potential of Base

As we have mentioned before, it is believed that the oxidation potentials of the nucleoside bases plays an important role in oxidative DNA damage. In guanine containing sequences, because of the lowest (among the all for nucleotides) oxidation potential of guanine, the migrating radical cation pause momentarily there and react with H_2O and O_2 leading damage.[5,6] Although, the role of relative reactivity of the bases have not been explored much. Apart from discovering the charge migration and reactions at A-T rich region in DNA, these studies will confirm if the reaction at the nucleosides are totally based on their oxidation potentials. The oxidation potentials of the four bases are listed below (figure 3.1).

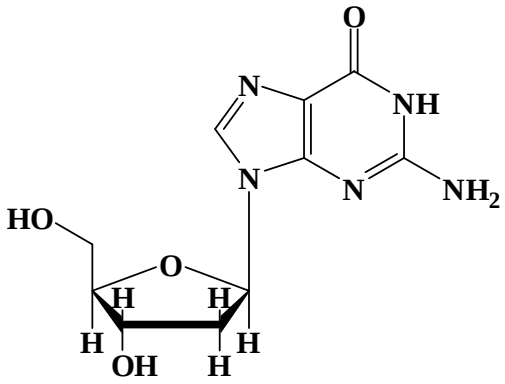

GUANINE
E_{OX} = 1.49 (vs NHE)

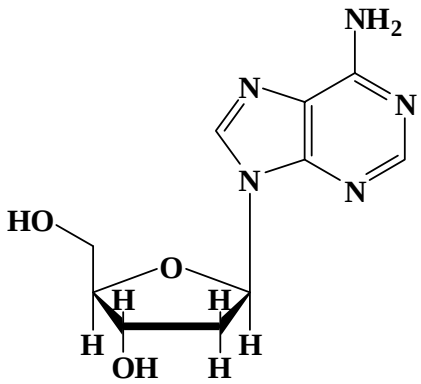

ADENINE
E_{OX} = 1.96 (vs NHE)

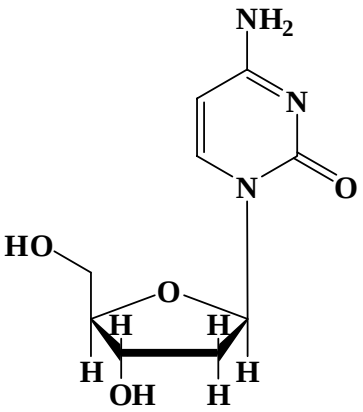

CYTOSINE
E_{OX}= 2.14 (vs NHE)

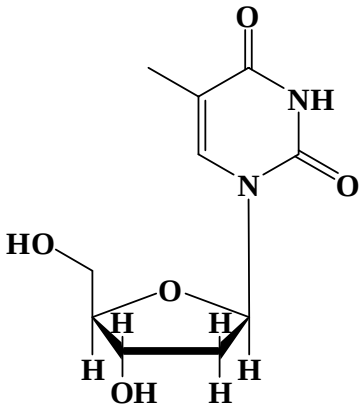

THYMIDINE
E_{OX}=2.11(vs NHE)

Figure 3.1 Oxidation potentials of the nucleosides measured by cyclic voltametry in acetonitrile. These values are estimated to be accurate to ± 0.05 V.[11]

It is evident from this table that, adenine has lower oxidation potential than thymidine. So, based on oxidation potential, the charge will reside momentarily at adenine during hole migration and oxidation reaction will lead damage at adenine.

3.3 Charge Migration in A-T Containing Sequences

3.3.1 The DNA Sequences

The DNA oligomers used for preliminary analysis have been listed in figure 3.2. DNA 1 consists of single strands S1 and S2, S1 has the anthraquinone charge injector (AQ) at the 5' end and S2 has alternate AA and TT segments. And one of the strands of DNA 2 has alternate TTT and AA segments (S4) and the other has the 5' anthraquinone (S3). As we have seen in the case of GG or GGG containing strands, when irradiated at 350 nm, the anthraquinone is expected to form AQ radical anion and the hole is expected to migrate through the bases of the DNA until it is trapped. Although, with DNA 1 and DNA 2, the trapping is expected to take place at the AA or AAA segments of either strands. DNA 3 is same as DNA 2 except it has a GG step after the AA and TTT steps.

DNA 1	**S1**	**5'-AQTTTTAATTAATTAATTAATATATTT-3'**
	S2	**3'-AAAATTAATTAATTAATTATATAAA-5'**
DNA 2	**S3**	**5'-AQTTTTAAATTAAATTAAATTAAATATATTT-3'**
	S4	**3'-AAAATTTAATTTAATTTAATTTATATAAA-5'**
DNA 3	**S5**	**5'-AQTTTTAAATTAAATTAAATTAAACCTATATTT-3'**
	S6	**3'-AAAATTTAATTTAATTTAATTTGGATATAAA-5'**

Figure 3.2 DNA oligomers used for preliminary experiments

3.3.2 Synthesis of DNA Oligomers

Nucleotide phosphoramidites for the oligomer synthesis were obtained from Glen research and used as received. These DNA oligonucleotides were synthesized in our laboratory by Dr. Abraham Joy on an Applied Biosystems Inc. Expedite DNA

Synthesizer and deprotected by ammonia treatment at 60 ^{0}C for overnight. These synthetic DNA oligonucleotides were purified by HPLC on a Hitachi 7000 HPLC system set with a Varian Dynamax 25x21.4 mm reverse-phase C-18 column using 5-20% Acetonitrile in 0.5 M Triethylammonium Acetate and then desalted. UV/Vis studies on DNA oligonucleotides were conducted at 260 nm on a Hewlett-Packard Spectrophotometer. The extinction coefficients of the oligomers were calculated using a biopolymer calculator, and their concentrations were determined from the absorbance at 260 nm. An adenine is substituted for the anthraquinone group in the extinction coefficient calculation. The mass of each oligonucleotide was determined by a Micromass Quattro Electrospray Ionization (ESI) mass spectrometer. . The mass spectrometry results are summarized in table 3.1 and it shows that we were able to synthesize the strands successfully.

Table 3.1: ESI MS analysis results of DNA oligomers S1-S6

DNA Strands	Expected Mass	Observed Mass
S1	**7990**	**7989**
S2	**7678**	**7678**
S3	**9243**	**9243**
S4	**8895**	**8895**
S5	**9811**	**9810**
S6	**9553**	**9551**

3.3.3 Characterization of DNA Oligomers

Thermal Denaturation

The thermal denaturation properties of DNA duplexes (DNA 1, 2 and 3) were characterized by UV absorption at 260 nm on a Cary 1E Spectrophotometer equipped with a multi-cell block, temperature controller and sample transport accessory. The first derivative of the absorbance vs. temperature curve gives the melting temperature of the DNA duplex. The DNA samples (5 μM DNA in 10 mM NaPi and 2 mM $MgCl_2$ solution at pH 7.0) are placed in a UV transparent quartz cell with a 1 cm path length and placed inside the Cary 1E Spectrophotometer. To verify the reversibility of the thermal transitions several temperature ramps from 25 to 90 ºC were investigated.

The results (Figure 3.3) show that all the three strands are forming stable duplexes at room temperature.

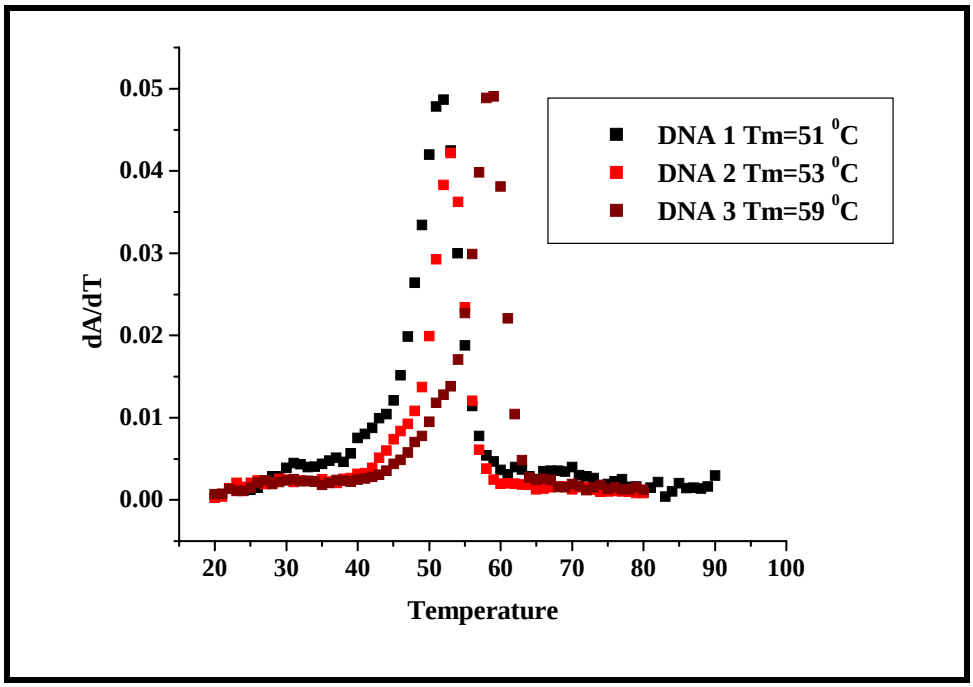

Figure 3.3: Plot of first derivative of absorbance against temperature for DNA 1 and DNA 2

Circular Dichroism

The secondary structure of DNA duplexes (1-3) were confirmed by circular dichroism (CD) experiment at room temperature on a JASCO-720 instrument. The exact samples used for the thermal denaturation experiments discussed above were used for the CD experiments. Under our experimental conditions the CD spectra of both the DNA molecules resemble B-DNA with no significant structural distortions (Figure 3.4).

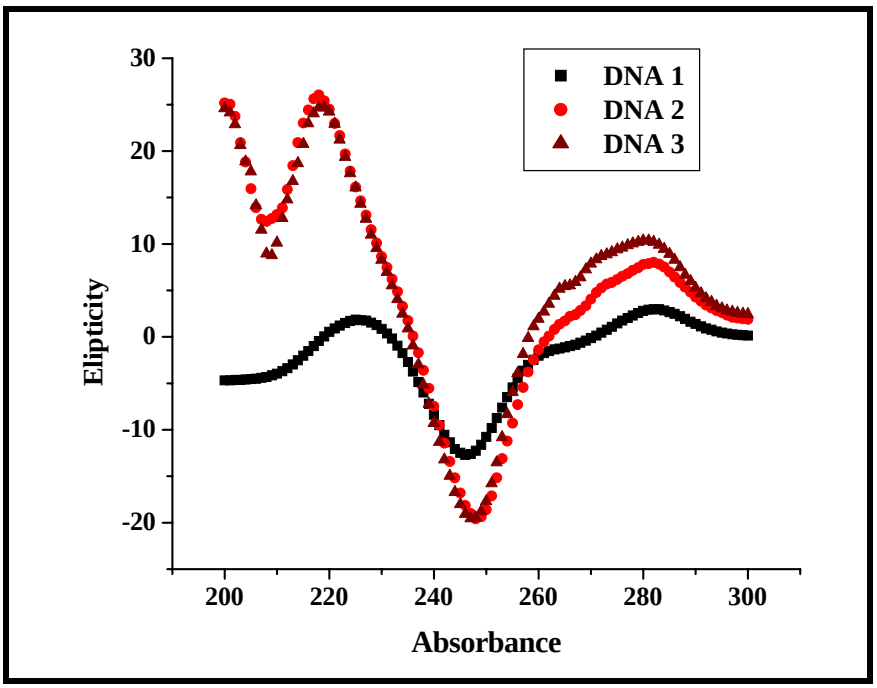

Figure 3.4: Circular dichroism spectra of DNA 1 and DNA 2

3.3.4 Preparation of Radiolabeled DNA

The DNA oligomers S2 and S4 were radiolabeled at the 5'-end using [γ-^{32}P]ATP and T4 PNK enzyme. A 5 µL sample of desired single stranded DNA was incubated with 1 µL of [γ-^{32}P]ATP and 2 µL of T4 PNK enzyme in a total volume of 20 µL at 37 ^{0}C for 45 min. After incubation, the DNA sample was suspended in a denaturing loading dye

and was purified on a 20% denaturing polyacrylamide gel. The desired DNA band was excised from the gel and eluted with 800 μL of elution buffer (0.5 M NH_4OAc, 10 mM $Mg(OAc)_2$/1.0 mM EDTA/0.1% SDS) at 37 ^{0}C for 12 h. The DNA was precipitated from the supernatant by addition of 600 μL of cold ethanol and 2 μL of glycogen. The mixture was vortexed, placed on dry ice for about 60 min, and centrifuged at 13000 rpm for 45 min. The supernatant was removed, and the residual DNA was washed with 100 μL of 80% ethanol and air-dried. Suitable volumes of water were added for further experimentation.

3.3.5 UV Irradiation and Gel electrophoresis

Samples for irradiation were prepared by hybridizing a mixture of unlabeled (5.0 μM) and radiolabeled (10000 cpm) oligonucleotides with complimentary AQ-linked DNA in sodium phosphate buffer solution at pH 7.0. Hybridization was achieved by heating the samples at 90 ^{0}C for 10 min, followed by slow cooling at room temperature for 3 h. Samples were irradiated at ca. 30 ^{0}C in microcentrifuge tubes in a Rayonet Photoreactor (Southern New England Ultraviolet Co., Bransford, CT) equipped with two 350 nm lamps. After irradiation, the samples were precipitated once with cold ethanol (100 μL) and 2 μL of glycogen. The precipitated samples were washed twice with 100 μL of 80% ethanol and dried. To identify the adenine damages[13] the dry DNA's were dissolved in 14 μL water and 2 μL of NaPi buffer (100 mM), 2 μL of NaCl (1M) and 2 μL of Na_2IrCl_6 (100 μM) were added to it. After 60 minutes of reaction at 37 ^{0}C, 2 μL of HEPES (20 mM) and 2 μL of EDTA (100 mM) were added to it to quench the reaction. Then the DNA was again precipitated from cold ethanol and dried. These samples were treated with 50 μL piperidine and heated at 90 ^{0}C for 30 minutes. Then the piperidine was

evaporated out and the samples were dissolved in denaturing loading dye and subjected to 20% 19:1 polyacrylamide gel electrophoresis. The gels were dried, and the cleavage sites were visualized by autoradiography.

3.3.6 Results and Discussion

The autoradiogram obtained from this experiment is shown in figure 3.5.

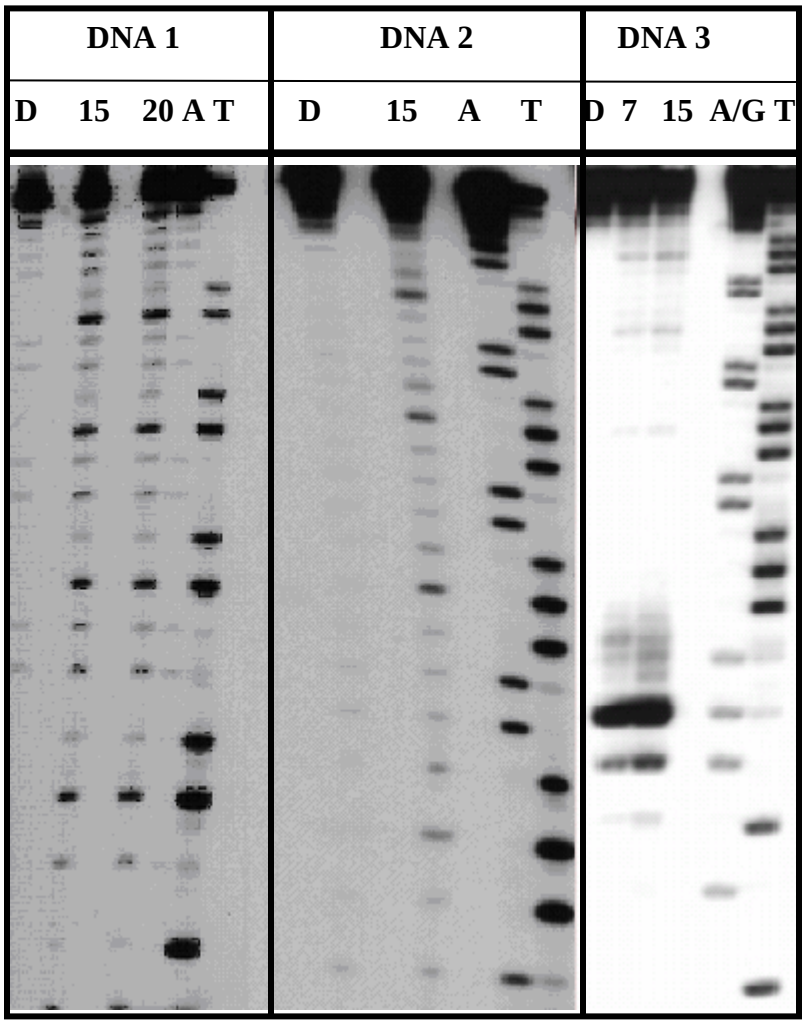

Figure 3.5: Autoradiogram showing the damage pattern in A-T containing strands. D, 7, 15, 20 represent 0, 7, 15 and 20 minutes of irradiation. A, A/G and T represents A, A and G and T sequencing lanes respectively.

For both the strands D represents the dark control and 15 and 20 represents 15 and 20 minutes of irradiation with eight lamps. A, T represent A and T sequencing lanes. It is evident from the autoradiogram that the damage is predominantly at the thymidines, not at the adenines. In DNA 1, the 5'-thymidines of the four 3'-TT-5' segment is damaged, with little damage at the 3'-thymidines. On the other hand, for DNA 2, the damage is predominantly on the middle thymidines of all 3'-TTT-5' segments, with little damage at the 3'-thymidines. DNA 3 is similar to DNA 2 except that it contains a GG step positioned directly after the fourth TTT site. Compared with DNA 2, the irradiation of DNA 3 shows a nearly complete absence of strand cleavage at the thymines. Instead, reaction occurs primarily at the 5'-G of the GG step, which is ca. 82 Å from the initial position of the radical cation. Since irradiation times are the same, the relative reaction efficiencies at the GG step and the TTT sites are comparable. In DNA 1 and DNA 2, the radical cation is trapped at a thymine, in DNA 3, the radical cation hops through the A/T base pairs and reacts at the remote guanines.

Remarkably, for these oligomers lacking guanines, one-electron oxidation results in reaction primarily at thymine even though adenine has a significantly lower E_{ox}. This is a circumstance that is readily understood by application of the Curtin-Hammett principle.[14] It is not the most stable (i.e., lowest E_{ox}) species in the equilibrated distribution of the radical cation among various locations on the oligomer that gives the major product but the one with the highest reactivity (i.e., reaction path with the lowest barrier). Evidently, the rate of irreversible radical cation trapping at T is much greater than it is at A, and it is this feature that controls the outcome of the reaction. The observation that a remote GG step inhibits reaction at preceding thymines shows that

hopping from (TTT/AAA) to (TTT/ AAA) through an (AA/TT) "bridge" is faster than trapping at T; however, trapping of the radical cation at the GG step is far more efficient than it is at a T.[15] In other words, in the DNA oligomers that lack guanines, the radical cation "visits" each T many times and will eventually react there, but the migrating radical cation much less frequently escapes encounters with the GG step.

3.4 Distance Dependence of Thymidine Damage

We have shown that in DNA oligomers containing TT segments (DNA 1) or TTT (DNA 2) segments separated by AA spacers, the Thymidines are damaged predominantly and there is an approximately equivalent amount of reaction at each of the TT (DNA 1) and TTT (DNA 2) sites, which indicates that in this case the rate of the radical cation hopping reaction is faster than trapping. The well-known guanine damage has typical distance dependence properties depending on the nature and number of bases between the reactive GG or GGG segments, which gives a clear idea on the relative rates of hopping and trapping.[15] In this part of our study we tried to investigate the distance dependence properties of thymidine damage.

3.4.1 The DNA Oligomers

The following strands have been designed for the distance dependence study of thymidine damage. For the DNA duplexes DNA 4, 5 and 6, one of the single strands (S8, S10 and S12) have four TTT or TT steps separated by different spacers. In S8 the TTT steps are separated by ATA spacers, and in S9 and S10 the TT's are separated by ATA and ATATA spacers respectively. For all the duplexes the complementary strands contain the anthraquinone charge injector.

DNA 4	**S7**	**5'-AQTTTTAAATATAAATATAAATATAAATATATTT-3'**
	S8	**3'-AAAATTTATATTTATATTTATATTTATATAAA-5'**
DNA 5	**S9**	**5'-AQTTTTAATATAATATAATATAATATATTT-3'**
	S10	**3'-AAAATTATATTATATTATATTATATAAA-5'**
DNA 6	**S11**	**5'-AQTTTTAATATATAATATATAATATATAATATATTT-3'**
	S12	**3'-AAAATTATATATTATATATTATATATTATATAAA-5'**

Figure 3.6: DNA oligomers for distance dependence study. The TTT and TT steps have been underlined and the spacers are colored blue.

3.4.2 Synthesis and Characterization of DNA Strands

The DNA single strands were synthesized and purified according to the procedure described earlier (chapter 3.3.2). These strands were characterized by mass spectrometry, Melting temperature and circular dichroism studies. All the concentrations and compositions were same as chapter 3.3.3. The results show that the strands have been synthesized properly and these strands form stable B-type DNA duplex at room temperature.

Table 3.2 ESI MS analysis results of DNA oligomers S7-S12

DNA Strand	Expected Mass	Calculated Mass
S7	10182	10182
S8	9807	9806
S9	8930	8929
S10	8688	8588
S11	10781	10781
S12	10441	10440

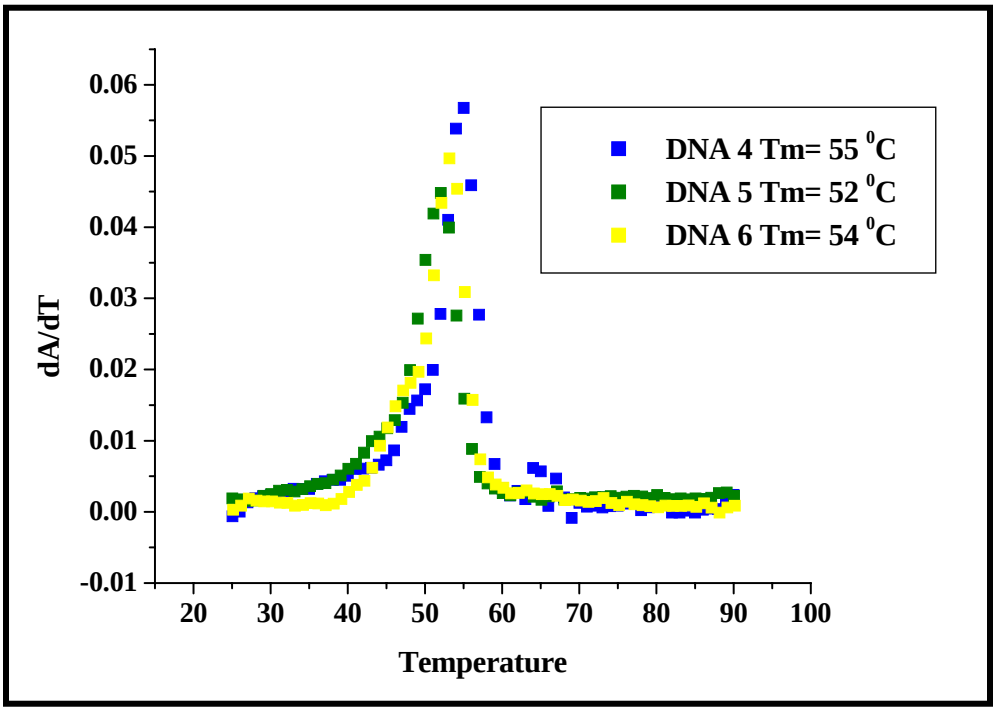

Figure 3.7: Melting temperature study of DNA 4, 5 and 6. The rate of change of absorption at 260 nm has been plotted against the temperature.

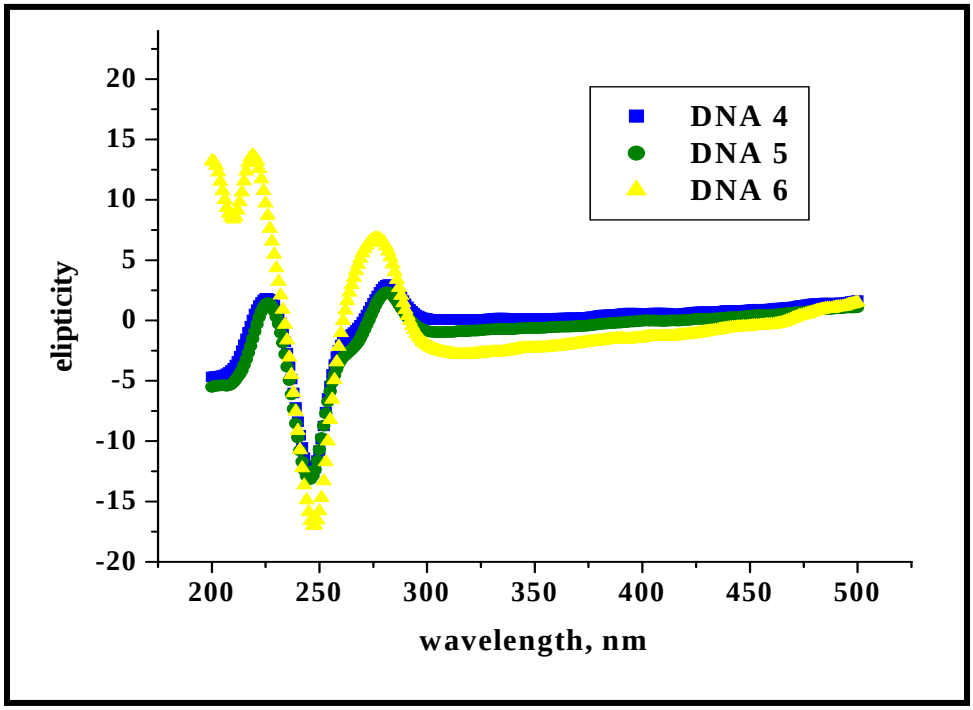

Figure 3.8: Circular dichroism spectra for DNA 4, 5 and 6

3.4.3 Preparation of Radiolabeled DNA & Gel electrophoresis

The DNA strands were radiolabeled by P32 using the same procedure described in chapter 3.3.4 and the gel electrophoresis experiments were run in accordance of chapter 3.3.5.

3.4.4 Quantitative Analysis through Phosphorimagery

Quantification of the amount of DNA damage at each TT step, which is relative to the efficiency of charge transfer through DNA, is accomplished by reading the gel image in a FUJI phosphorimager. The gel is exposed to a FUJI imaging plate, and read in the FUJI 2340 BAS-Image system. ImageGuage software is then used to determine the relative intensity of radiolabel at each TT step, revealed as dark spots in the

autoradiogram. This relative intensity is directly related to the amount of DNA oligomer at the position on the gel.

3.4.5 Results and Discussion

In the first experiment, the damage pattern of DNA 2 (see, figure 3.2) was compared with the same of DNA 4. DNA 2 has four TTT steps separated by AA spacers and DNA four has four TTT steps separated by ATA spacers. The autoradiogram obtained from this experiment is shown in figure 3.9.

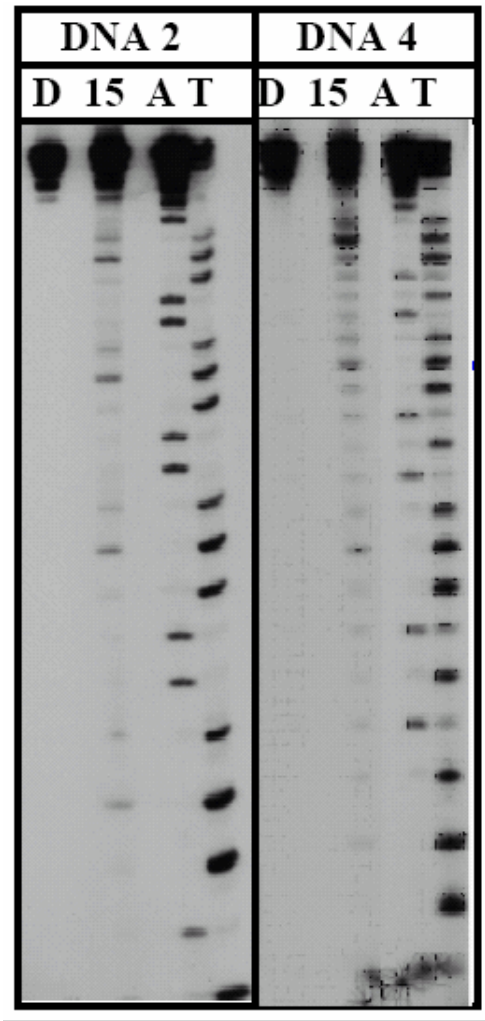

Figure 3.9: Autoradiogram showing the damage patterns of DNA 2 and DNA 4. D and 15 represents 0 and 15 minutes of irradiation, A and T represents A and T sequencing lanes.

The next experiment was carried out to investigate the relative damage pattern of DNA 1, DNA 5 and DNA 6.These strands have four TT steps separated by AA, ATA and ATATA spacers respectively. Figure 3.10 represents the autoradiogram obtained from this experiment.

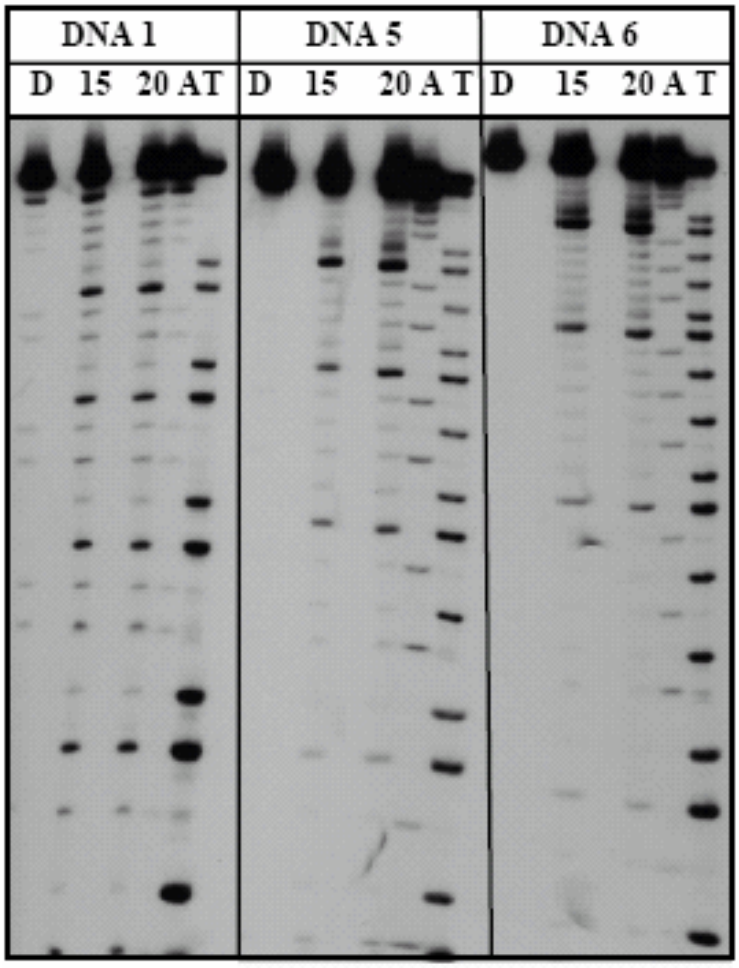

Figure 3.10: Autoradiogram representing the damage patterns of DNA 1, DNA 5 and DNA 6. D, 15 and 20 represent 0, 15 and 20 minutes of irradiation respectively. A and T represent A and T sequencing lanes.

The quantitative analysis results of these two experiments have been shown in table 3.3. And figure 3.11 shows the semilog plot representing the distance dependence of these five DNA strands.

Table 3.3: Results obtained from phosphor image of PAGE autoradiogram in distance dependence study of thymidine damage. T1, T2, T3, and T4 indicate four TTT(for DNA 2 and DNA 4) and TT(for DNA 1, DNA 5 and DNA 6) steps. Relative damage indicates the ratio of damage at that site to the total damage in that strand.

DNA	Relative Damage				Slope of semilog plot	k_{ratio}
	T1	T2	T3	T4		
DNA 1	0.31	0.25	0.23	0.20	-0.009 ± 0.001	20
DNA 2	0.33	0.23	0.23	0.20	-0.009 ± 0.002	20
DNA 4	0.48	0.24	0.18	0.11	-0.02 ± 0.002	10
DNA 5	0.47	0.23	0.18	0.12	-0.02 ± 0.004	10
DNA 6	0.58	0.24	0.13	0.05	-0.03 ± 0.001	3

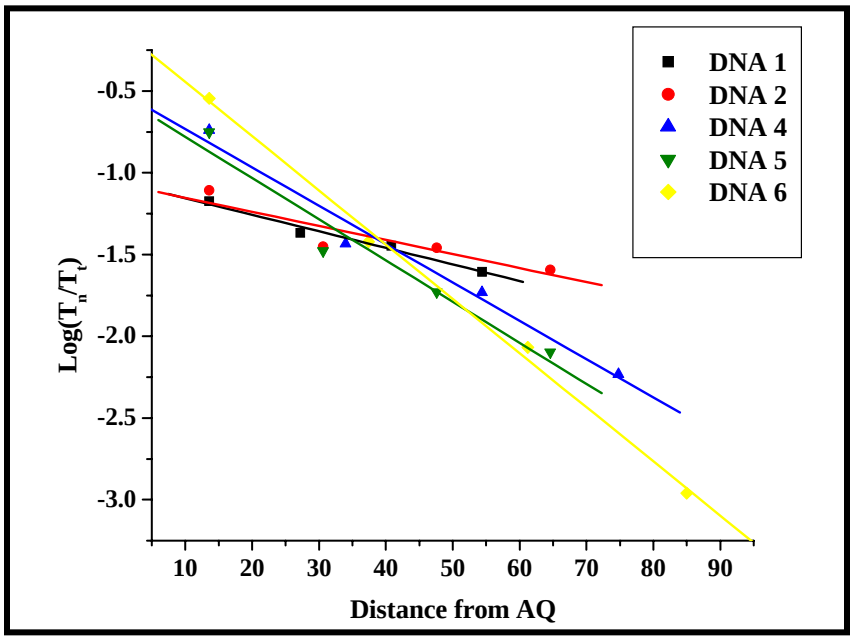

Figure 3.11: Semilig plot of distance from AQ against the log of relative damage at each TTT (for DNA 2 and DNA 4) and TT (for DNA 1, DNA 5, DNA 6) sites. T_n/T_t indicates the ratio of damage at a particular site to the total damage in that strand.

There are obvious patterns in this data that depend upon the relative magnitudes of rate of hopping (k_{hop}) and the rate of trapping (k_{trap}). These experiments provide the data to calculate a unitless parameter, k_{ratio}, which is the ratio of k_{hop} to k_{trap}.

As described earlier, for DNA 2, the damage is on the middle T predominantly and the 3'-T is damaged also, and there is not much distance dependence indicating a much higher k_{hop} than k_{trap}. In DNA 4, where the TTT segments are separated by ATA segments, the damage pattern is same. But, the semilog plot of the amount of reaction observed at TTT steps of DNA 4 versus the distance from the AQ is apparently linear with a slope of 0.02 ± 0.002 A^{-1} (Figure 3.11). Thus, in this case k_{hop} does not completely overwhelm k_{trap}.

Investigation of the other set of DNA oligomers, DNA 1, DNA 5 and DNA 6, where TT segments are separated by AA, ATA and ATATA segments respectively, reveals similar results. For these oligomers, the predominant damage is at the 5'-T (67%) and there is more than one damage at 3'-T indicating multiple products at that site. In each of these cases, the irreversible trapping reaction competes kinetically with radical cation migration, as indicated by obtaining non-zero slopes from the semilog plots of reaction versus distance (Table 3.3 and Figure 3.11). The slope of the line showing the distance dependence for reaction of DNA 1 is less than the slope for DNA 5, which is in turn less than DNA 6.

These experiments show that the distance dependence of thymidine damage is similar to that of the well known guanine damage[15]. This indicates that the radical cation migrates through the DNA oligomers lacking guanine and reacts at TTT or TT sites in a similar way as it does in the case of guanine containing strands where it reacts at $(G)_n$

sites. That is the thymidine damages obtained in these experiments are resulting from one electron hole migration from the anthraquinone charge injector, any other process is not involved in here.

3.5 Role of the C5-Methyl Group in Thymidine Damage

From the previous two chapters it is clear that the reaction is taking place at the thymidines by long range charge migration through the DNA strands containing only A and T. The next things to be investigated are the exact reactions involved in thymidine damage and the mechanism of these reactions. Radical formation and oxidation at the thymidine C5-methyl is known[16]. So, we decided to check first if that methyl group is playing any role in the thymidine reaction.

3.5.1 The DNA Oligomers

To investigate the role of C5-methyl of thymidine in thymidine reactions and damage, we designed the following strands (figure 3.12). These strands are similar to the strands used in the previous experiments, only some of the thymidines (T) have been replaced by 2'-deoxyuridines (U). The only difference between thymidine and 2'-deoxyridine is the C5-methyl group (see, figure 3.12) and the relative damage pattern of thymidine and deoxyuridines containing strands will reveal the role of that methyl group in thymidine damage.

DNA 7 consists of single strands S3 and S13. S13 is similar to S4; only the first and third TTT steps have been replaced by UUU steps. DNA 8 consists of S1 and S 14. S 14 is similar to S2, only it has alternate 3'-UT-5' and 3'-TU-5' steps in place of the four 3'-TT-5' steps. DNA 9 has all possible two base combinations with T and U, i.e. 3'-TT-5', 3'-UT-5', 3'-TU-5' and 3'-UU-5'. DNA 10 and DNA 11 have all possible three base

combinations, i.e. 3’-TTT-5’, 3’-UTT-5’, 3’-TUT-5’, 3’-TTU-5’, 3’-UUT-5’, 3’-UTU-5’, 3’-TUU-5’ and 3’-UUU-5’.

DNA 7	**S3**	**5’-AQTTTTAAATTAAATTAAATTAAATATATTT-3’**
	S13	**3’-AAAAUUUAATTTAAUUUAATTTATATAAA-5’**
DNA 8	**S1**	**AQ 5’-TTTTAATTAATTAATTAATATATTT-3’**
	S14	**3’-AAAATUAAUTAATUAAUTATATAAA*-5’**
DNA 9	**S1**	**AQ 5’-TTTTAATTAATTAATTAATATATTT-3’**
	S15	**3’-AAAAUTAATTAATUAAUUATATAAA*-5’**
DNA 10	**S3**	**AQ 5’-TTTTAAATTAAATTAAATTAAATATATTT-3’**
	S16	**3’-AAAAUTTAAUTUAATTUAATUTATATAAA*-5’**
DNA 11	**S3**	**AQ 5’-TTTTAAATTAAATTAAATTAAATATATTT-3’**
	S17	**3’-AAAAUUTAAUUUAATUUAATTTATATAAA*-5’**

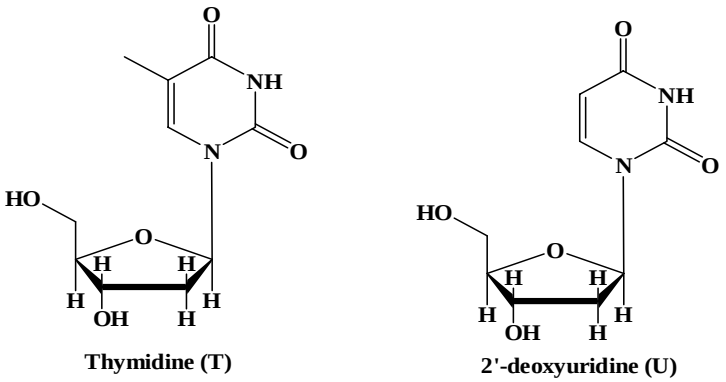

Figure 3.12: DNA oligomers for investigating the effect of C5-methyl group

3.5.2 Synthesis and Characterization of DNA strands

The DNA single strands were synthesized and purified according to the procedure described earlier (chapter 3.3.2). These strands were characterized by mass spectrometry, Melting temperature and circular dichroism studies. All the concentrations and compositions were same as chapter 3.3.3.

Table 3.2: ESI MS analysis results of DNA oligomers S13-S17

DNA Strand	Expected Mass	Observed Mass
S13	8497	8496
S14	7620	7620
S15	7620	7620
S16	8825	8824
S17	8797	8796

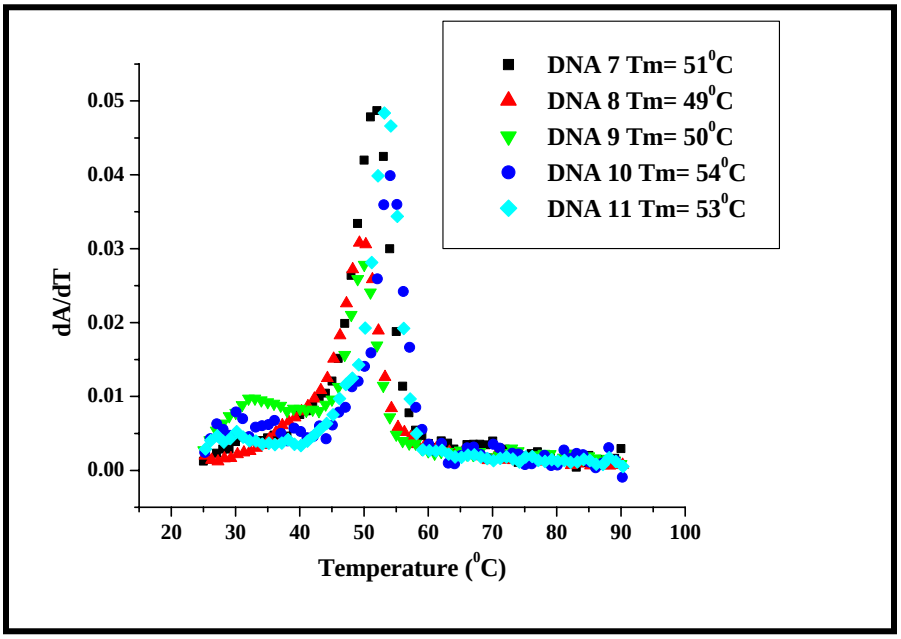

Figure 3.13: Melting temperature of DNA7-DNA11

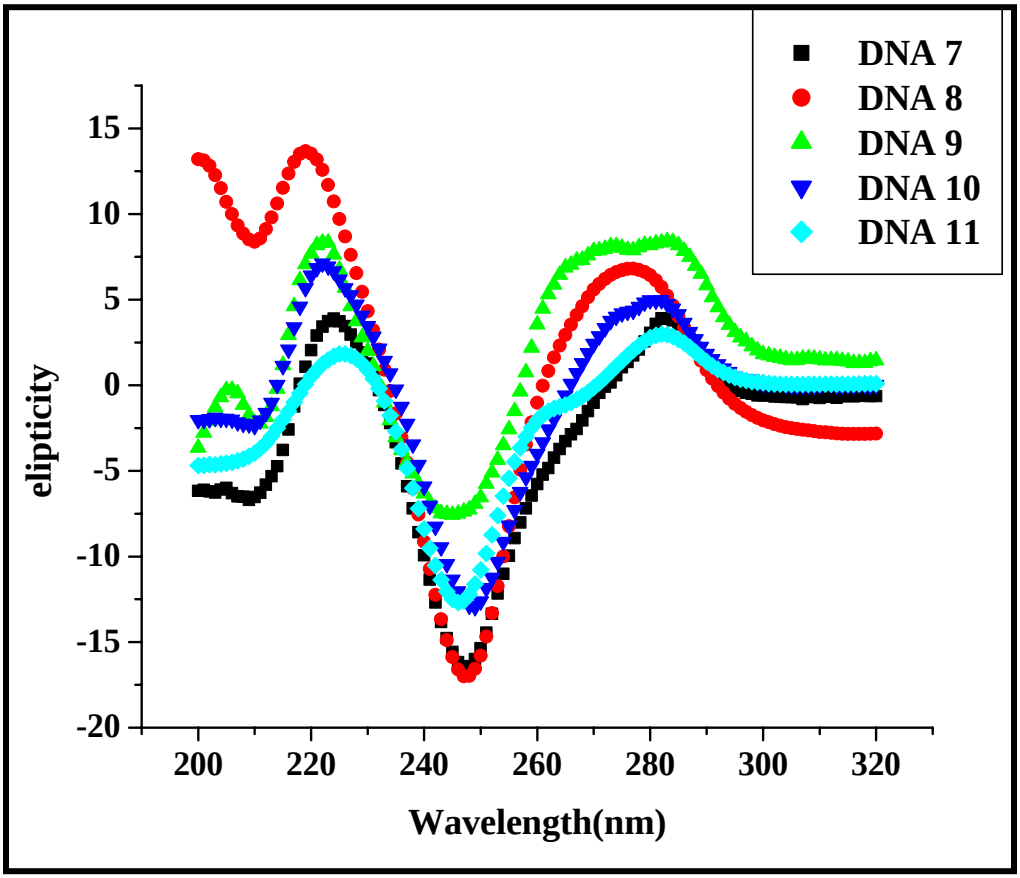

Figure 3.14: Circular dichroism spectra for DNA 7-11

From the mass spectrometry results it is clear that the single strands were synthesized properly. The melting temperature analysis and circular dichroism spectra show that all the DNA's form stable B form DNA duplexes.

3.5.3 Preparation of Radiolabeled DNA & Gel electrophoresis

The DNA strands were radiolabeled by P32 using the same procedure described in chapter 3.3.4 and the gel electrophoresis experiments were run in accordance of chapter 3.3.5. For ECORIII treatment, after irradiation and precipitation 6 μL ECORIII enzyme, 4 μL ECORIII buffer (10x rxn buffer 4) and 10 μL water was added to the

samples. Then those were kept at 37^0C for overnight and reprecipitated with ethanol before loading into the gel.

3.5.4 Quantitative Analysis through Phosphorimagery

Quantification of the amount of DNA damage at each TT step, which is relative to the efficiency of charge transfer through DNA, is accomplished by reading the gel image in a FUJI phosphorimager. The gel is exposed to a FUJI imaging plate, and read in the FUJI 2340 BAS-Image system. ImageGuage software is then used to determine the relative intensity of radiolabel at each TT step, revealed as dark spots in the autoradiogram. This relative intensity is directly related to the amount of DNA oligomer at the position on the gel.

3.5.5 Results and Discussion

In the first experiment we investigated the relative damage patterns of DNA2 and DNA 7. DNA 2 has four 3'-TTT-5' steps separated by AA steps in one of its strands. On the other hand, DNA 7 has two 3'-UUU-5' and two 3'-TTT-5' steps in one of its strands. The autoradiogram for this experiment has been shown in figure 3.15. As described in the previous chapters, the middle T's of each of the 3'-TTT-5' are damaged predominantly, with little damage at 3'-thymidines. And this is true for both the strands. Interestingly, the scenario is totally different for 3'-UUU-5' segments; there is no damage in these parts. This indicates that the C5-methyl group plays an important role in the thymidine reactions and absence of it stops the reaction. Although, this does not stop the hole migration, the 3'-TTT-5' steps after the 3'-UUU-5' has been damaged normally. However, the exact role played by the methyl group and the mechanism of the reactions are not clear from this experiment.

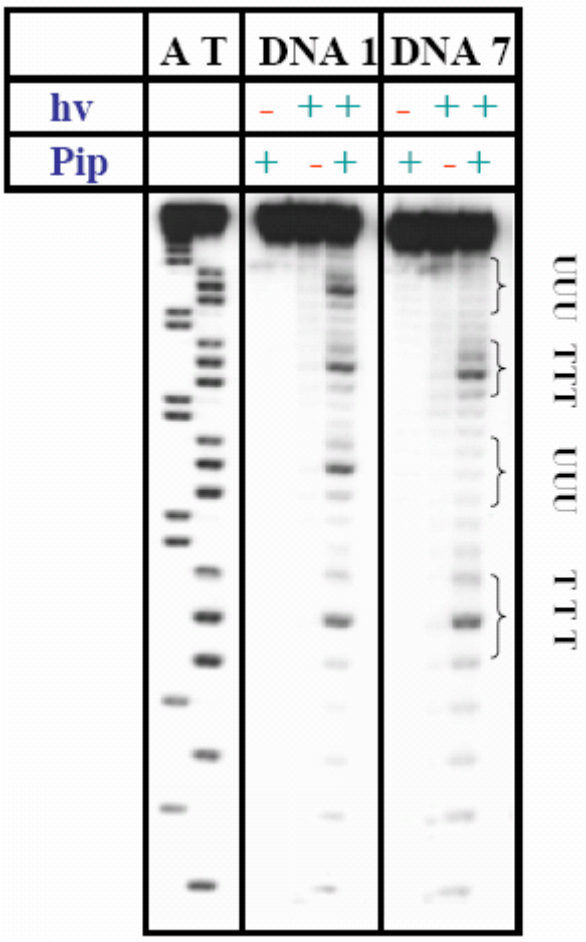

Figure 3.15: Autoradiogram showing the importance of C5-methyl group of thymidines in the reactions leading to its damage in DNA. hv indicates the irradiation and pip indicates piperidine. A and T indicates A and T sequencing lanes for DNA 1. The 2'-deoxyurdines and thymidines are indicated as U and T in DNA 7.

To figure out the exact role played by the C5-methyl groups in thymidine damage, we used DNA 8 and DNA 9. DNA 8 contains alternative 3'-UT-5' and 3'-TU-5' steps separated by AA spacers and DNA 9 contains 3'-UT-5', 3'-TT-5', 3'-TU-5' and 3'-UU-5' steps. The autoradiogram obtained from this experiment came with a very interesting damage pattern (fig 3.16).

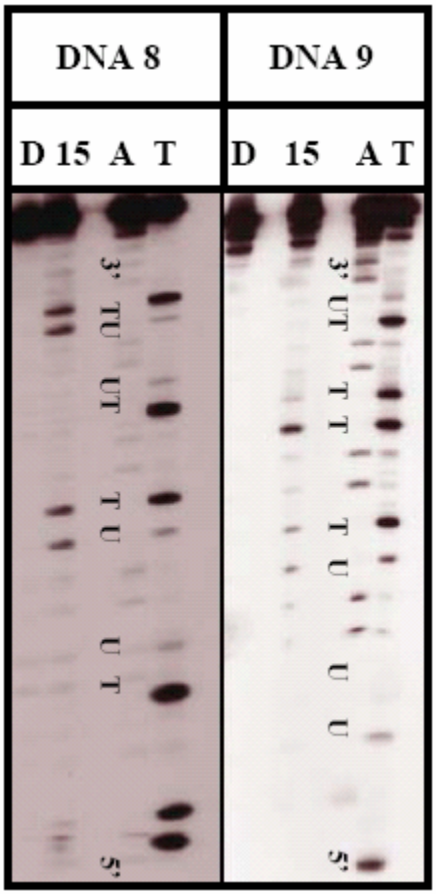

Figure 3.16: Autoradiogram showing the damage patterns of DNA 8 and DNA 9. The TU and UT steps have been labeled and 3' and 5' sides are indicated. D and 15 represents 0 and 15 minutes of radiation and A and T represents a and T sequencing lanes.

As expected, the damage pattern of the 3'-TT-5' segment of DNA 7 is exactly same as the 3'-TT-5' segment of DNA 3 and there is no damage at either of bases at the 3'-UU-5' segment. However, both the bases are damaged in a 3'-TU-5' segment and neither of them is damaged in a 3'-UT-5' segment and this observation is true for both the oligomers. The same experiment was repeated several times at different concentrations of sodium phosphate buffer and magnesium chloride to examine if there is any effect of sodium and magnesium salts (fig 3.17), but this unexpected damage pattern of 3'-TU-5' and 3'-UT-5' segments was consistent at all the conditions.

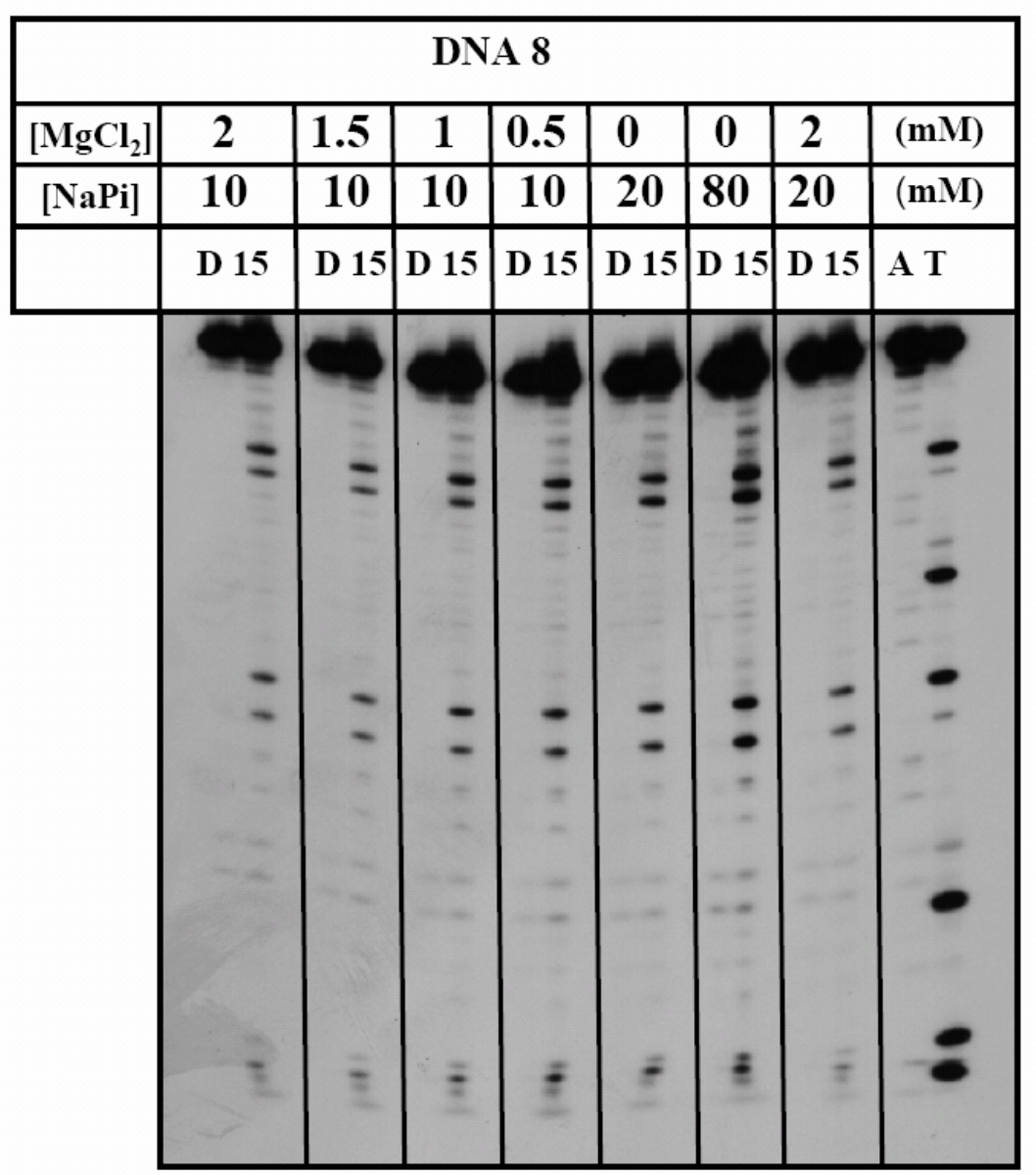

Figure 3.17: Autoradiogram showing the effect of Mg and Na salts on the damage patterns of 3'-TU-5' and 3'-UT-5' segments. NaPi represents sodium phosphate buffer. D and 15 represents 0 and 15 minutes of irradiation and A and T indicates A and T sequencing lanes.

The most common oxidation product of uracil is 5,6-dihydroxyl-uracil or uracil glycol[17]. During the sequencing experiments of DNA 8 it has been observed that although the reaction rate of $KMnO_4$ oxidant with Thymine and Uracil to produce thymine glycol and uracil glycol are comparable[18], piperidine labile damage is much prominent in case of

thymine than in uracil (Lane T in Figure 3.17). This observation leads to a possibility that uracils in DNA8 and DNA9 are actually oxidized to uracil glycol but results in no cleavage due to its less reactivity with piperidine. To explore on this prospects DNA 12 is used where all the TT segments of one strand is replaced with UU segments. And instead of chemical cleavage with piperidine, Ecoli endonuclease III (ECORIII) enzymatic cleavage is used, as uracil glycol is known to be an efficient substrate for this enzyme[19]. The PAGE analysis shows (Fig 3.18) no damage at UU segments, confirming absence of uracil glycol as an oxidation product. Treatment of irradiated DNA 1 and DNA 8 with ECORIII reveals same damage pattern as the piperidine treated samples, only there is a change in product distribution.

DNA 12: 5'-AQTTTTAATTAATTAATTAATATATTT-3'
3'-AAAAUUAAUUAAUUAAUUAUAUAAA-5'

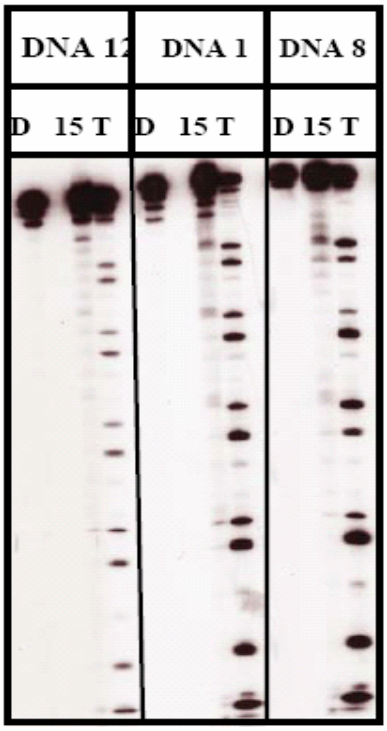

Figure 3.18: Autoradiogram showing the ECORIII mediated damage of DNA 12, DNA 1 and DNA 8. D and 15 represents 0 and 15 minutes of irradiation and T indicates T sequencing lane.

To investigate the same effects in thymidine damage at TTT segments, DNA 10 and DNA 11 are used. DNA 10 has four of the possible combinations possible with T and U at TTT segments (3'-UTT-5', 3'-UTU-5', 3'-TTU-5', and 3'-TUT-5') while DNA 11 has the other four (3'-UUT-5', 3'-UUU-5', 3'-TUU-5', and 3'-TTT-5'). PAGE analysis of these two strands (fig 3.19) comes up with a similar result as the previous experiment. As expected, the 3'-TTT-5' segments has predominant middle T damage with some damage at 3'-T, and no reaction is observed at 3'-UUU-5' segment. There is no damage at the segments having a U at 3' side (3'-UTT-5', 3'-UTU-5', and 3'-UUT-5') and the damage pattern for 3'-TTU-5' is same as 3'-TT-5', the damage pattern at 3'-TUT-5' and 3'-TUU-5' are same as 3'-TU-5'.

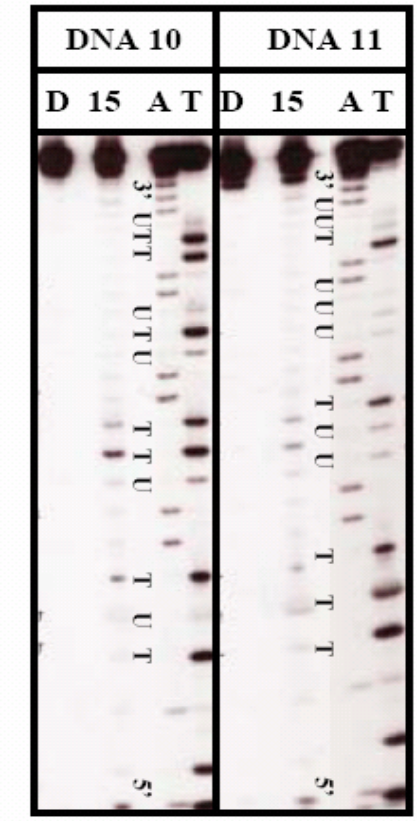

Figure 3.19: Autoradiogram representing the damage pattern of DNA 10 and DNA 11. The U and T's and 3' and 5'-ends are indicated. D, 15 represents 0 and 15 minutes of irradiation and A and T represents A and T sequencing lanes.

These experiments show that, although, a U at 5'side only effects the product distribution slightly, presence of this nucleoside at 3' side totally stops the reactions at T's and TT's 5' to it. So, it is the C5-methyl group of 3'-T only, that plays an important role in oxidative thymidine damage. Also, as the absence of methyl group in one nucleobase is affecting the reactions at next nucleobases, it is more likely that tandem lesion is generated by nucleobase radical or nucleobase oxygen radical. The radical reactions involving thymidine or thymidine peroxyl radicals are widely known. The mostly known radical species (figure 3.20) generating from thymidine and 2'-deoxyurdines are 5,6-dihydro-thymidine-6-yl, 5-hydroxy-6-hydro-thymidine-6-yl, 5,6-dihydro-2'-deoxyuridine-6-peroxyl, 5,6-dihydro-thymidine-5-yl, thymidine-5-methyl radical, thymidine-5-methylperoxy radical etc[16,20-22].

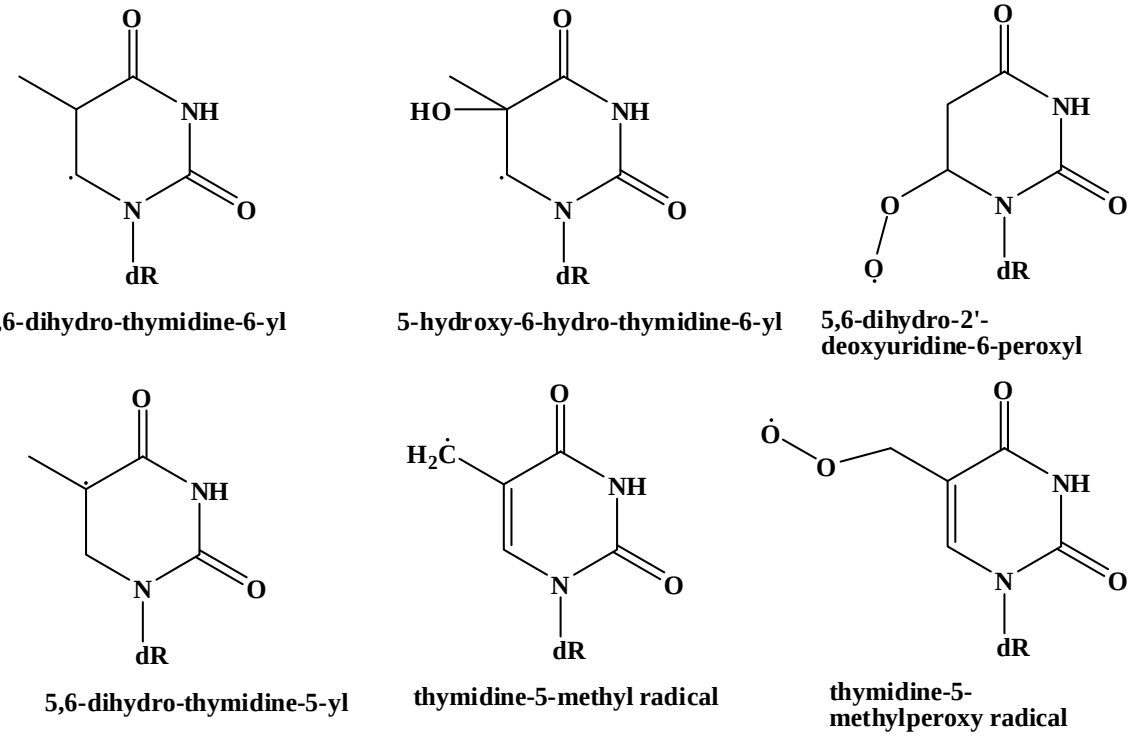

Figure 3.20: Radicals generated from thymidine and 2'-deoxyuridines.

Using these radicals and radical generating reactions, a couple of possible mechanisms has been designed, which can explain the results obtained from our previous experiments. Figure 3.21 and 3.22 illustrate the possible tandem lesions involving the methyl group of 3'-thymidine; one involving Me-H abstraction (fig 3.21) and other involving C1'-H abstraction (fig 3.22). In the first one, by charge migration from AQ, the radical cation 2 is generated from a 3'-TT-5' segment (1), where the radical is at the C5 position of 5'-T and the C5 position of the same base has the positive charge. This radical cation can react with water or/and oxygen to first form the 6-hydroxythymidine-5-yl radical (3) and then the 6-hydroxythymidine-5-peroxyl radical (4). This peroxyl radical can abstract a hydrogen radical from the C5-methyl group of 3'-thymidine, to form 5 which have the thymidine-methyl radical at the 3' position. This species now can react with water and/or oxygen to form the modified dinucleotide 6. In this modified 3'-TT-5' portion, the 5'-T has been converted to cis or trans thymidine glycol and the 3'-T is converted to 5-hydroxymethyl-2'-deoxyuridine or the aldehyde/acid generated from it by further oxidation. For the dinucleotide sections having a 2'-deoxyuridine at the 3' position, the peroxyl radical at the C6 of 5' thymidine forms; but as there is no methyl group at the 3'-base to abstract hydrogen from, it goes back to more stable normal thymidine and there is no net reaction. But, for a 3'-TU-5' segment, the formation of 5-hydroxy-2'-deoxyuridine-6-peroxyl is feasible and that can abstract hydrogen from the C5 methyl of 3'-thymidine leading similar products to 3'-TT-5' segments.

In the other mechanism, C1'-H abstraction (figure 3.22), the radical cation is first generated at the 3'thymidine (11) of a 3'-TT-5' segment. This radical cation then can lose a proton and form a methyl radical at the C5 position of the 3'-thymidine (12). This

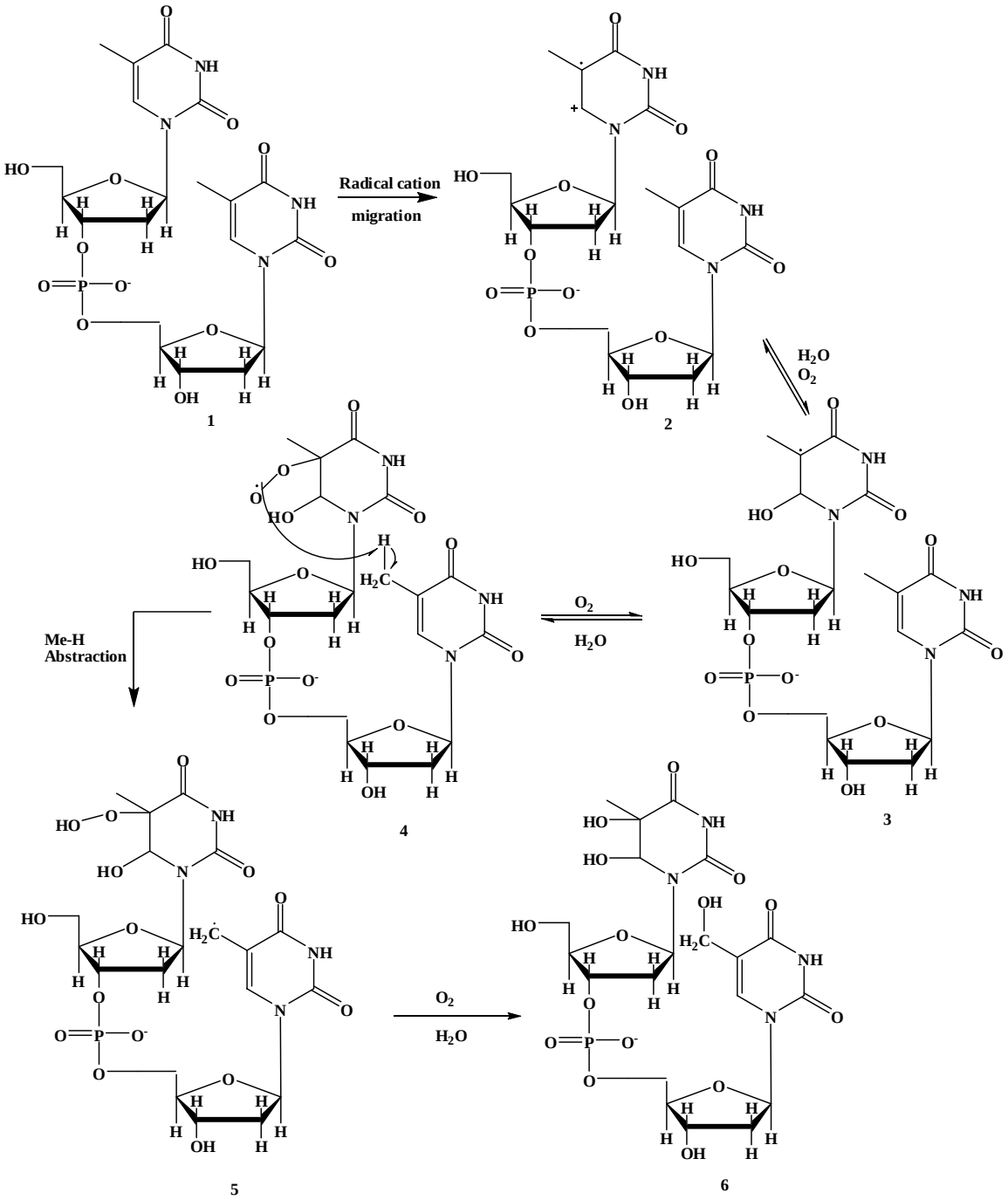

Figure 3.21: Me-H abstraction pathway and mechanism of thymidine damage

radical can react with oxygen and/or water to form a peroxyl radical (13) at the same position; and this peroxyl can abstract the C1'-H of the 5'-thymidine (14). These

reactions will lead to modified dinucleotide with an abasic site at the 5'-thymidine and 5-hydroxymethyl-2'-deoxyuridine or it's oxidized derivatives at the 3'-thymidine (15). When the 3'-thymidine is replaced by 2'-deoxyurdine, the methyl radical formation is inhibited. This will stop the reaction and would not lead to any piperidine labile damage.

Apart from these tandem lesions, the C5-methyl radical formed at 3'-thymidine (8) can react with water or oxygen to form 5-hydroxymethyl-2'-deoxyuridine and/or 5-formyl-2'-deoxyuridine at that position (Figure 3.23). There are other possible mechanisms that can lead to piperidine labile damages at the thymidines. But, these are the three are the most probable ones as these mechanisms can perfectly explain the result that the C5-methyl group at the 3'-thymidine is essential for this reaction. Although, these mechanisms do not explain anything about the relative damage intensity at 3' and 5' positions of a 3'-TT-5' segment, but that will depend on the relative orientation of the two thymidines and the relative reactivity of the different modified thymidines with piperidine. It is very difficult to figure out which one of these mechanisms is actually leading to the damage. That will depend on the reactivities of the generated radicals and the distance between the reactive species. It is very much possible that more than one of these pathways is working simultaneously. In the next few chapters we have described our modeling experiments to figure out the theoretical distance between the reactive centers, experiments with radical scavengers and spin traps to figure out the radical intermediates involved in the pathway and enzymatic treatment and HPLC-MS experiments to find out the exact product.

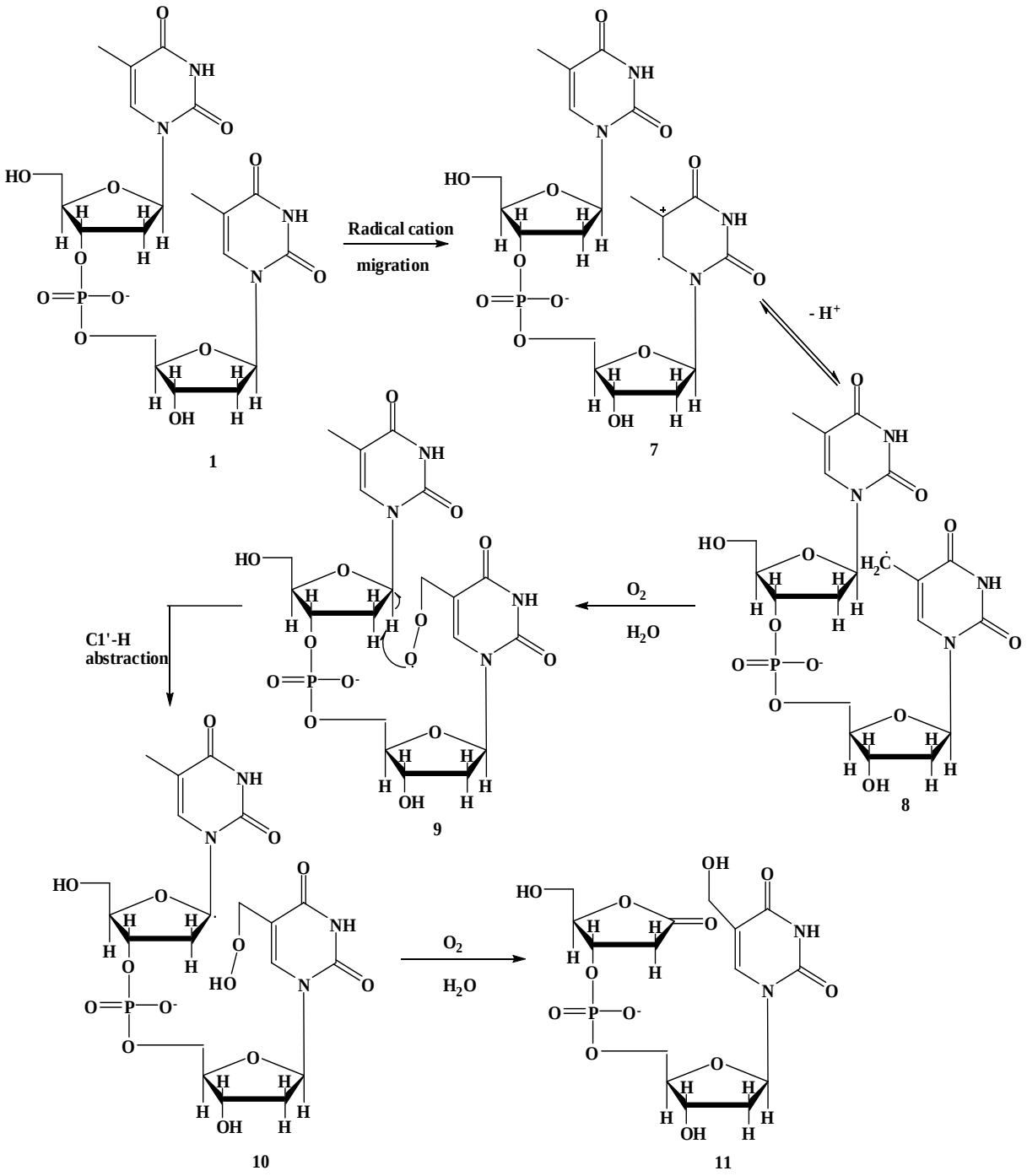

Figure 3.22: C1’-H abstraction pathway and mechanism for thymidine damage

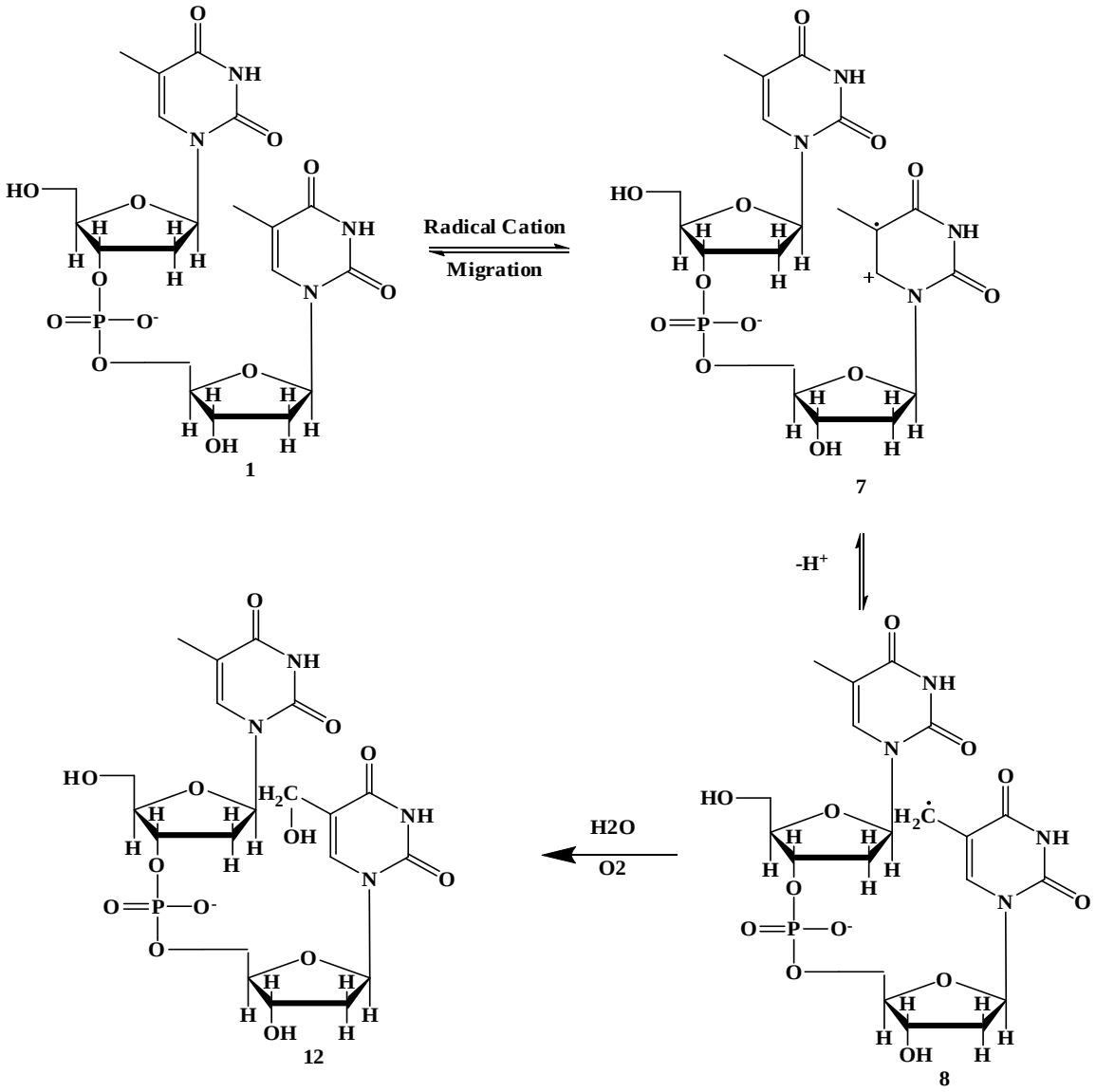

Figure 3.23: Direct oxidation of C5-methyl group of 3'-thymidine

3.6 Molecular Modeling Studies

Molecular modeling studies were performed to figure out the theoretical distances between the reactive species involved in the two pathways descried in previous chapter. Hyperchem software was used to perform these modeling experiments. At first DNA 8 was build to calculate the distances for 3'-TT-5', 3'-TU-5' and 3'-UT-5' segments and its most stable structure was determined using geometry optimization function. Then

different modifications were drawn according to the different pathways described in chapter 3.5 and those structures were energy minimized similarly. On the basis of these models relative feasibility of the two possible thymidine damage pathways were assessed.

3.6.1 Me-H Abstraction

To estimate the viability of Me-H abstraction pathway models of DNA double strands were constructed with the following modifications (figure 3.23).

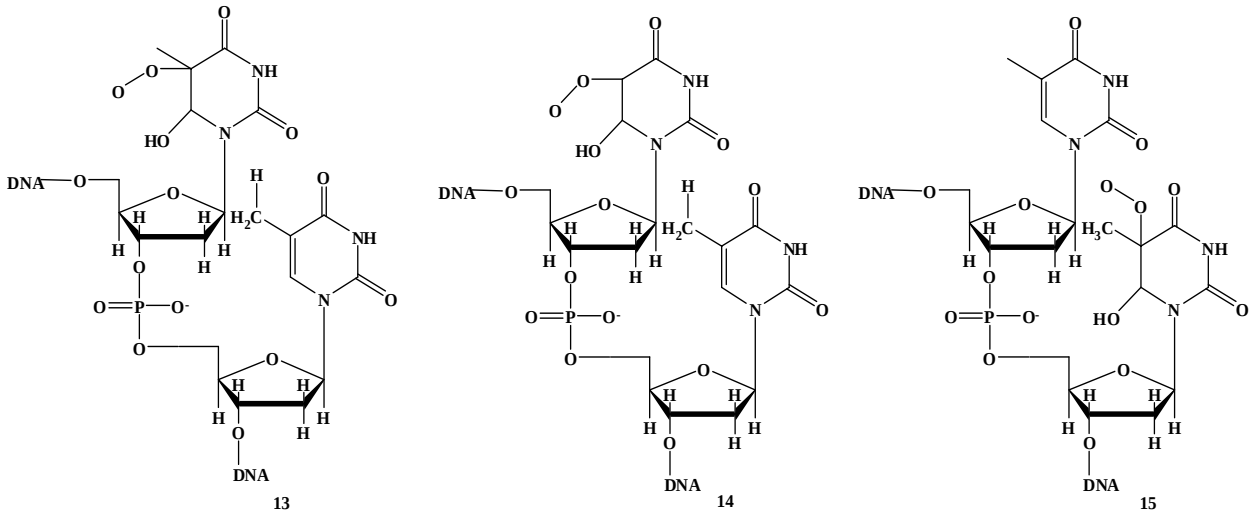

Figure 3.24: Structure of the modified 3'-TT-5' and 3'-TU-5' segments used to generate the models of reactive species representing Me-H abstraction pathway

Modified 3'-TT-5' segment 13 and modified 3'-TU-5' segment 14 represent the 6-hydroxy-thymidine-5-peroxyl radical (4) or 6-hydroxy-2'-deoxyuridine-5-peroxyl radical at the 5'-thymidine or 5'-uridine respectively. On the other hand, 15 represents a modified 3'-TT-5' segment where a peroxyl radical has been generated at C5 position of 3'-thymidine. This is to see if C5-Me hydrogen abstraction from the 3'-thymidine is theoretically feasible by the peroxyl radical generated at the C5 of 5'-thymidine. The energy minimized models for 13 and 15 have been shown in figure 3.25 and in figure 3.26 respectively.

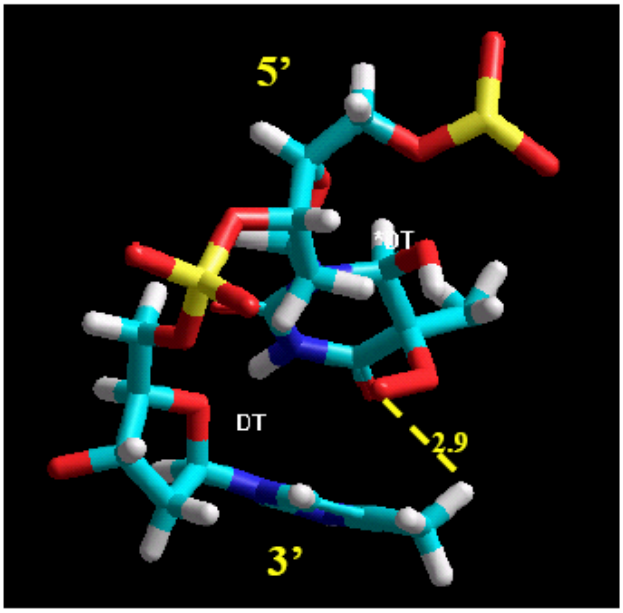

Figure 3.25: Hyperchem model of structure 13 as a part of double stranded B form DNA. Cyan, white, blue, red and yellow represent carbon, hydrogen, nitrogen, oxygen and phosphorous. 5’ and 3’ sides have been indicated and the distance between the peroxyl radical at C5 of 5’-thymidne and C5-methyl hydrogen of 3’-thymidine has been also shown.

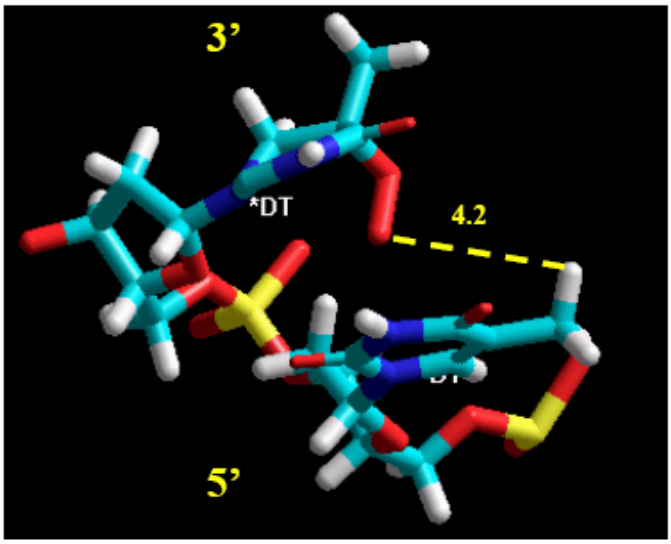

Figure 3.26: Hyperchem model of structure 15 as a part of double stranded B form DNA. Cyan, white, blue, red and yellow represent carbon, hydrogen, nitrogen, oxygen and phosphorous. 5’ and 3’ sides have been indicated and the distance between the peroxyl radical at C5 of 3’-thymidne and C5-methyl hydrogen of 5’-thymidine has been also shown.

3.6.2 C1'-H Abstraction

The following modified nucleotide (16) was modeled to figure out the theoretical feasibility of C1'-H abstraction pathway. This model represents the C5-methyl peroxyl radical 9. Figure 3.17 shows the Hyperchem molecular modeling picture of 16 as a part of double strand B DNA

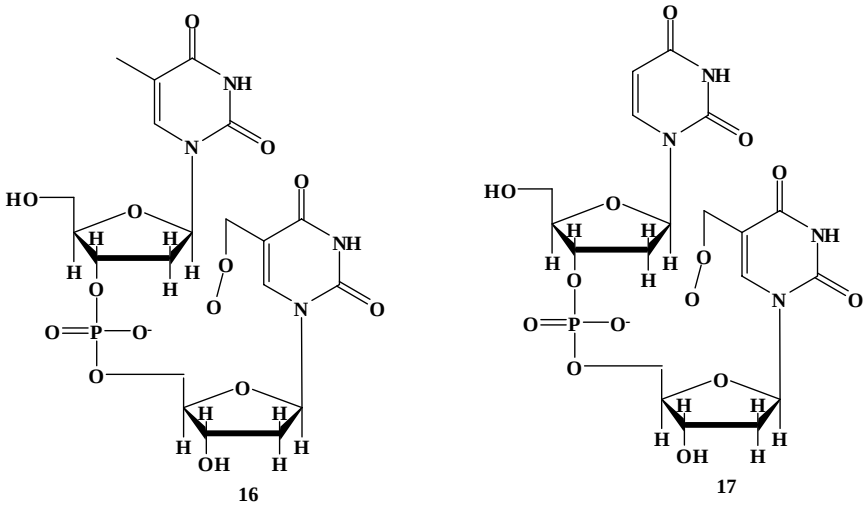

Figure 3.27: Modified nucleoside modeled to study the C1'-H abstraction pathway

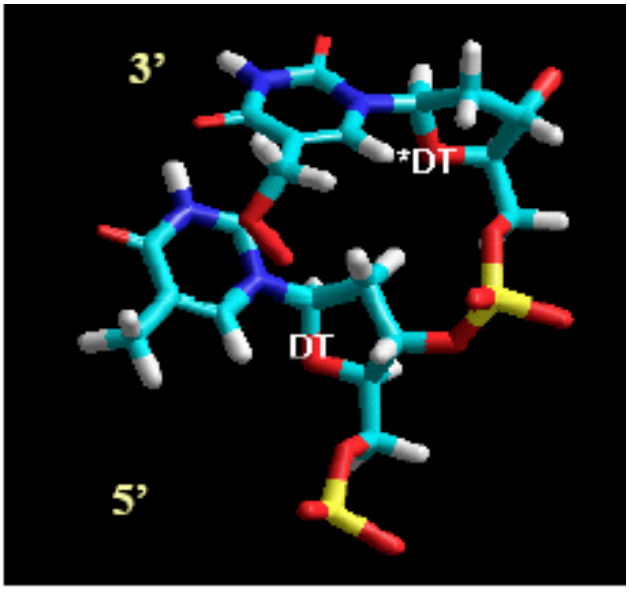

Figure 3.28: Hyperchem model of structure 16 as a part of double stranded B form DNA. Cyan, white, blue, red and yellow represent carbon, hydrogen, nitrogen, oxygen and phosphorous.

The calculated distances between the different reaction centers for the above mentioned pathways have been summarized in table 3.5. These results indicates that when the radical is generated at the 5'-thymidine and forms 6-hydroxy-thymidine-5-peroxyl, it is feasible for the radical to abstract the C5-methyl-H of the 3'-thymidine (distance between the reaction centers 2.9 Å). This observation holds for a 2'-deoxyuridin at the 5' position too. On the other hand, if the radical cation is generated at the 3'-thymidine both of the possible tandem reactions are less feasible. When a 6-hydroxy-thymidine-5-peroxyl radical is generated the C5-methyl-hydrogen of 5'-thymidine is more than 4 Å away. And the C1'-H abstraction is less feasible when a C5-methyl-peroxy radical is generated as it is also more than 4 Å away from the C1'-H of 3'-thymidine.

Table 3.5: Theoretical distances between different reactive species involved in C5-Me-H abstraction and C1'-H abstraction pathways. C5-O-O represents C5-peroxyl radical, C5-Me-O-O represents the C5-methyl peroxyl radical and (3') and (5') indicates the 3'-thymidine and 5'-thymidine or 2'-deoxyuridine respectively.

DNA segment	Distance from	Distance to	Distance (Å)
3'-TT-5'	C5-O-O (5')	C5-methyl-H (3')	2.9
3'-TU-5'	C5-O-O (5')	C5-methyl-H (3')	2.87
3'-TT-5'	C5-O-O (3')	C5-methyl-H (5')	4.23
3'-TT-5'	C5-Me-O-O (3')	C1'-H (3')	4.72
3'-TU-5'	C5-Me-O-O (3')	C1'-H (3')	4.68

3.6.3 NMR Structure Study

These modeling studies have been done considering a regular B-DNA structure of the strand. Although, it is known that A-T tracts often to a bending in the regular B-DNA structure[23,24]. To account for any of the bending effects, we calculated the distances between the reaction centers in a NMR structure (PDB ID: 1CQO) that has AA-TT

segments, using Pymol. Although, the sequence of this DNA is totally different from the DNA we are using, this study will give a rough idea on the distances between different atoms in a 3'-TT-5' segment. Figure 3.28 shows a 3'-TT-5' segment of pymol generated picture of NMR structure of duplex DNA $d(GCGTTAACGC)_2$.

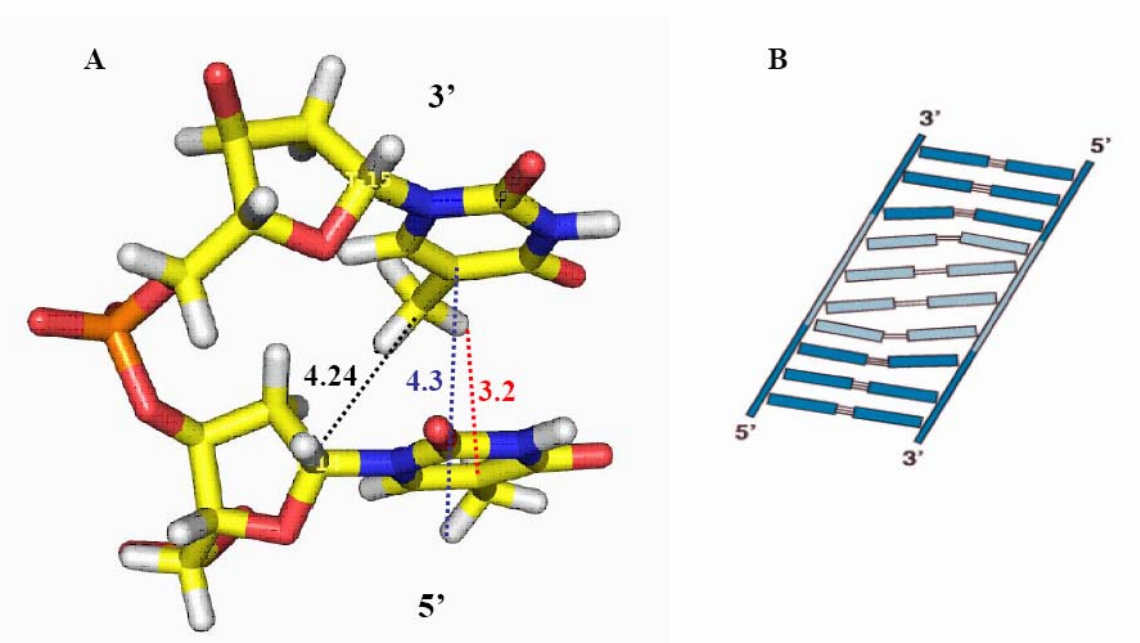

Figure 3.29: (A) T14 and T15 of Pymol generated picture of published NMR structure of DNA $d(GCGTTAACGC)_2$ (PDB ID: 1CQO). Distances between C5-methyl carbon of 3'-T and C1'-H of 5'-T (C1'-H abstraction), C5 of 3'-T and C5-methyl hydrogen of 5'-T, C5 of 5'-T and C5-methyl hydrogen of 3'-T (Me-H abstraction) have been shown in black, blue and red doted lines respectively. All the distances are in angstroms. (B)[23]Bending of A-T tract in same DNA duplex.

The distances between different reaction centers involved in the pathways described earlier have been calculated. The distance between the C5 of 5'-T and C5-methyl hydrogen of 3'-T is 3.2 Å and the distance between C5 of 3'-T and C5-methyl hydrogen of 5'-T is 4.3 Å. These two distances represent the distance between the reaction centers for Me-H abstraction pathway by radical generated at C5 position of 5'-thymidine and 3'-thymidine respectively. And the distance between the C5 methyl carbon

of 3'-thymidine and C1'-H of 5'-thymidine is 4.28 Å and this represent the C1'-H abstraction pathways. The peroxyl radical has not been generated for any of these structures, but that's going to decrease the distance for all the possibilities equally. From these calculations it is evident that the C5-methyl hydrogen abstraction of 3'-thymidine by radical generated at C5 of 5'-thymidine is the most feasible pathway even if we consider the bending at A-T region.

3.7 Effect of Radical Scavenger

The mechanisms that we have proposed involve radical intermediates. So, these reactions must be affected by radical scavengers. Radical scavengers will react with radical intermediates generated in the reactions depending on their lifetime and reactivity. We studied the thymidine damage in presence of radical scavenger glutathione to provide a proof that the reactions leading to thymidine damage are actually going through radical intermediate.

3.7.1 Radical Scavenger: Glutathione

The radical scavenger used in our experiment is glutathione. Glutathione is a tripeptide γ-glutamylcysteinylglycine and it contains an unusual peptide linkage between the amine group of cysteine and the carboxyl group of the glutamate side chain (Figure 3.30).This is an antioxidant and known to protect cells from toxins such as free radicals[25]. The thiol groups of glutathione are kept in reduced form (GSH) in normal animal cell. In reaction with radicals it loses a hydrogen radical from thiol to reduce the radical and two oxidized glutathion radicals form dimer (GS-SG).

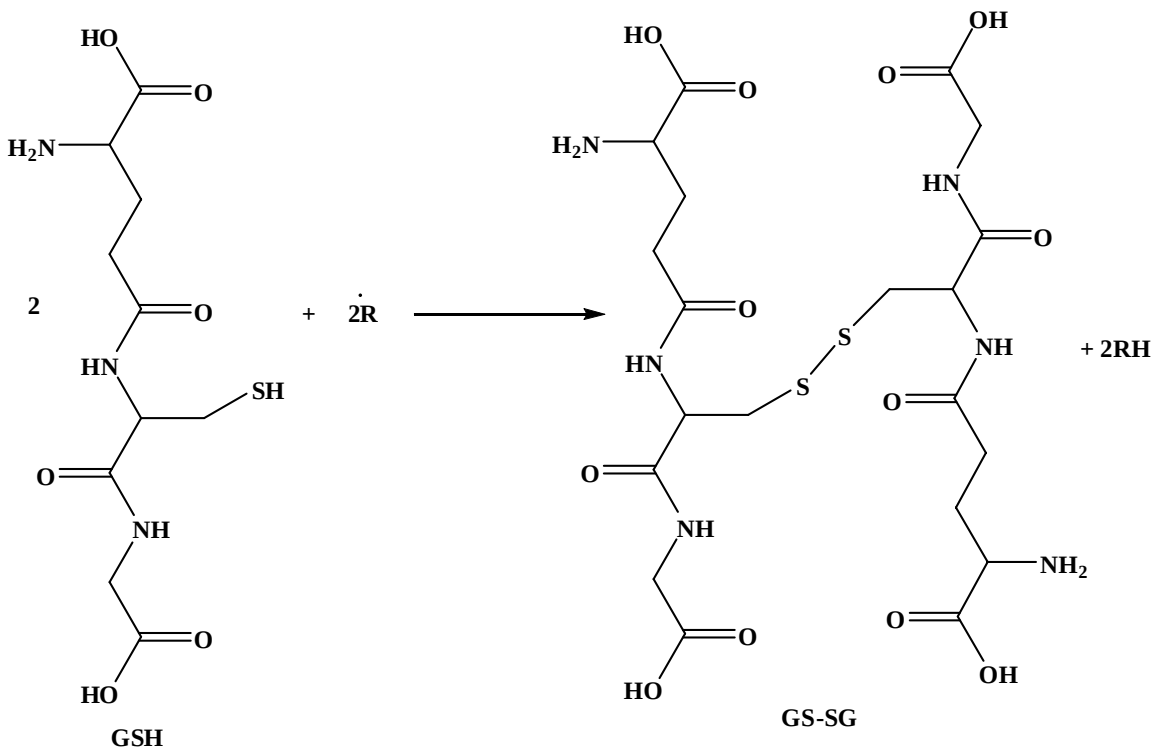

Figure 3.30: Mechanism of radical scavenging action of glutathione (GSH)

3.7.2 Experimental

The DNA duplexes used for this experiment are DNA1, DNA 3 (Figure 3.2) and DNA 8 (Figure 3.8). These strands have been labeled and hybridized as mentioned earlier. Before irradiation different concentrations of glutathione (0 to 5 mM) was added to the samples. Then these were irradiated, precipitated, treated with piperidine and the damage patterns were studied using gel electrophoresis and phosphorimaging in same way as described in previous segments (3.3.4 and 3.3.5).

3.7.3 Results and Discussion

At first, the affect of glutathione on thymidine reaction was studied using DNA 3. This duplex has a GG step at the TT containing strand. Glutathione can react with the anthraquinone radical cation and thus quenching the charge migration process, resulting

decrease in thymidine damage. In that case, the results will be misleading, as glutathione will affect the thymidine damage even if no radical intermediate generates during thymidine damage reactions. However, if the anthraquinone radical cation is quenched by glutathione, the damage at the GG step will also be affected. Thus, this GG step works as an indicator. If glutathione affects only TTT steps but not GG steps it will definitely indicate that the decrease in damage at thymidines results in from radical intermediate quenching at those thymidines not from anthraquinone radical quenching. On the other hand, if both TTT and GG steps are affected by glutathione the anthraquinone radical cation might be quenched. The autoradiogram and quantitative results obtained from this experiment are shown in figure 3.31 and 3.32.

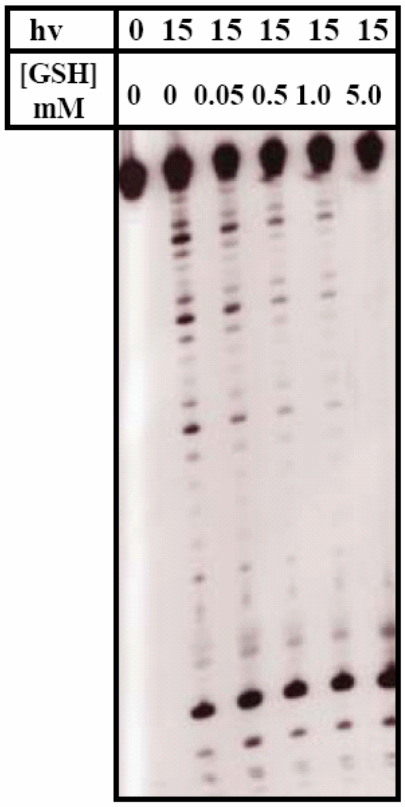

Figure 3.31: Autoradiogram showing the affect of glutathione (GSH) on thymidine damage in DNA 3. hv indicates the times of irradiation in minutes and glutathione concentrations are given in mM.

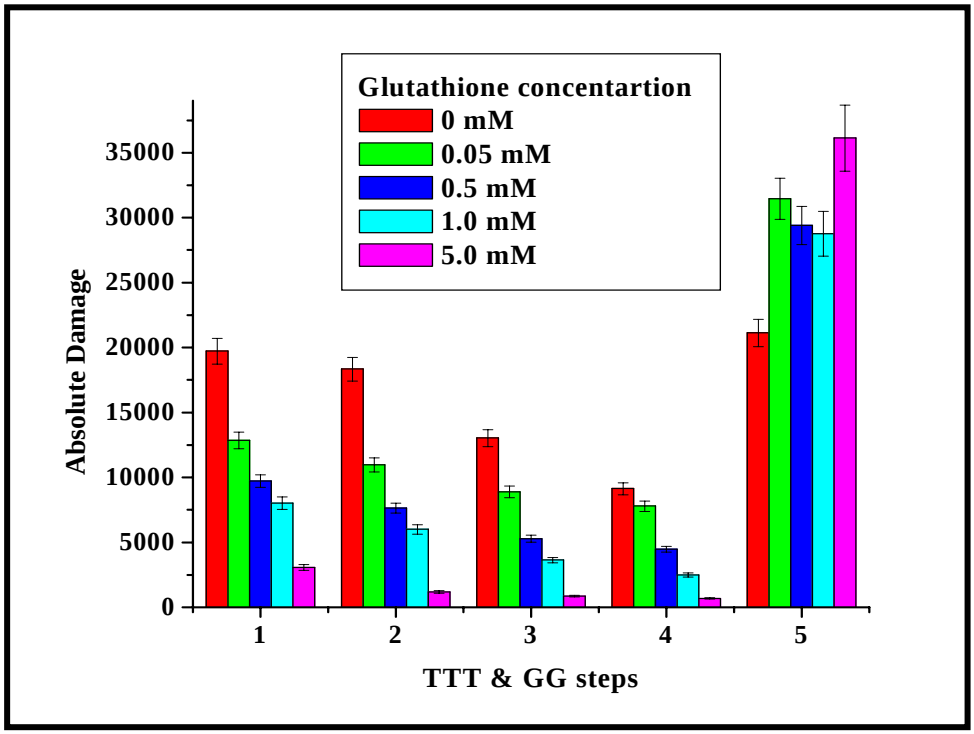

Figure 3.32: Quantitative analysis showing affect of glutathione on reactions at TTT and GG steps in DNA 3. 1, 2, 3, 4 represent the four TTT steps and 5 represent the GG step.

From the gel electrophoresis and the quantitative analysis it is clear that the thymidine damage at the TTT steps are seriously affected glutathione radical scavenger. A regular decrease in thymidine damage has been observed with increasing concentration of glutathione (GSH). But there is no regular pattern observed in guanine damage at the GG step with increase in GSH concentration. There is no decrease in guanine damage and actually the guanine damage increases as the concentration of glutathione goes from 0 to 5 mM. From this result it is clear that the GSH is not quenching the anthraquinone radical cation. However, it is quenching the reaction at the TTT steps. This indicates the reactions taking place at TTT steps leading to the thymidine damage definitely involve radical intermediates. The same experiment has been done with DNA 1 and DNA 8. These strands don't have any GG steps, but has four TT steps and alternative 3'-TU-5'

and 3'-UT-5' steps respectively. The quantitative results are shown in Figure 3.33 and the effect of glutathione is same for these strands too. This further proves that the reactions leading to damage at 3'-TT-5' and 3'-TU-5' steps do involve radical intermediates.

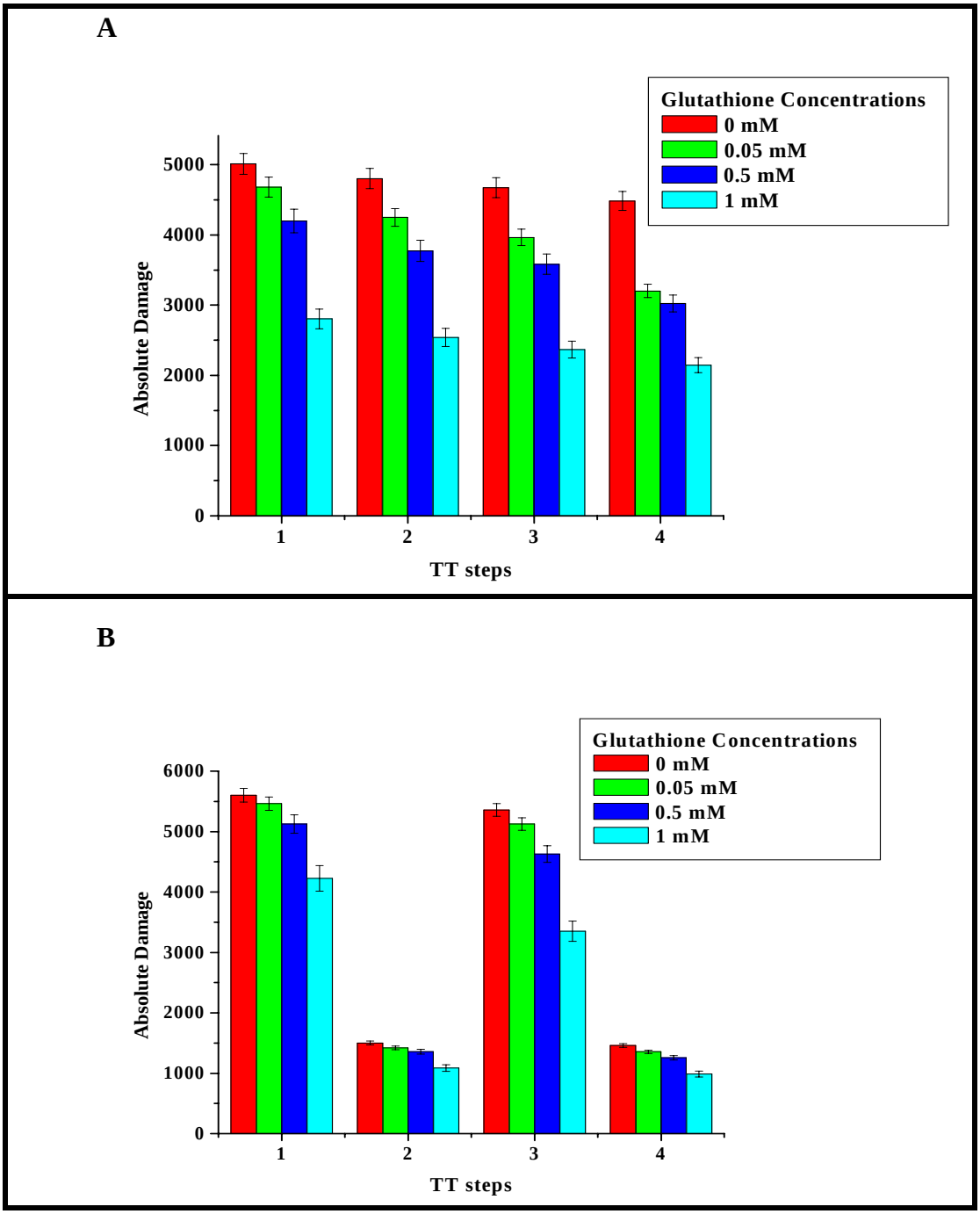

Figure 3.33: Effect of GSH in reactions at (A) DNA 3 and at (B) DNA 6. 1, 2, 3, 4 represent the four TT steps in DNA 3 and alternate 3'-TU-5' and 3'-UT-5' steps in DNA6.

3.8 EPR Studies

The experiments with glutathione proved that there are radical intermediates involved in the reactions leading to thymidine damage. This result leads us to perform EPR studies to find out the radicals involved. We tried to use different spin-traps that will react with these radicals and from the EPR spectra of those adduct information about the radicals can be obtained.

3.8.1 Spin-traps

Spin-traps are compounds that are used to trap radicals. The known spin-traps used for detection of radicals involved in DNA reactions are 2-methyl-2-nitrosopropane (MNP) and α-(l-oxy-4-pyridyl)-N-tert-butylnitrone (4-PyOBN)[26-28]. This compound forms adduct with radicals and adduct is also a radical which gives strong EPR signals (Figure 3.34). Generally, these EPR signals have secondary splitting due to the interaction of unpaired electron with the nuclei of adducts. From these secondary splitting the structure of the radicals can be deduced.

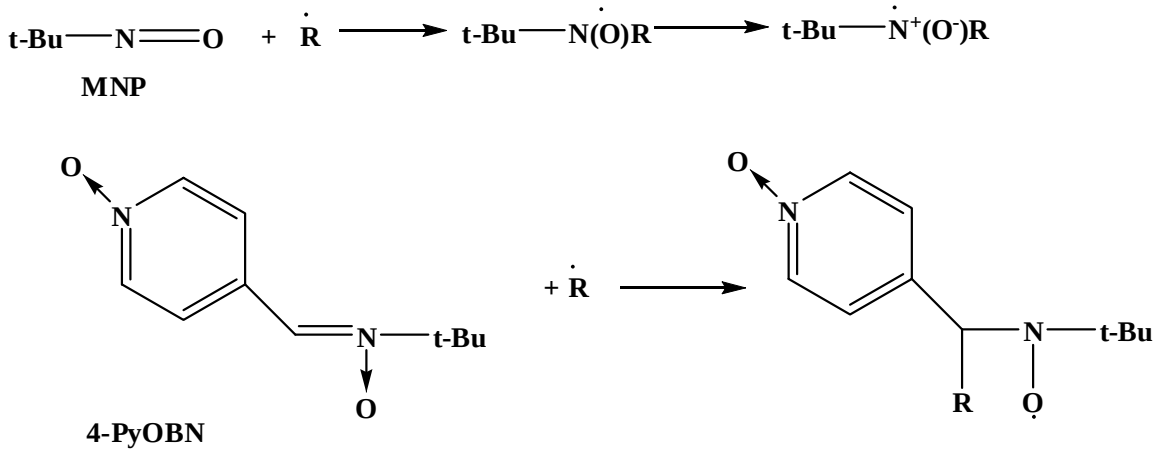

Figure 3.34: Reaction of MNP and 4-PyOBN with radicals generating another radical adduct

The spin-traps that will be useful for our experiments should have three characters. It should form a radical adduct by reaction with the radicals form in the thymidine damage reactions. It should not react with anthraquinone radical cation and should not absorb in the region of anthraquinone absorption (around 360 nm). And the spin-trap should be soluble in water. The spin-traps described here do form radical adducts in reactions with radicals generated from reaction involving thymidine. But, MNP is not soluble in water and 4-PyOBN has absorption tail around 360 nm. So, we explored the feasibility of another well-known spin-trap 4-hydroxy-2,2,6,6-tetramethylpiperidine-1-oxyl (TEMPOL) in our experiments. This spin-trap is soluble in water and does not absorb around 360 nm. However, the interaction of TEMPOL with radicals generated in this reaction is not known.

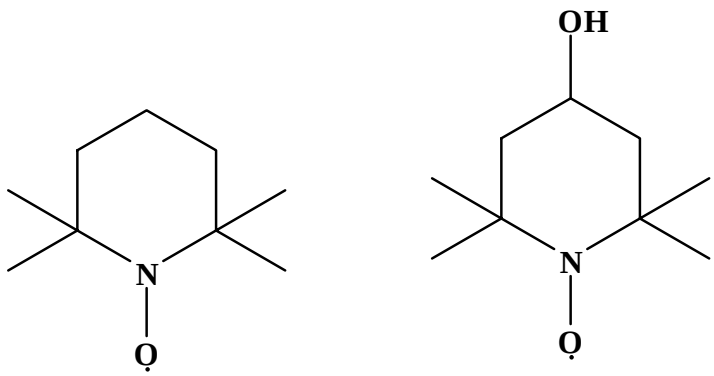

TEMPO **TEMPOL**

Figure 3.35: Structure of spin-traps TEMPO and TEMPOL

3.8.2 Experimental

To figure out the interaction of the spin-traps with the anthraquinone radical cation DNA 3 was used. The experimental set-ups were similar to the experiments with glutathione. Two sets of DNA samples were prepared and one set was treated with different concentrations of 4-PyOBN and other with TEMPOL. Then those were

irradiated and gel electrophoresis was done. For EPR study DNA 1 was used. 500 μL of DNA samples were prepared (same concentrations as used before for gel electrophoresis studies) and treated with the spin-trap TEMPOL. After irradiation those samples were used for EPR study. The EPR experiments were performed by David Jenson in Bruker EMX EPR spectrometer at Dr. Bridget Barry's lab.

3.8.3 Results and Discussion

The autoradiogram obtained from the preliminary experiments with 4-PyOBN and TEMPOL are shown in figure 3.36. This experiment gives us an idea about the interaction of these spin-traps with anthraquinone radical cation and the radicals generated in thymidine reactions.

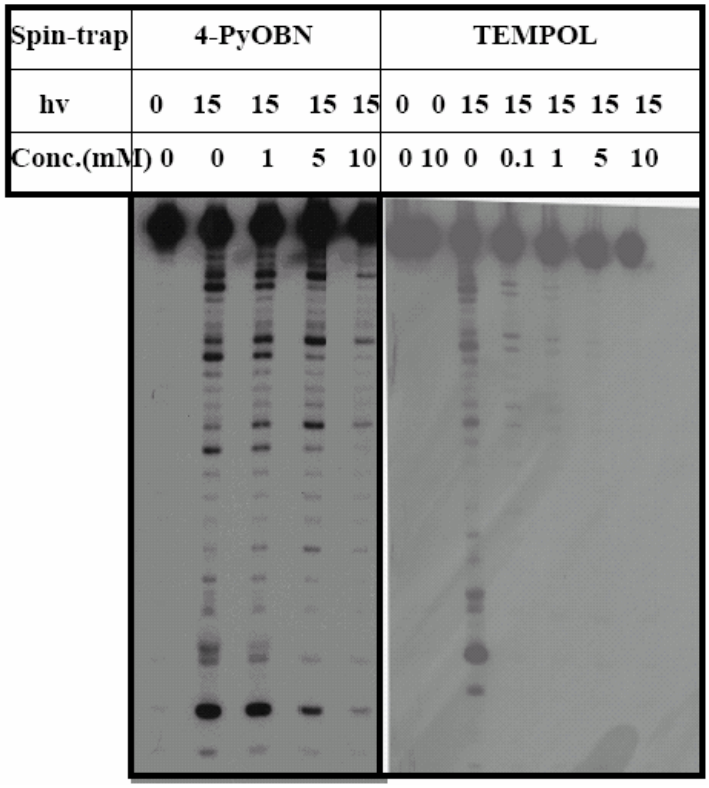

Figure 3.36: Autoradiogram showing the effect of spin-traps 4-PyOBN and TEMPOL in thymidine damage in DNA 3. hv indicates the irradiation times in minutes and conc. indicates concentrations of spin-traps in mM.

From the gel electrophoresis study it is clear that the damage at thymidine is not much affected by the increasing concentration of spin-trap 4-PyOBN. Only at 10 mM concentration there is considerable decrease in thymidine damage. However, there is decrease in guanine damage too. That indicates the spin-trap might be quenching the anthraquinone radical resulting decrease in thymidine and guanine damage. With TEMPOL the situation is bit different. This spin-trap is also affecting the guanine damage along with the thymidine damage. But its effect is stronger than the 4-PyOBN. 0.1 mM of TEMPO is sufficient to decrease the thymidine damage over 50%. So, this might be an effective spin-trap for EPR studies as very low concentration will be required to affect the thymidine reactions and it would reduce any secondary reactions that might interfere our study.

Now, the spin-trap can affect the guanine damage in two ways. First, it can quench the anthraquinone radical cation and thus affect the charge migration process resulting decrease in damage at every step. Secondly, it can quench the radicals generated at thymidines and thus decrease the amount of radical cation that reach to the guanine. This will also decrease the guanine damage. If it quenches the anthraquinone radical cation the EPR will not come up with any conclusive results. However, in case of the second possibility there is a chance of obtaining good results from EPR. To explore on this topic, we studied the effect of TEMPO on guanine damage in a sequence which have six GG steps separated by TT spacers (DNA 13, Figure 3.36). As mentioned in previous chapter, this strand will lead damages at the GG steps and the intensity of damage will decrease with increase in distance from anthraquinone. If the spin-trap does not affect the guanine damage in a same way as DNA 3, then it might be concluded that it is not

quenching the anthraquinone radical cation. The autoradiogram obtained from this experiment has been shown in Figure 3.36.

DNA 13 5'-AQAATTGGTTGGTTGGTTGGTTGGTTGGATAT-3'
3'-TTAACCAACCAACCAACCAACCAACCTATA-5'

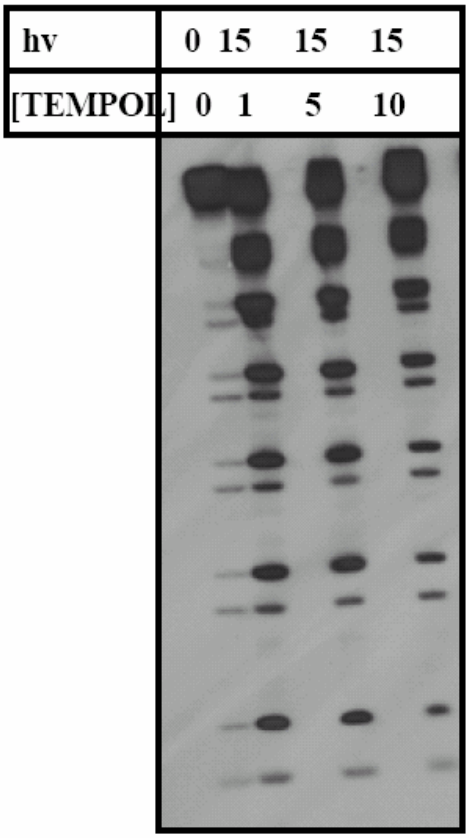

Figure 3.36: Effect of TEMPOL in guanine damage at DNA 13. hv indicates the irradiation times in minutes. The TEMPOL concentrations are in mM. The structure of DNA 13 has been shown also.

The autoradiogram shows that the guanine damage in DNA 13 is not much affected by TEMPOL. Even with TEMPOL concentrations as high as 10 mM, there is very little decrease in guanine damage. So, it might be concluded that in DNA 3 TEMPOL was not quenching the anthraquinone radical cation and decrease in guanine damage was a result of less radical cation reaching to that site.

From these experiments we decided to try the EPR study with TEMPOL spin-trap. The DNA samples were hybridized in same way as the gel experiments. 1000 μL of 10 μM DNA was prepared, 500 μL of it was irradiated for 15 minutes and other part was kept as dark control. 1 μL of TEMPOL was added to each of the fractions to make the effective TEMPOL concentration 100 μM. The EPR of these samples were studied and figure 3.37 shows the EPR spectra of the dark and irradiated samples.

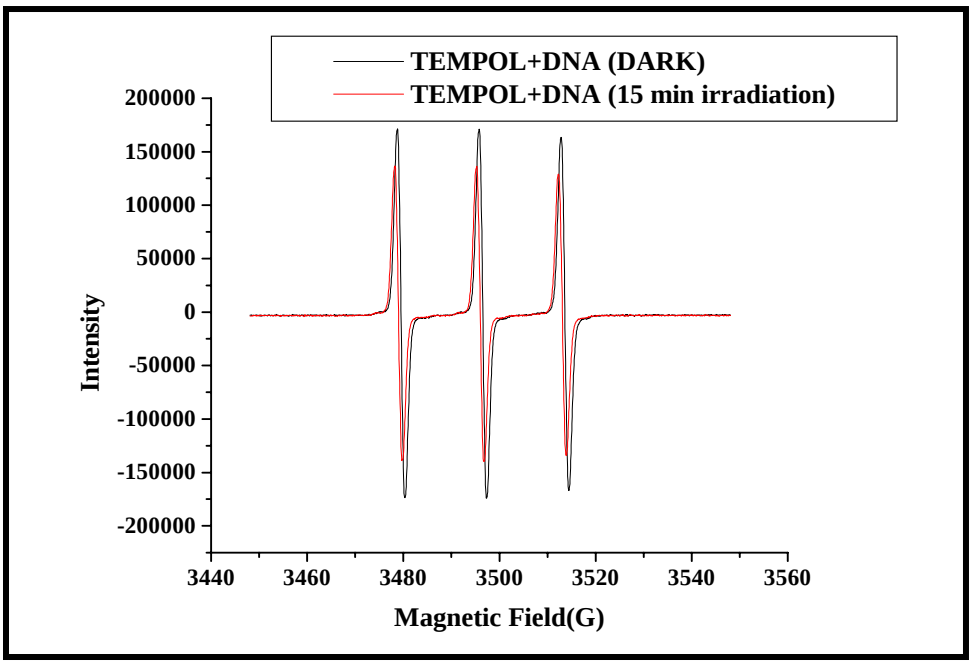

Figure 3.37: EPR spectra of TEMPOL with DNA in dark and after 15 minutes of irradiation

The EPR spectra of TEMPOL with DNA without any irradiation (black line) shows three clear peaks resulting from primary coupling of unpaired electron with ^{14}N nucleus of TEMPOL. Spectra of TEMPOL with irradiated DNA (red line) shows similar signal with a little decrease in intensity. But, there was no additional secondary coupling observed in that case. There could be several explanations of this result. The TEMPOL might be just neutralizing the radicals generated during the thymidine damage reactions. In that way some of the TEMPOL radicals are neutralized and that is evident in the

decrease in TEMPOL signal. Also the DNA concentrations might be low to produce any secondary coupling in TEMPOL signal. Although, this experiment would be able provide us with some information about the radical produced in the thymidine damage reactions, it will only give information about the radicals that react with TEMPOL. That radical might not be the one leading to reactions at thymidines. More reliable information about the mechanism and products from thymidine damage reaction could be obtained from HPLC-MS/MS product analysis of the reactions.

3.9 Product Analysis

The product analysis was performed in collaboration with Dr. Jean Cadet at Grenobole, France. We prepared the DNA samples and irradiated those. Samples were sent to France and the enzymatic cleavage of the DNA and HPLC-MS/MS analysis were performed over there.

3.9.1 Preparation of Samples

We planed to analyze the thymidine oxidation products in DNA 1, with a modification (DNA 14). One of the strands of DNA 1 has four TT steps separated by AA steps and the complementary contains the anthraquinone charge injector. All the thymidines of the complementary strands have been replaced by deoxyuridines to get rid of any secondary oxidation that might take place due to direct interaction of anthraquinone with thymidines (Figure 3.38). Only the last thymidine could not be

DNA 1: 5'-AQTTTTAATTAATTAATTAATATATTT-3'
3'-AAAATTAATTAATTAATTATATAAA-5'
DNA 14: 5'-AQUUUUAAUUAAUUAAUUAAUAUAUUT-3'
3'-AAAATTAATTAATTAATTATATAAA-5'

Figure 3.38: DNA strands for product analysis by HPLC-MS/MS

changed due to synthetic difficulties. However, that thymidine is far away from anthraquinone to have an interaction with. The piperidine labile damage pattern of this DNA is same as that of DNA 1.

50 µL of each single strand (100 µM) was mixed with 100 µL of sodium phosphate buffer (pH 7.0, 100 mM), 25 µL of magnesium chloride (80 mM) and 775 µL of nanopure water. The samples were hybridized and irradiated for 0, 1, 2, 5, 7, 10 and 15 minutes. Then the samples were precipitated with ethanol and the solvent was removed from the samples. These dry DNA samples were sent to France for enzymatic hydrolysis and HPLC-MS/MS study.

3.9.2 Results and Discussion

The four thymidine oxidation products showed up in the product analysis are cis-thymidine glycol (cis-Thdgly), trans-thymidine glycol (trans-Thdgly), 5-hydroxymethyl2'-deoxyuridine (5-HMdUd) and 5'-formyl-2'-deoxyuridine (5-FordUd). The structures of these products and a plot describing the % yield of these products against the unreacted thymidine at different irradiation times have been shown in figure 3.39 and 3.40.

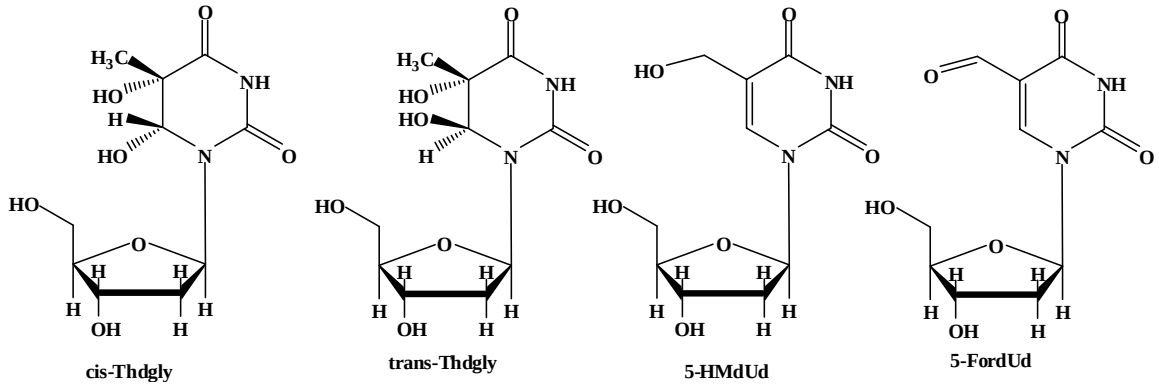

Figure 3.39: Thymidine oxidation products obtained from HPLC-MS/MS study

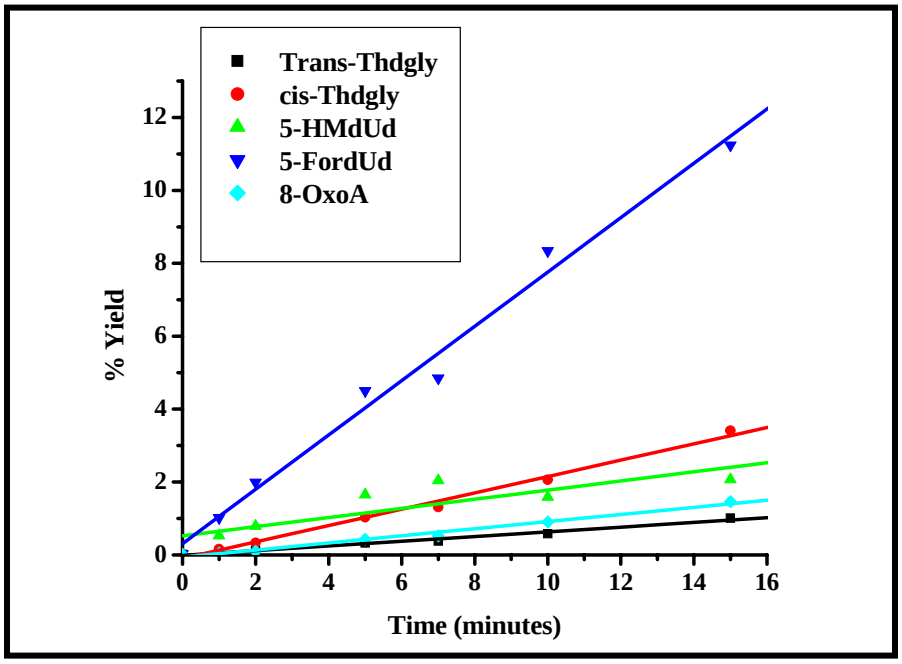

Figure 3.40: Plot showing formation of different thymidine oxidation products at different irradiation times

The percentage yield (against thymidine yield) of each of these products has been calculated at different irradiation times and the plot shows linear relationship of yields with time of irradiation for each of them. Among these four modified nucleotides, 5-FormdU has the highest yield followed by 5-HMdU, cis-ThdGly and trans-ThdGly. We have also tried to find out if there is any production of adenine oxidation product 8-oxo-adenine (8-OxoA) and the result shows that the formation of this product is very little compared to the thymidine oxidation products.

From our experiments we have previously proposed two tandem reaction pathways that might lead to thymidine damage along with direct oxidation, and the molecular modeling studies indicated that the C5-Me-H abstraction pathway by generation of radical cation at the 5'-thymidine of a 3'-TT-5' segment is the more

feasible pathway. The products obtained from the HPLC-MS/MS studies can be perfectly explained by that pathway. The pathway has been described briefly here again for better understanding (Figure 3.41).

When a radical cation visit a 3'-TT-5' segment (1) of DNA, it can results in radical cation 2, where a radical cation is generated at 5'-T. This can react with water to produce the radical 3, where the 5'-T has become a 6-hydroxythymidine-5-yl radical. Reaction of this radical with oxygen may produce 6-hydroxythymidine-5-peroxyl radical 4, which can abstract hydrogen from the methyl group of 3'-T to form another radical 5. In 5, the radical is at the methyl group of 3'-T. Reaction of 5 with oxygen and /or water will produce 6, where 5'-T has become a thymidine glycol and the 3'-T has become 5-hydroxymethyl-2'-deoxyluracil or other higher oxidation product (5-formyl-2'-deoxyuridine). Orientation of the peroxyl radical would be very important in this pathway. It can be cis or trans to the hydroxyl group at the C5 position. However, in one orientation it would be close to C5-methyl hydrogen of 3'-thymidine and in other orientation it would be away from that hydrogen. This will implicate stereoselectivity in the thymidine glycol formation and HPLC-MS/MS results confirm that the thymidine glycol formation is indeed stereoselective (more cis glycol than trans glycol).

On the other hand, there is a possibility of generation of the radical cation at 3'-thymidine (7, Figure 3.40). This can form similar peroxyl radical as the 5'-thymidine but can not abstract hydrogen from C5-methyl group of 5'-thymidine as it is too far away (From molecular modeling and NMR structure analysis, see segment 3.6). Now, it can release a proton from C5-methyl and form a radical there (8). This radical will react with

oxygen and water to produce 5-hydroxymethyl-2'deoxyurdine and 5-formyl-2'-deoxyuridine (9).

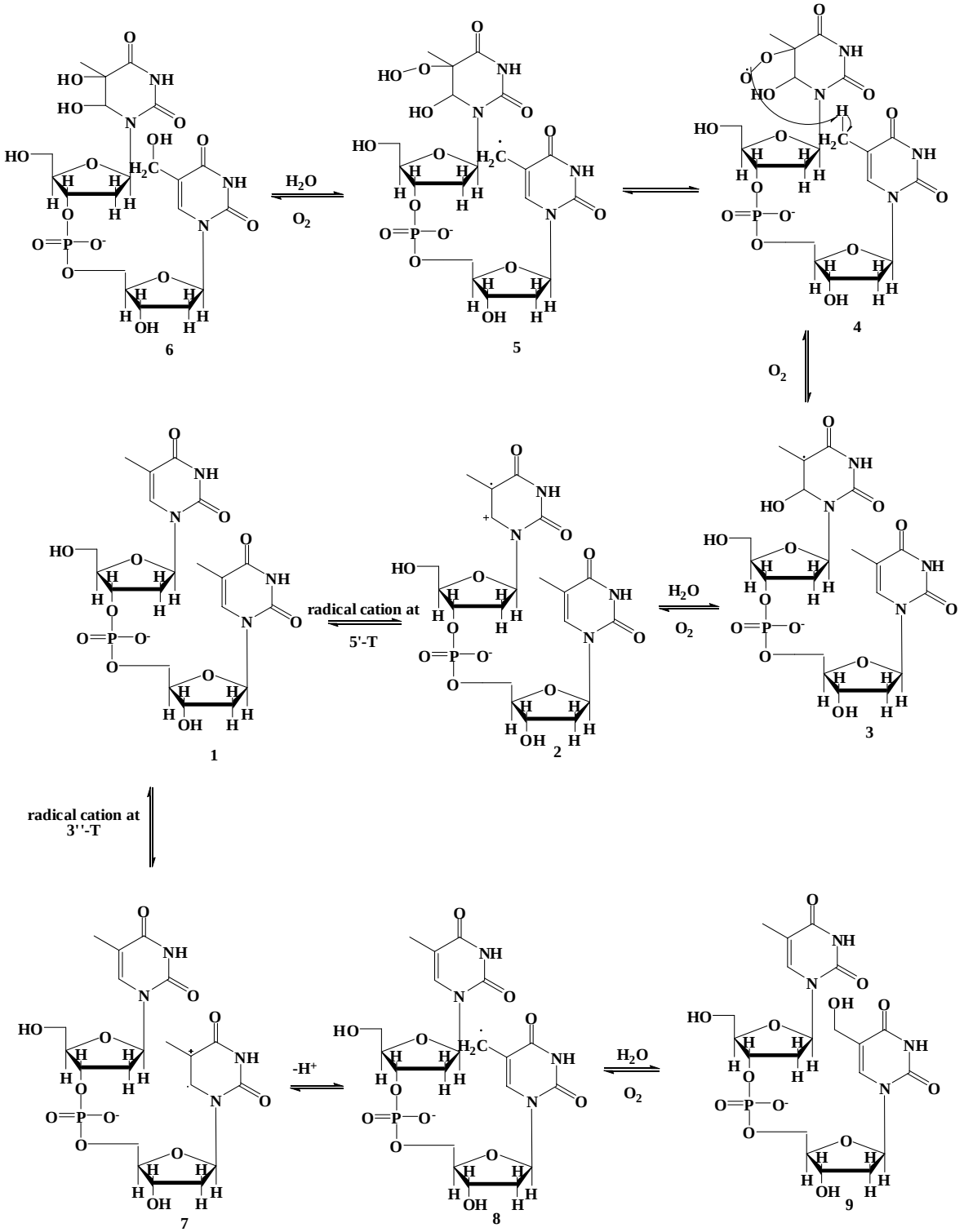

Figure 3.41: Reactions leading to thymidine damage by one-electron oxidation

From the product distribution obtained from HPLC analysis it is evident that the formation of 5-hydroxymethyl-2'-deoxyurdine and 5-formyl-2'-deoxyuridine are much higher than the thymidine glycols. This implies that both the pathways described here are operating. Both these pathways result in 5-hydroxymethyl-2'-deoxyuridine and 5-formyl-2'-deoxyuridine, but only the pathway involving the radical cation generation at the 5'-thymidine generates thymidine glycols.

3.10 Cross-link Formation

It has been reported that when a 5-(2'-Deoxyuridinyl) methyl radical is generated in DNA, an interstrand crosslink between the methyl group of thymidine and amine of adenine base paired to it, is observed.[29,30] In our experiments we have not seen any cross-link formation. To detect any cross-link we studied the gel electrophoresis of DNA 1 before piperidine treatment, But only very little crosslink was found (Figure 3.42)

The mechanism of this crosslink formation involves a rotation of thymidine base around its glycosidic bond[30] (figure 3.43) and for that it has to overcome the hydrogen bonding interaction between that thymidine and adenine base paired with it. The DNA strand used by Greenberg and coworkers has a bulky Phenyl selenium group attached to the methyl group of thymidine, which on γ-radiation generates the radical at that position. That might change the conformation of the DNA to some extent and can affect the hydrogen bond interaction between the O4 of thymidine and amine hydrogen of adenine. This might make that hydrogen bonding weaker and it would be easier for the thymidine

to rotate around its glycosidic bond. On the other hand, the DNA strands used in our work do not have any such kind of distortion. So, it is difficult for the thymidine to

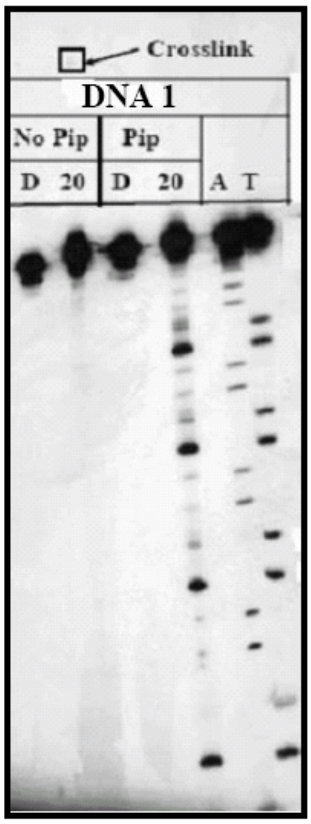

Figure 3.42: Autoradiogram showing very little cross-link formation. pip and no pip represents piperidine treated and not treated samples. D and 20 represents 0 and 20 minutes of irradiation.

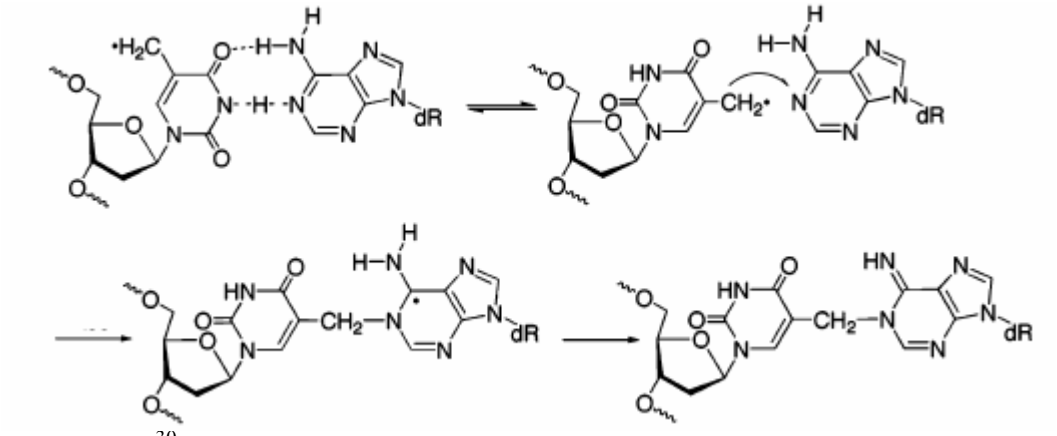

Figure 3.43[30]: Mechanism of cross-link formation

overcome the hydrogen bond energy to rotate and the methyl radical remains at its normal position, away from the adenine amine group. We tested this hypothesis by molecular modeling. In the DNA we used, the distance between the O4 of thymidine and amine hydrogen of adenine is 2.09 angstroms. While, the same distance is 2.79 angstroms when the thymidine has a phenyl selenium attached to the methyl group. This distance is much higher than a normal hydrogen bond distance of 1.97 angstroms. Thus, the hydrogen bond interaction between this modified thymidine and adenine is not strong enough and the rotation around the thymidine glycosidic bond is possible. But, for the DNA's used in our work the distance is close to normal hydrogen bond distance and the hydrogen bond is strong enough to prevent rotation and crosslink formation.

3.11 Determination of Quantum Yield of Thymidine Reaction

The quantum yield of the reactions leading thymidine damage (strand cleavage) has been calculated using DNA 14. The photoreactor has been calibrated using Anthraquinone-2,6-disulphonate[31] and the rate of thymidine damage is calculated from the disappearance of the DNA by HPLC.

3.11.1 Determination of Light Flux

AQDS (100 μM) was prepared in NaOH solution (pH 14.07). The solution was deoxygenated by freeze-pump-thaw process thrice. Then it was irradiated at 350 nm (6 lamps) for 0, 0.5, 1, 1.5, 2, and 2.5 minutes and UV absorption spectra has been taken at each time interval. The formation of AQDS radical anion has been monitored at 520 nm.

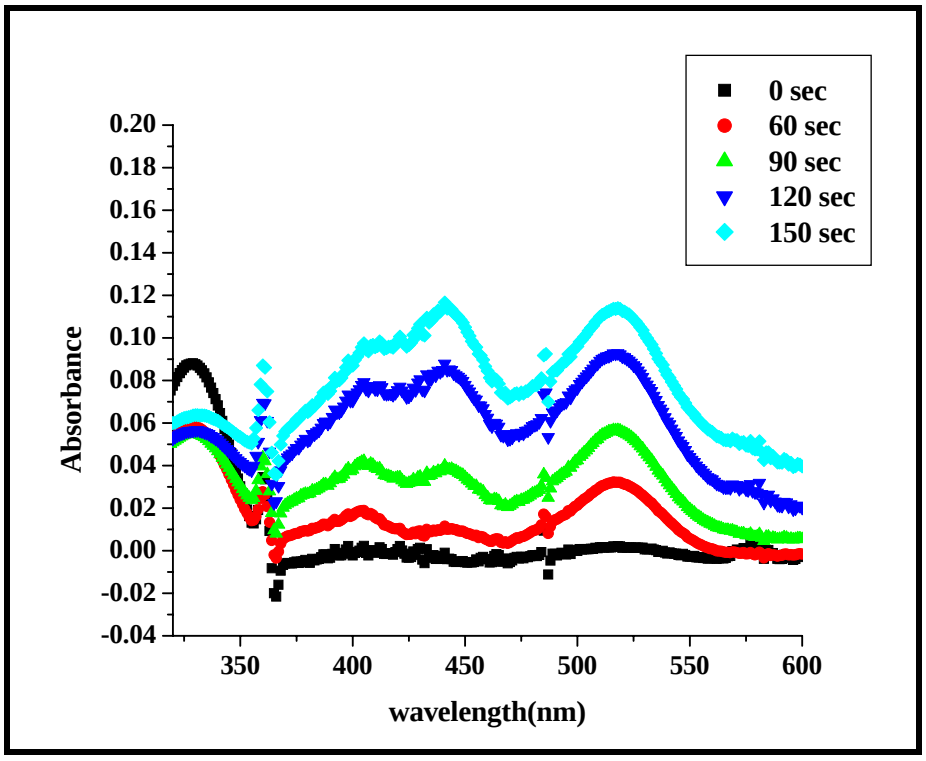

Figure 3.44: UV absorption spectra of AQDS at different irradiation times.

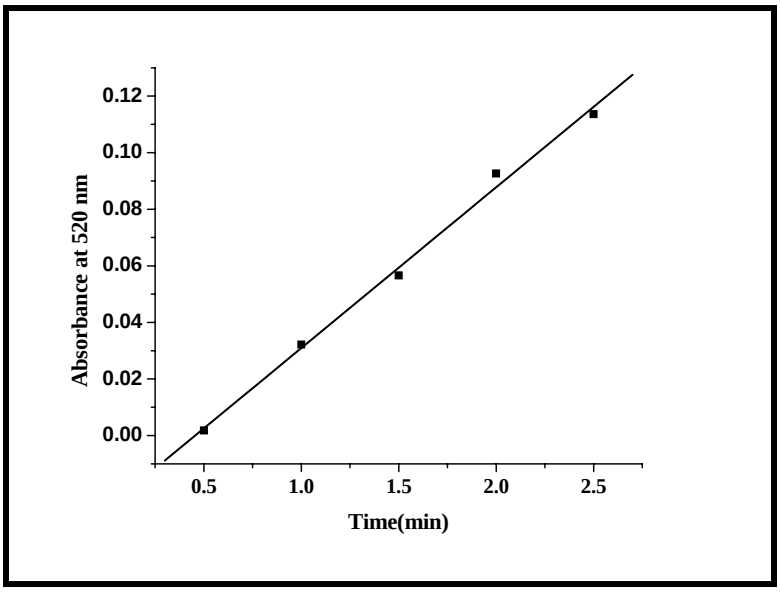

Figure 3.45: Rate of formation of AQDS radical anion

Rate of change in concentration (dx/dt) = (slope of the straight line)/ (ε x l)

ε = 8700 $mol^{-1}cm^{-1}L$

l = 0.25 cm

slope of the straight line (figure 2) = 0.0582 min^{-1}

dx/dt = 0.0582 / (8700 x 0.25) mol L^{-1} min^{-1}

1 mL solution has been used for the experiment.

hence, dx/dt = 0.0582 x 10^{-3} / (8700 x 0.25) moles min^{-1}

= 2.6 x 10^{-8} moles min^{-1}

Light flux η = dx/dt / quantum yield at pH 14 (Φ)

= 2.6 x 10^{-8} / 0.2 moles min^{-1}

= 1.3 x 10^{-7} moles min^{-1}

Light flux = 1.3 x 10^{-7} einstein min^{-1}

3.11.2 Calculation of Quantum Yield

To determine the rate of thymidine reactions, the following DNA duplex has been used. (DNA 14)

5′-AQUUUUAAUUAAUUAAUUAAUAUAUUT-3′
3′-AAAATTAATTAATTAATTATATAAA-5′

1.5 mL of duplex DNA has been used. The concentration of DNA was 10 μM. 500 μL of this DNA solution has been kept as dark after hybridization. The other 1 mL solution has been irradiated at 350 nm (6 lamps) for 7 minutes. Then it was divided into 2 aliquots of 500 μL and each of them along with the dark sample were treated with 200 μL of 1 M

piperidine for 30 minutes at 90 ^{0}C. After piperidine treatment the samples were dried under vacuum and used for HPLC. Prior to HPLC 500 μL of nanopure water and 200 μL of 1 mM 2′-deoxycytidine has been added to all the samples as internal standard. The internal standard come out at about 8 minutes, the TT containing strand comes out after 32 minutes and the AQ containing strand comes out at about 34 minutes. The rate of the thymidine reaction has been determined from the change in peak area of the signal at 32 minutes.

Table 3.6: HPLC analysis results of dark and 7 minutes irradiated samples.

Sample	Area for internal standard	Area for DNA signal
Dark	11867116	2910998
Irradiated	9961251	1639663

For the **DARK** sample:

area under the peak at 32 minutes/ area for internal standard = 0.24

For the **IRRADIATED** sample:

area under the peak at 32 minutes/ area for internal standard = 0.16

The dark sample contains 500 μL of 10 μM DNA= **5×10^{-9} moles of DNA**

The irradiated sample contains 5×10^{-9} x (0.16/0.24) moles of unreacted DNA

= **3.3×10^{-9} moles of unreacted DNA**

Rate of the thymidine damage reaction = (5- 3.3) x 10^{-9} moles / 7 min

= **2.5×10^{-10} moles min^{-1}**

For the calculation of quantum yield the relative absorbance of AQDS and AQ in DNA has to be considered. To determine the absorbance of AQ at 350 nm, another DNA

duplex has been used, which has same sequence as the AQ containing duplex but does not have any AQ. The difference in absorbance of AQ containing duplex and the non-AQ duplex has been used as the absorbance of AQ.

Table 3.7: Relative absorptions of AQDS and AQ at 350 nm

Sample	Absorbance at 350 nm
DNA (no AQ)	0.05078125
DNA (with AQ)	0.074585915
AQDS	0.224449158

Relative absorbance = 0.224/ (0.0746-0.05078) = **9.4**

Quantum yield of the reaction = (Rate of the reaction / Light flux) x 9.4

= (2.5 x 10^{-10} moles min^{-1}/ 1.3 x 10^{-7} moles min^{-1}) x 9.4

= **1.8 x 10^{-2}**

3.12 Conclusion

In this chapter a systematic analysis of the long range charge migration and one-electron oxidations in DNA strands lacking guanine has been reported. Although, on the basis of oxidation potential it has been predicted that the reaction will occur at adenines, the real scenario is different. It is the thymidines in adenine-thymidine containing strands that are actually getting damaged. This indicates that the relative reactivity of the nucleobases also play an important role in determining the site of damage.

The different characteristics of this thymidine damage have been studied thoroughly. The efficiency of damage is dependent on the distance of the damaged site

from the anthraquinone charge injector, which shows that the damage is resulting from the long range charge migration from anthraquinone. The effect of radical scavenger glutathione on the reactions at thymidine has been studied and the damage decreased with increasing concentration of glutathione. However, glutathione does not affect the damage at remote guanines present in the same strand. This indicates that the charge injector anthraquinone radical anion is not quenched by the glutathione and it is decreasing the thymidine damage by reacting with the radicals generated during the reactions. It has been also found that the C5-methyl group of thymidine plays an important role in thymidine damage. Replacing all or some of the thymidines (T) with 2'-deoxyuridines (U) we found out an interesting trend in the reactions. When the 3'-thymidine of a 3'-TT-5' segment is substituted by U, there is no reaction. On the other hand, if the 5'-thymidine is substituted by U the damage is not inhibited. This implies that the C5-methyl group of 3'-thymidine only plays important role in the reactions and tandem reaction is involved. On the basis of these studies a number of pathways have been proposed and the feasibility of those is predicted by molecular modeling. Lastly, the products of thymidine damage reaction have been revealed by HPLC-MS and the results can be perfectly explained by one of the proposed mechanisms.

REFERENCES

1. Ly, D.; Kan, Y.; Armitage, B.; Schuster, G. B. *J. Am. Chem. Soc.* **1996**, *118*, 8747-8748.

2. Schuster, G. B. *Acc. Chem. Res.* **2000**, *33*, 253-260.

3. Giese, B.; Spichty, M.; Wessely, S. *Pure Appl. Chem.* **2001**, *73*, 449-453.

4. O'Neill, M. A.; Barton, J. K. *J. Am. Chem. Soc* **2004**, *126*, 11471-11483.

5. Steenken, S.; Jovanovic, S. V. *J. Am. Chem. Soc.* **1997**, *119*, 617-618.

6. Senthilkumar, K.; Grozema, F. C.; Guerra, C. F.; Bickelhaupt, F. M.; Lewis, F. D.; Berlin, Y. A.; Ratner, M. A.; Siebbeles, L. D. A. *J. Am. Chem. Soc.* **2005**, *127*, 14894-14903.

7. Saito, I.; Takayama, M.; Kawanishi, S. *J. Am. Chem. Soc.* **1995**, *117*, 5590-5591.

8. Douki, T.; Cadet, J. *Int. J. Radiat. Biol.* **1999**, *75*, 571-581.

9. O'Neill, P.; Parker, A. W.; Plumb, M. A.; Siebbeles, L. D. A. *J. Phys. Chem. B* **2001**, *105*, 5283-5290.

10. Fukuzumi, S.; Miyao, H.; Ohkubo, K.; Suenobu, T. *J. Phys. Chem A* **2005**, *109,* 3285-3294.

11. Seidel, C. A. M.; Schulz, A.; Sauer, M. H. M. *J. Phys. Chem.* **1996**, *100*, 5541-5553.

12. Bergeron, F.; Houde, D.; Hunting, D. J.; Wagner, J. R. *Nucleic Acids Res.* **2004**, *32*, 6154-6163.

13. Muller, J. M.; Duarte, V.; Hickerson, R. P.; Burrows, C. J. *Nucleic Acids Res.* **1998**, *26*, 2247-2249.

14. Curtin, D. Y. *Rec. Chem. Prog.* **1954**, *15*, 111-128.

15. Liu, C.-S.; Hernandez, R.; Schuster, G. B. *J. Am. Chem. Soc.* **2004**, *126*, 2877-2884

16. Mrtini, M.; Termini, J *Chem. Res. Toxicol.* **1997,** *10,* 234-241

17. Saladino, R.; Carlucci, P.; Danti, M. C.; Crestinib, C.; Mincione, E. *Tetrahedron* **2000**, 56 10031-10037

18. Bui, T. C.; Cotton, R.G. H. *Bioorganic Chemistry* **2002**, 30**,** 133–137

19. Purmal, A. A.; Lampman, G. W.; Bond, J. P.; Hatahet, Z.; Wallace, S. S. *J. Biol. Chem*. **1998**, 273, 10026-10035

20. Carter, K. N.; Greenberg, M M. *J. Org. Chem.* **2003**, *68*, 4275-4280

21. Carter, K. N.; Greenberg, M M. *J. Am. Chem. Soc.* **2003**, 125, 13376-13378

22. Tallman, K. A.; Greenberg, M. M. *J. Am. Chem. Soc.* **2001**, 123, 5181-5187

23. Hizver, J.; Rozenberg, H.; Frolow, F.; Rabinovich, D.; Shakked, Z *Proc. Nat. Acad. Sci*. **2001**, 98, 8490-8495

24. Sarma, M. H.; Gupta, G.; Sarma, R. H.; *Biochemistry* **1988**, 27, 7909-7919

25. Strużńka, L; Chalimoniuk, M.; Sulkowski, G. *Toxicology* **2005**, 212, 185-194

26. Janzen, E. G. *Acc. Chem. Res.* **1971**, 4*,* 31-40.

27. Janzen, E. G.; Wang, Y. Y.; Shetty, R. V. *J. Am. Chem. Soc.* **1978**, 100, 2923-2925

28. Kuwabara, M.; Inanami, O.; Endoh, D; Sato, F. *Biochemistry* **1987**, 26, 2458-2465

29. Hong, I. S.; Greenberg, M. M. *J. Am. Chem. Soc.* **2005**, *127*, 3692-3693.

30. Hong, I. S.; Greenberg, M. M. *J. Am. Chem. Soc.* **2006**, 128, 485-491